PhiX174 GENOME-CAPSID INTERACTIONS: EVIDENCE FOR A SCAFFOLDING-LIKE FUNCTION FOR THE GENOME DURING MORPHOGENESIS

by

Susan Lynette Hafenstein

A Dissertation Submitted to the Faculty of the

DEPARTMENT OF VETERINARY SCIENCE AND MICROBIOLOGY

In Partial Fulfillment of the Requirements
For the Degree of

DOCTOR OF PHILOSOPHY
WITH A MAJOR IN PATHOBIOLOGY

In the Graduate College

THE UNIVERSITY OF ARIZONA

2003

UMI Number: 3106995

ProQuest Information and Learning Company
300 North Zeeb Road
P.O. Box 1346
Ann Arbor, MI 48106-1346

THE UNIVERSITY OF ARIZONA ®
GRADUATE COLLEGE

As members of the Final Examination Committee, we certify that we have read the dissertation prepared by Susan Lynette Hafenstein entitled PhiX174 Genome-Capsid Interactions: Evidence for a Scaffolding-like Function for the Genome During Morphogenesis

and recommend that it be accepted as fulfilling the dissertation requirement for the Degree of Doctor of Philosophy

James K Collins	6/14/03
Dr. James Collins	Date
David L Besselsen	6/16/03
Dr. David Besselsen	Date
Bentley A Fane	6-16-03
Dr. Bentley Fane	Date
	Date
	Date

Final approval and acceptance of this dissertation is contingent upon the candidate's submission of the final copy of the dissertation to the Graduate College.

I hereby certify that I have read this dissertation prepared under my direction and recommend that it be accepted as fulfilling the dissertation requirement.

Bentley A Fane	6-16-03
Dissertation Director	Date
Dr. Bentley Fane	

STATEMENT BY AUTHOR

This dissertation has been submitted in partial fulfillment of requirements for an advanced degree at The University of Arizona and is deposited in the University Library to be made available to borrowers under rules of the Library.

Brief quotations from this dissertation are allowable without special permission, provided that accurate acknowledgment of source is made. Requests for permission for extended quotation from or reproduction of this manuscript in whole or in part may be granted by the copyright holder.

SIGNED: Susan Hafenstein

IN ACKNOWLEDGEMENT:

Thanks to my parents for nurturing a sense of humor and curiosity and for providing me with a strong work ethic and a belief in my capabilities. They taught me by their own example that hard work and perseverance pay off and that any fishing trip is a good fishing trip.

Thanks to my mentor, Bentley Fane. His enthusiasm for the science and his ability as my teacher go unequaled. I have been exceedingly fortunate to begin my scientific training in the Fane lab, these years have been pivotal years in my life, and I am emerging as a happy scientist. Thank you. I am proud and honored to go forth without fear, to trust my data, to bless the centrifuge, and to continue to ask questions and challenge the answers.

To April Burch, thanks for showing me that the best thing to serve with an ice-cold beer is a scientific discussion, even better when mixed with a riverbank or a mountain view, but truly enjoyed anywhere at all.

To Min Chen. Thank you for thousands of agar plates and the DNA sequence of all the mutants who were and the ones who were not. And for being my good friend.

To Asako Uchiyama, thank you for sacrificing the time and the tubies and your place in the incubator so that my research here could finish while yours was starting. I will miss your smile.

My gratitude to my friend Karie Brentlinger, forever. You have done so much to help me along the way that it is impossible to list here. Kiss the pig for me and stop stealing cable.

Thanks to Trish Fairweather for the workout of the body and the mind. Keep on pumping both and consider gene therapy instead of physical therapy.

Special thanks to Ole and the boys. You brightened the path and lightened the load. I am especially grateful to the Olsen grandparents for being there every time I needed them.

To all of you, my friends and family, thanks for the tolerance and support and love. It hasn't all been smooth sailing and I couldn't have done it without you.

IN DEDICATION

To my best friend,

David Erling Olsen, Jr.

TABLE OF CONTENTS

TABLE OF CONTENTS - *CONTINUED*

TABLE OF CONTENTS - *CONTINUED*

LIST OF FIGURES

LIST OF FIGURES – *continued*

LIST OF FIGURES – *continued*

LIST OF TABLES

LIST OF TABLES – continued

ABSTRACT

The assembly of viral proteins and nucleic acids into mature and biologically active virions involves a diverse spectrum of macromolecular interactions. After capsid formation, structural and packaging proteins must interact with viral nucleic acids. These interactions may confer packaging specificity, spatially organize the genome, enhance particle stability, or contribute directly to capsid quaternary structure. In the*Microviridae*, packaging and capsid proteins are tightly associated, tethering the genome to the inner surface and guiding it into the overall icosahedral symmetry of the particle. All of these factors may influence the final stages of maturation, which involves an inward collapse of coat proteins around the packaged genome.

These packaging parameters were altered in three ways. 1) The DNA binding residues of the DNA binding protein were altered. Although the genome and protein are in the interior of the capsid, alterations were expressed on the capsid's outer surfaces. The results of second site genetic analyses illustrate how coat protein modifications can compensate for defective phenotypes. 2) Non-DNA binding amino acid residues believed to be of structural importance were mutated. The results of these analyses elucidate the function of these residues in optimizing DNA-protein interactions and organizing the DNA into the capsid's symmetry. Again, the results of second site genetic analyses demonstrate the inherent evolutionary plasticity of the system. 3) Packaged DNA was changed by altering base composition and folding parameters. The experimental results

support a model in which the secondary structure of the packaged genome acts in a scaffold-like manner during the final stage of virion morphogenesis, affecting the biophysical and biological properties of the mature virion.

Finally a chimeric particle was constructed by placing a wild type DNA binding protein in a wild type, but foreign environment. The biophysical characterization of these particles is consistent with the mentioned model. A structural analysis was performed, in collaboration with Dr. Rossmann's group (Purdue University), to provide a structural context in which to interpret the observed biophysical effects. While not all questions were answered or hypotheses verified, the results elucidate the limitations and interpretation of structural analyses, a current debate in the structural biology field.

CHAPTER I: INTRODUCTION

Das große Bild

1.1 PROBLEM DEFINITION

The assembly of viral proteins and nucleic acids into mature and biologically active virions involves a diverse spectrum of macromolecular interactions. After capsid formation, structural and packaging proteins must interact with viral nucleic acids. These interactions may confer packaging specificity, spatially organize the genome, enhance particle stability, or contribute directly to capsid quaternary structure (Larson *et al,* 1998, Fox *et al*, 1998, Choi *et al,* 2000, Fisher and Johnson, 1993). Typically, packaging proteins are extremely basic, neutralizing the negative charges associated with the genome (Alestrom *et al.*, 1984; Anderson *et al.*, 1989, Davis *et al.*, 1976; Copeland *et al.* 1984).

In *Microviridae*, packaging proteins are tightly associated with the capsid protein (McKenna *et al.*, 1992, 1994), which tethers the genome to the inner surface and may guide it into the overall icosahedral symmetry of the particle. All of these factors may influence the final stages of maturation, especially since they involve an inward collapse of coat proteins around a packaged genome. Altering these packaging parameters could

affect particle dimension, surface topography and stability, which, in turn, may affect infectivity. The development of medically significant gene delivery systems will be governed by tissue and animal tropism. Viruses with icosahedral symmetry, such as *Togaviridae* (Bredenbeek *et al.*, 1993; Dubensky *et al.*, 1996), *Adenoviridae* (Gorziglia *et al.*, 1996; Lieber *et al.*, 1996), *Spumavirinae* (Russell and Miller, 1996), and the small T=1 *Parvoviridae* (Kotkin, 1996; Zolotukhnin *et al.*, 1996), are currently being investigated for the treatment of a variety of genetic diseases. If icosahedral virions are to be successfully employed, mechanisms that affect packaging and the ability to generate infectious recombinant vectors must be elucidated.

The T=1 icosahedral Microviruses (canonical members: øX174, G4 and α3) are ideally suited for the DNA packaging and structural research. The atomic structures of the øX174 virion, the øX174 procapsid, a degraded G4 procapsid, and the α3 virion have been determined (McKenna *et al.*, 1992, 1994, 1996; Dokland *et al.*, 1997, 1999; Bernal *et al.* 2003). Therefore, the results of genetic and biochemical analyses can be interpreted within a structural context. However, atomic structures derived from X-ray crystallography are static images of the virion form most susceptible to crystallization

conditions. Transient interactions, flexible components, and capsid dynamics in solution remain better defined and investigated via genetic and biochemical assays.

The specific aims of the research included in this dissertation were the following:

1) To investigate the mechanisms by which the DNA binding protein guides the genome during packaging into the overall the icosahedral symmetry by genetic, second-site genetic and biochemical analyses.
2) To examine the biophysical effects of packaged DNA on particle characteristics analyzed by altering genome base composition and folding parameters, and the DNA binding protein.
3) To provide a more detailed structural context in which to interpret the results from specific aims 1 and 2, by solving the atomic structure of a chimeric virus with altered protein-genome interactions: α3 virions packaged with the øX174 DNA binding protein. These studies, conducted in collaboration with Dr. M. G. Rossmann (Purdue University), also included solving the atomic structure of wild-type α3 (Bernal *et al* 2003).The experimental results support a model in which the secondary structure of the packaged genome acts in a scaffold-like manner during the final stage of virion morphogenesis, affecting the biophysical and biological properties of the mature virion.

LITERATURE REVIEW

1.2.1 THE *MICROVIRIDAE*

Of the 15 members of the family *Microviridae*, øX174, G4, and α3 have been the most extensively studied and characterized. They are small (260 Å in diameter), T=1, icosahedral viruses, with single stranded DNA genomes 5.3 -6.1 kb in length. Mature particles have a buoyant density in the range of 1.4 g/cm^3, and sediment at approximately 115S. All three genomes have been sequenced (Sanger *et al.* 1978, Godson *et al.*, 1978, Kodaira *et al.*, 1992) and contain the identical arrangement of overlapping reading frames. Sequence homologies range from 59 to 67%, with øX174 and α3 being the most distantly related.

Mature microvirus virions contain four structural proteins. There are 60 copies each of the coat protein, F, the minor spike protein G, and the DNA binding protein, J. The capsid is comprised of pentamers of F protein joined in T=1 symmetry, producing 12 vertices, 20 faces with 60 asymmetric units. Pentamers of protein G decorate each five-fold axis of symmetry. Each copy of J protein is complexed with the DNA and a viral coat protein, effectively tethering the genome to the inner surface of the capsid at each asymmetric unit. There are 12 copies of H, the minor spike protein, one at each five-fold axis of symmetry residing in a hydrophobic channel that runs through capsomer. Thus,

the relative stoichiometry of these structural proteins in øX174 is 5:5:5:1 (F:G:J:H) and is dictated by the icosahedral symmetry of the mature virion. This stoichiometry has been verified by both biochemical and structural analyses (Hayashi *et al.* 1988; McKenna *et al.* 1992, 1994). While the stoichiometry of coat, spike and DNA binding proteins in G4 and α3 virions is identical to the øX174 values. Differences in the relative amount of the minor spike protein have been observed (Bernal *et al.* 2003).

1.2.2 *Microviridae* Virion Morphogenesis

Microviridae morphogenesis is illustrated in Figure 1 and is dependent on two species of scaffolding proteins and a packaged single-stranded DNA genome (Hayashi *et al.* 1988, Hafenstein and Fane, 2002). Initially, assembly proceeds via two independent pathways, procapsid morphogenesis and DNA synthesis through the formation of the stage III pre-initiation complex (Hayashi *et al.*, 1988; Ekechukwu *et al.*, 1995, Burch and Fane, 2000). The first capsid intermediates are the 9S and 6S particles, pentamers of the coat and major spike proteins respectively (Tonegawa and Hayashi 1970). In a reaction dependent on B, a 9S and 6S particle are joined, creating the 12S particle (Siden and Hayashi, 1074). Twelve 12S particles then associate with 240 molecules of the external scaffolding protein, D, to form the procapsid (Tonegawa and Hayashi 1970; Fujisawa and Hayashi 1977a).

The mechanisms involved in *Microviridae* packaging differ substantially from those found in other bacteriophages. Packaging and single-stranded genome biosynthesis are concurrent processes. Genome length is strictly governed by a single origin of replication, which determines both the commencement and termination of biosynthesis and packaging. DNA concatamers, unique translocating vertices, and headful packaging are not involved. After the procapsid is assembled, the pre-initiation complex associates with the viral procapsid in a depression along the two-fold axis of symmetry, forming the 50S complex allowing genome replication and packaging to commence (Hayashi, 1978, Mukai *et al.*, 1979, Ekechukwu *et al.*, 1995). The viral A protein binds to the origin of replication in the RF II DNA. This is both necessary and sufficient for packaging specificity (Fluit *et al.*, 1985, Aoyama and Hayashi, 1985, Hafenstein and Fane, 2002). Any circular DNA molecule with a *Microviridae* origin of replication can serve as a template (Aoyama and Hayashi, 1985). Upon binding, protein A nicks the origin (Van Mansfeld *et al.*, 1984) and forms a covalent ester bond with the DNA (Eisenberg and Kornberg, 1979). After one round of rolling circle synthesis, it cuts the newly generated origin and acts as a ligase, generating a covalently closed circular molecule (Eisenberg *et al.* 1977, Brown *et al.*, 1984).

The highly basic DNA binding protein (J) enters the morphogenetic pathway during packaging (Fujisawa and Hayashi, 1976), associating with the genome via charge-charge interactions (Jennings and Fane, 1997). The C-terminus of J, highly conserved within the *Microviridae*, associates with a cleft in the coat protein (F) in each asymmetric unit

(Figure 2). This is a common binding cleft occupied by B in the procapsid. Interactions by protein J during packaging result in displacing the internal scaffolding protein (B) from the common binding cleft in the coat protein (Dokland *et al.,* 1997) and may facilitate further interactions between the genome and a small cluster of adjacent basic capsid amino acids located in the coat protein, (F). Morphogenesis completes with the dissociation of the external scaffolding protein (D) and an 8.5 Å radial collapse of coat protein pentamers around the single stranded genome. No pentamer-to-pentamer contacts have yet been made and the genome itself, tethered to the inner surface of the capsid at each pentameric subunit, may function as a scaffold, directing the final collapse and maturation of the virion. The impact of the genomic tether on the biophysical characteristics of the mature virion has been established by changing the characteristics of the DNA binding protein and by direct manipulation of the packaged DNA (Hafenstein and Fane, 2002).

1.2.3 Assembly of small icosahedral viruses:

There are three general mechanisms for the assembly and packaging of small icosahedral viruses. (1) Through highly cooperative interactions between the nucleic acid and the viral proteins, usually the capsid protein, the genome is enclosed during the capsid morphogenesis and assumes a level of icosahedral order through interactions with the capsid proteins. The packaging of the ss RNA genome of Satellite tobacco mosaic virus (STMV), and therefore its capsid assembly, appears to follow this mechanism. As the

genome is replicated, local regions of secondary structure (hair-pin loops) form to which dimers of coat protein bind. Loosely formed, fluid-like aggregates of protein and RNA are then proposed to form pentamers which would concurrently assume the T=1 icosahedral structure (Larson and McPherson, 2001).

(2) In a second packaging mechanism, the genome folds upon itself, forming both local and distal viral structural proteins then encloses the globular genomic structure. Virions that utilize this mechanism characteristically have an extensively basic capsid interior, very few protein-protein interactions between coat proteins before morphogenesis, and a coat protein tail with a highly basic nucleic acid binding domain. As proposed for the *Bromoviridae*, when the ssRNA genome of BMV folds into secondary structure through intergenomic interactions, a negatively charged surface is presented that attracts the positively charged RNA binding domains of the coat protein. After the positively charged extensions of the coat proteins interact with the genome, the capsid subunits are brought into contact, which leads to the requisite protein-protein interactions to achieve the virion structure.

(3) Finally, the third mechanism involves packaging the genome into a preformed immature capsid, called a procapsid in some assembly systems. Viruses that utilize this mechanism are characterized by strong coat protein-protein interactions, clearly needed to form a pre-formed icosahedral lattice, as observed in the T=3, ssRNA tymoviruses, physalis mottle virus and turnip yellow mosaic virus. Specifically there is N-terminal arm

extending from one A subunit underneath and interacting with the trimer in the next subunit, producing an interlocking network. Packaging of polyamines is required for particle stability and a unique hairpin (C.C or C.A mismatch) seems to bind specifically to the interior of the protein shell and may represent a genome encapsidation initiation signal (Bink *et al.,* 2002).

The *Microviridae* genome packaging and morphogenesis appears to utilize aspects of all three above systems. While procapsids initially assemble via protein-protein interactions, which includes coat-coat protein interactions in pentamer formation, procapsid integrity is dependent on coat-scaffolding interactions, as opposed to the coat-coat interactions as seen in the T=3 capsids discussed above. Although local genomic structure does not nucleate capsid morphogenesis as it does with STMV nor does a global structure act as template on which capsid proteins assemble as in the *Bromoviridae*, both levels of genomic structure may influence the final stages of morphogenesis after the genome is packaged

1.2.4 GENOME DEPENDENCE IN OTHER SYSTEMS

The nodoviruses, Flock house virus, (FHV), Black beetle virus (BBV), and Pariocoto, (PaV) are T=3 insect viruses with ssRNA bipartite genomes. Atomic structures have been solved for all three (Fisher and Johnson, 1993, Wery et al, 1994, Tang et al, 2001)

and all have ordered RNA density. In FHV the ribose phosphate backbone and base density can be visualized as a duplex at each twofold axis of symmetry. In BBV the genome is less ordered and only the phosphate backbone can be visualized; however, 34% of the RNA is ordered in Pariacoto, forming a cage-like structure on the interior. Despite these differences, in all three the highly ordered conformation of the genome at the twofold axes is a result of RNA-protein interactions. Specifically, it has been established in FHV, that interactions between a 10 bp RNA duplex and residues 20-30 of the N-terminal coat protein, interact to form a molecular switch which must be present to allow proper T=3 assembly to proceed. The amino terminus of the coat protein contains 11 basic residues and four proline residues. The specificity in this region has been demonstrated with N-terminal deletion mutants (Marshall and Schneemann, 2001). Either native or foreign RNA will allow T=3 particle formation, however, particles packaged with cellular RNA have different solution properties than wild type FHV (Bothner *et al.* 1999).

Satellite tobacco mosaic virus (STMV) is the satellite virus to tobacco mosaic virus (TMV) and the structure has been solved by X-ray diffraction (Larson et *al.,* 1993, Larson *et al.,* 1998). Almost 60% of the single stranded RNA genome is visible due to extensive interactions with the coat protein. Each coat protein dimer is complexed with a double stranded section of the genome comprised of seven base pairs. With the genome this constrained and ordered by interactions with the coat, less than half of the continuous RNA genome is left free within the capsid linking the bound sections of RNA. Thus,

Satellite tobacco mosaic virus demonstrates the flip side of protein-genomic interactions by illustrating the spatial constraint of the genome, ordering it into symmetrical units, and the entire arrangement suggests a packaging model unique to STMV (see above).

In the Sobemoviruses: Southern cowpea mosaic virus (SCMV) and Sesbania mosaic virus (SeMV) a highly basic N-terminal extension of the coat protein has been shown to interact with the genome and this interaction serves as a molecular switch directing correct capsid assembly (Lokesh *et al.* 2001). The N-terminus has a conserved binding domain (RRKRRAKRR) that is directly preceded by a proline-rich segment (PNPP), a motif similar to the øX174 DNA binding protein. The importance of the N-terminal binding domain was established by deletion mutants. In separate studies conducted to investigate the specificity of the binding domain, proline residues introduced into the RNA binding domain did not disrupt binding of the genome, but did alter the secondary structure of the protein (Lee and Hacker, 2001).

The Bromovirus family has two members that have been extensively studied, Brome mosaic virus (BMV) and cowpea chlorotic mottle virus (CCMV). The biochemical studies in conjunction with the structures solved for these viruses have contributed a proposed new packaging model for BMV and elucidated the biological significance and importance of the packaged genome as a structural element. In work by Krol *et al.* (1999), it was found that the viral RNA genome initiates interactions with the coat protein and dictates the final structure formed. Altering the RNA's for encapsidation

results in polymorphic capsids with a breakdown in quasi-equivalency. However the protein component can be altered without effect as long as the relative basicity remains the same (Choi and Rao 2000a). And in recent studies with CCMV (Willits *et al.*, 2003), it has been established that the packaged genome confers stability to the mature virion.

In all of these studies, the role of single-stranded viral genomes in virus of assembly was initially hypothesized from atomic structures. Later, biochemical and genetic analyses were used to verify the initial hypotheses. In some cases, hypotheses were substantiated and in others they were not. Traditionally x-ray structures were considered to contain the final answers in questions regarding biological activity. However, extremely compelling *in vitro* and *in vivo* results have not always been confirmed by x-ray studies. This has led to a more critical view on the effects of the crystalline environment on organic complexes. Perhaps these new concerns were best expressed by J. E. Johnson; "Our experience raises a cautionary note: that critical roles assigned to particular motifs based solely on structural analysis must be experimentally tested *in vivo* and *in vitro* to ensure proper validation."

1.3 DISSERTATION FORMAT

The first chapter is an introduction to define the problems studied; describe the *Microviridae* as a model system for the study of viral morphogenesis; to review assembly of small icosahedral virions in general terms; to review the literature about genomic affects on assembly in more specific terms; and to describe the dissertation format.

A version of Chapter 2 exists as a publication in the Journal of Virology and is included as a reprint as Appendix A. The chapter 2 version is placed in sequence because it is essential to the continuity of the dissertation. A version of Chapter 3 has been submitted to the Journal of Virology. Therefore, both of these chapters are in the publication format for that journal. Min Chen, a research technician, assisted me with the DNA sequencing and plating assays reported in Chapter 3.

Chapter 4 is a work in progress. The crystallographic data presented in this dissertation and appended papers are the result of a long time collaboration between Dr. Bentley A. Fane and Dr. Michael G. Rossmann at Purdue University. All viral mutants and particles used for crystallographic studies were generated by me in the laboratory of Dr. Bentley A. Fane. Although further investigation of H incorporation is necessary, a version of Chapter 4 is in preparation in conjunction with Michael G. Rossmann's lab at Purdue for submission to the Journal of Molecular Biology.

Appendix B contains the manuscript of bacteriophage $\alpha 3$ structure. Therein, the construction of the viral and host-cell mutants and viral preparations were performed by me and shipped to Purdue for crystallization, or in the case of procapsids, cryo-image reconstruction. All further purifications and crystallographic work were performed in the Michael G Rossmann Lab. The interpretation of the structural data and its biological significance, and to some extent manuscript preparation, was the result of a joint effort of

authors in round table forum with vigorous discussion and some debate, in which I was honored to take part.

All other experimentation and interpretation of the genetic and biochemical analyses described and detailed within this dissertation and appended papers were conducted by me in the laboratory of Dr. Bentley A. Fane at the University of Arkansas (1998) and at the University of Arizona (1998-2003).

FIGURE LEGENDS

FIG. 1. *Microviridae* morphogenesis.

FIG. 2. Association of the DNA binding protein to the major capsid protein. The DNA binding protein is illustrated in psychedelic green.

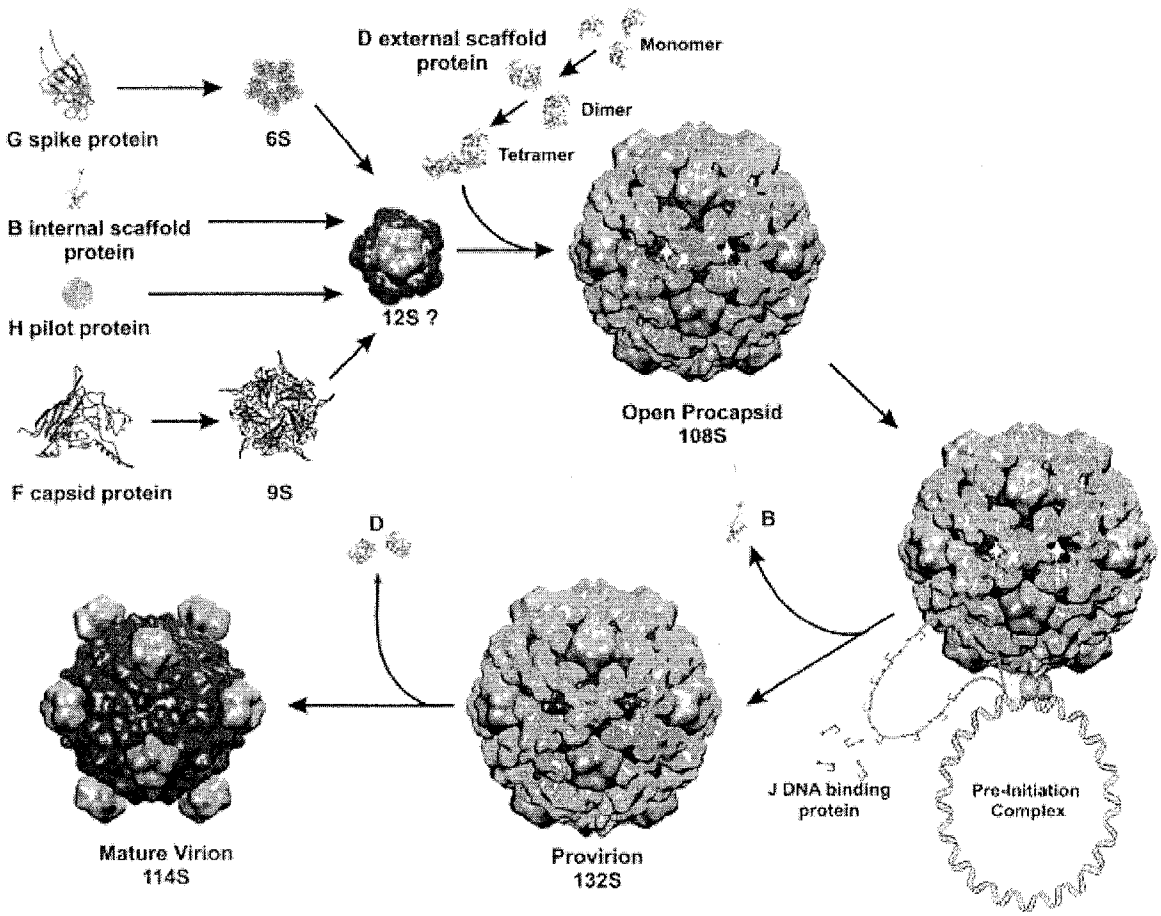
D external scaffold protein
Monomer
Dimer
Tetramer
G spike protein
6S
B internal scaffold protein
H pilot protein
12S ?
F capsid protein
9S
Open Procapsid
108S
B
D
J DNA binding protein
Pre-Initiation Complex
Provirion
132S
Mature Virion
114S

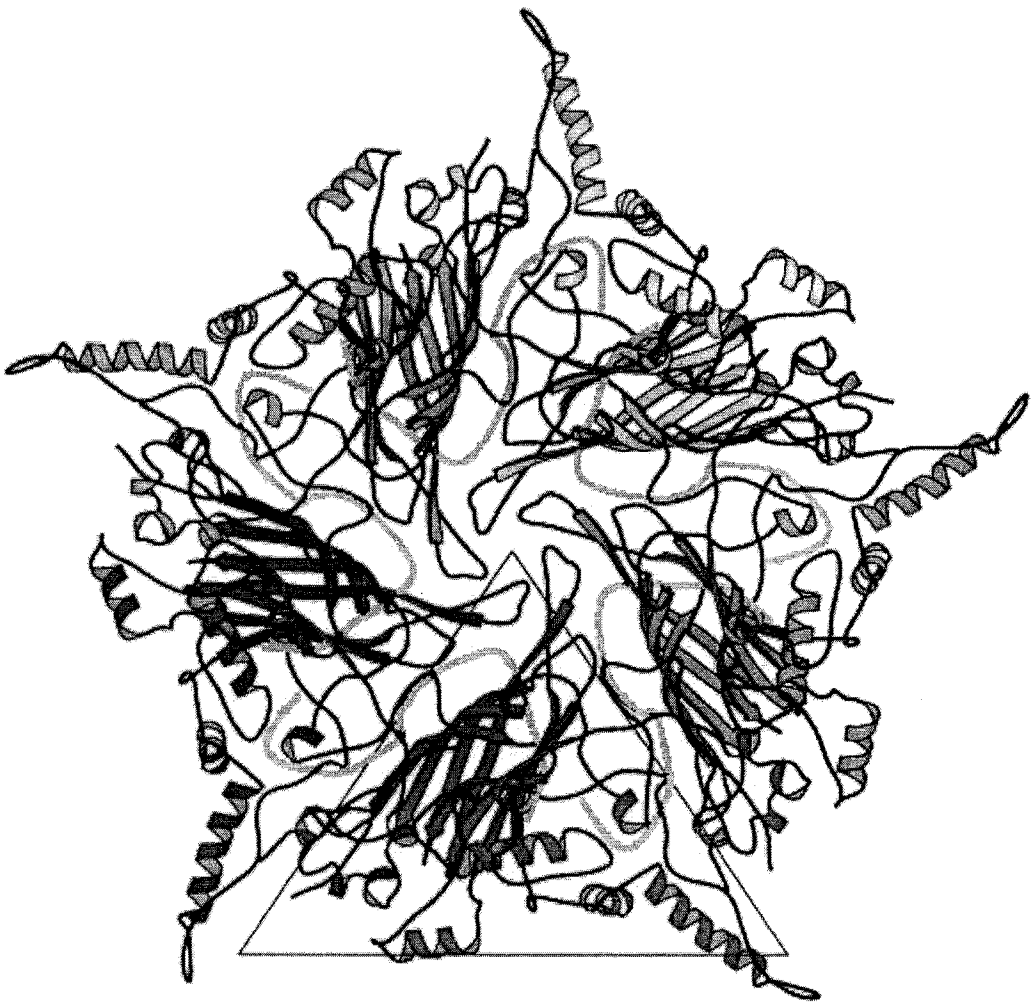

CHAPTER 2

ØX174 GENOME-CAPSID INTERACTIONS INFLUENCE THE BIOPHYSICAL PROPERTIES OF THE VIRION: EVIDENCE FOR A SCAFFOLDING-LIKE FUNCTION FOR THE GENOME DURING THE FINAL STAGES OF MORPHOGENESIS

ABSTRACT

During the final stages of øX174 morphogenesis, there is an 8.5 Å radial collapse of coat proteins around the packaged genome, which is tethered to capsid's inner surface by the DNA binding protein. Two approaches were taken to determine whether protein-DNA interactions affect the properties of the mature virion, and hence the final stages of morphogenesis. In the first approach, genome-capsid associations were altered with mutant DNA binding proteins. The resulting particles differed from wild type virion in density, native gel migration, and host cell recognition. Differences in native gel migration were especially pronounced. However, no differences in protein stoichiometries were detected. An extragenic second-site suppressor of the mutant DNA binding protein restores all assayed properties to near wild type values. In the second approach, øX174 was packaged with foreign, single-stranded, covalently closed, circular DNA molecules identical in length to the øX174 genome. The resulting particles exhibited native gel migration rates that significantly differed from wild type. The results of these experiments suggest that the structure of the genome and/or its association with the capsid's inner surface may perform a scaffolding-like function during the procapsid to virion transition.

INTRODUCTION

Unlike many double-stranded (ds) DNA viruses which use one scaffolding protein (Desai, P., *et al.*., 1994, King, J., and S. Casjens. 1974), øX174 morphogenesis is dependent on two species (Hayashi, M., *et al.*, 1988). Together, these two proteins perform the full spectrum of functions found in one-protein systems. However, after procapsid assembly, the final stages of øX174 morphogenesis differ. In ds DNA systems, procapsids expand during packaging (Jardine, P. J., and D. H. Combs, 1998, Lata, R.,*et al.*, 2000, Prasad, B. V., *et al.*, 1993) and the genome forms a dense core (Earnshaw, W. C., and S.R. Casjens. 1980). In contrast, øX174 morphogenesis concludes with the collapse of coat proteins around the single-stranded (ss) genome, which is associated with the inner surface of the capsid (Dokland, T., *et al.*, 1997, Dokland, T., *et al.* 1999, McKenna, R., *et al.*, 1992, McKenna, R., *et al.*, 1994).

As illustrated in Figure 2.1, øX174 genome replication is coupled to DNA packaging. The pre-initiation complex, consisting of the host cell *rep* and viral A and C proteins, associates with the procapsid forming the 50S complex (Ekechukwu, M. C., *et al.*, 1995, Mukai, R., *et al.*, 1979). The viral A protein binds the origin of replication in replicative form DNA. This is both necessary and sufficient for packaging specificity (Aoyama, A., and M. Hayashi. 1985, Fluit, A. C., *et al.*, 1985). Upon binding, protein A nicks the origin (Van Mansfeld, A. D., *et al.*, 1984) and forms a covalent ester bond with the DNA

(Eisenberg, S., and A. Kornberg. 1979.). After one round of rolling circle synthesis, protein A cuts and ligates the newly generated origin, generating a circular ss molecule (Brown, D. R., *et al.*, 1984, Eisenberg, S., *et al.*, 1977). This packaging mechanism produces precise genomes of identical length (Aoyama, A., and M. Hayashi. 1985).

The highly basic DNA binding protein (J) enters the procapsid along with the ssDNA genome, (Fujisawa, H. and M. Hayashi. 1976), associating with the genome via charge-charge interactions (Jennings, B. and B. A. Fane. 1997). Once in the procapsid, the C-terminus binds to a coat protein cleft (McKenna, R., *et al.*, 1992, McKenna, R., *et al.*, 1994). This may facilitate further interactions with a small cluster of adjacent basic capsid amino acids. Accordingly, a portion of the packaged DNA (8-10%) is icosahedrally ordered, tethered to the inner surface (McKenna, R., *et al..*, 1992, McKenna, R., *et al.*, 1994). This tether constrains the spatial orientation and secondary structure of the remaining nucleotides (Benevides, J. M., *et al.*, 1991). Morphogenesis completes with the dissociation of the external scaffolding protein and an 8.5 Å radial collapse of capsid pentamers. Whether the tethered genome influences the integrity and/or magnitude of this collapse is addressed in this report.

The interaction of icosahedral capsid proteins with single-stranded genomes is a well-documented phenomenon. Many viral RNA capsid proteins have internally localized basic N-termini extensions that nonspecifically bind genomes (Chen, Z.G., *et al.*, 1989, Choi, Y. G. and A. L. N. Rao, 2000b, Larson, S. B., *et al.*, 1998, Rossmann, M. G. and J.

E. Johnson. 1989, Vriend, G., *et al.*, 1986, Wikoff, W. R., *et al.*, 1997). The phenomenon has been documented in single-stranded animal viruses as well (Agbandje-McKenna, M., *et al.*, 1998, Chapman, M. S. and M. G. Rossmann. 1995, Fisher, A. J., and J. E. Johnson. 1993, Tang, L., *et al.*, 2001). To investigate the functions of the øX174 genome tether, both the protein and nucleic acid components were altered. The protein component was altered by mutations in the DNA binding protein. The DNA component was altered by packaging foreign, unit-length, single-stranded, circular DNA molecules. In both instances, the altered particles were infectious but exhibited different biophysical properties.

MATERIALS AND METHODS

Phage plating, stock preparation, media, DNA purification, bacterial strains, and plasmids. Plating protocols, media, and stock preparation have been previously described (Fane, B. A. and M. Hayashi. 1991). *E. coli* C strains: C122 (sup^0) is the wild type host; BAF 5 contains a *supE* mutation (Fane, B. A. and M. Hayashi. 1991). BAF 30 is a *rec* A- derivative of C122 (Fane, B. A., Head, S., and M. Hayashi. 1992). Plasmids pøXB and pøXDJ contain IPTG inducible clones of the denoted øX174 genes (Burch, A. D., *et al.*, 1999, Burch, A. D. and B. A. Fane. 2000). The *sly* D host mutation confers resistance to øX174 E-protein mediated lysis (Roof, W. D., *et al.*, 1994). The *gro89* host mutation blocks DNA packaging (Ekechukwu, M. C., *et al.*, 1995).

Phage mutants. The øX174 J mutants, *J3K->LI*, *JK->ALL*, and *J3K->LII/su(J)-FS1F* have been previously described (Jennings, B. and B. A. Fane. 1997). The *su(J)-FS1F* mutation was placed into the *J3K->LI* background by oligonucleotide mediated mutagenesis (Fane, B. A., Shien, S., and M. Hayashi. 1993). Progeny that had acquired the *su(J)-FS1F* mutation were identified by selecting against the temperature sensitive phenotype of the *J3K->LI* parent. Two rounds of oligonucleotide mutagenesis were performed to place the *su(J)-FS1F* mutation in the wild type background. Genotypes of all strains were verified by direct DNA sequence analysis.

Buoyant density gradients. For small-scale experiments in which two or three different particles were analyzed within the same gradient, 10^5-10^6 particles were mixed into a 1.4 g/cm^3 CsCl solution and spun for 47.5 hr at 23,000 rpm in an SW51 rotor (Beckmann). Gradients were divided into 80-85 fractions. The location of infectious particles was determined by a plaque assay. For large-scale preparations of *JK->ALL* 70S particles, 100 ml of *slyD* cells (2.0 X 10^8 cells/ml) were infected (MOI=5) at 33°C and incubated for two hours. To generate wild type procapsids, *gro89* cells were infected with lysis deficient øX174 *am(E)W4*. Infected cells were harvested, resuspended in 10 ml BE buffer, and lysed with T4 lysozyme. Cellular debris was eliminated by centrifugation. The supernatant was layered atop CsCl step gradients and spun as previously described (Fane, B. A. and M. Hayashi. 1991). Exogenous virions (1.0 X 10^6) were added to gradients as a density marker. Procapsid and 70S particle bands were clearly visible after centrifugation. Fractions were titered to determine the location of the wild type marker phage.

Native agarose gel electrophoresis. To examine particles by native gel electrophoresis, 10 µl samples, containing 1.0 X10^8 pfu, were mixed with 6 X gel loading buffer (0.25% bromophenol blue, 0.25% xylene cyanol FF, 30% glycerol). Samples were bi-directionally electrophoresed through 0.8% (w/v) agarose TBE gels (TBE: 45 mM tris-borate; 1.0 mM EDTA) for 10 hours at 24 volts/cm^2. After electrophoresis, lanes were cut into 2.0-mm horizontal sections with a modified egg-slicer. Particles were eluted from

the gel by vortexing in 0.1 ml HFB buffer. The location of infectious particles was determined by a plaque assay.

Attachment assays. *E. coli* C122 cells were grown to a concentration of 1.0 X 10^8 cells/ml and concentrated 5-fold in growth media (1.0 % tryptone, 0.5% KCL). $MgCl_2$ and $CaCl_2$ were added to a concentration of 10 mM and 5.0 mM, respectively. Approximately 1.0 X10^8 phage were added to 1.0 ml of cells and incubated at 37^0 C for specified time intervals (see figures). At sampling times, attached phage were removed by centrifugation. Supernatants were titered to determine the level of unattached virions.

Construction of *amp*^{R} packaging plasmids and transducing particles. øX174 DNA containing the øX174 origin of replication was amplified. The 5' PCR primer was designed to introduce an *Nco* I site into the fragment that was then initially cloned into TOPO 2.1 vector (Invitrogen). The TOPO vector was digested with *Nco* I and *EcoR* I (adjacent to cloning site), and the fragment was placed into PSE420 (Invitrogen) digested with the same enzymes (PORI). To bring the size of PORI up to 5386 base pairs, additional material was cloned behind the øX174 origin. These DNA sequences were obtained by amplifying pSE420 DNA between bases 3302 and 3776. This PCR fragment was first placed into a TOP0 2.1 and the orientation of the insert was determined. Depending on orientation, plasmids were cut with *Bam* HI and *Xba* I, or *Not* I and *Sac* I; then cloned into PORI that had been prepared with *Bam* HI and *Nhe* I, or *Not* I and *Sac* I. Plasmids were transformed into BAF 30 *recA* cells. Transducing particles were produced

by infecting cells harboring the packaging plasmids with wild type øX174. The presence of the origin of replication in the plasmid is both necessary and sufficient for packaging a single-stranded version of the vector (Aoyama, A., and M. Hayashi. 1985, Fluit, A. C., *et al.*, 1985). Lysates contain both virion and transducing particles. The titer of transducing particles was determined by infecting 1.0 X 10^8 *slyD* cells at an MOI of 0.1 and subsequent plating on ampicillin (100 μg/ml) plates. The low MOI and *slyD* cells were used to prevent co-infections and a second round of infection by progeny virions, respectively. The ratio of progeny virions to amp^R transducing particles was approximately 50:1 in both infections. This represents typical values for these types of experiments (Ekechukwu, M. C., *et al.*, 1995).

RESULTS

Complete genome encapsidation is not required for the completion of genome biosynthesis. *Microviridae* genome biosynthesis and DNA packaging are concurrent processes (Fujisawa, H. and M. Hayashi. 1976). Previous work with the øX174 *J* mutants used in these studies demonstrated that mature packaged particle formation was a function of the number of charged residues of the protein (Jennings, B. and B. A. Fane. 1997). For example mutant J proteins with only nine basic amino acid residues (wild-type contains 12) could produce packaged particles with wild-type S values, 114S. However, several other biophysical properties differ (see below). Mutant proteins with only six basic residues produce particles that sediment at 70S (Jennings, B. and B. A. Fane. 1997). Analyzing the nature of the DNA associated with the 70S particles (partial v complete genomes), its susceptibility to DNAse, and the density of the 70S particles would determine if genome biosynthesis terminates with a cessation in packaging, or whether these two processes can be partly uncoupled *in vivo*.

The mutant genotypes and phenotypes used in these studies are summarized in Table 1. DNA associate with *J K->L ALL* 70S particles was extracted and analyzed by electrophoresis (data not shown). It was identical to virion DNA, indicating that single-stranded DNA biosynthesis went to completion. The density of the particles was determined to 1.36 gm/cm^3 (Table 2) by buoyant density centrifugation, midway between the densities of the 114S virion (1.39 gm/cm^3) and the 108S procapsid (1.31 gm/cm^3)

used as standards. These data indicate that the mutant J protein had no effect on genome biosynthesis, but the genome was not fully packaged. To test this hypothesis, particle densities were re-determined after DNAse treatment (Aoyama, A., Hamatake, R. K., and M. Hayashi. 1981). While the densities of the virion and empty procapsid were not affected, the density of the 70S particle was reduced (Table 2).

Further characterization of infectious particles packaged with mutant DNA binding proteins. Unlike mutant J proteins with less than six basic residues, proteins with nine basic residues, *J3K->LI,* produce infectious particles with wild-type S values. However, the mutant has a small plaque phenotype and is both temperature and cold sensitive. Particles packaged with the *J3K->LI* and wild-type *J protein* were characterized by buoyant density centrifugation. The results of these analyses along with stoichiometric studies (see below) could determine whether the genomic DNA is fully encapsidated, more mutant J protein is needed for packaging, or other possibilities. For these experiments particles packaged with wild type J protein contained an amber mutation in gene B. Since particles could be independently titered (see figure legend), it was possible to characterize both types of virion within the same gradient. As seen in Figure 2.2, panel A, particles packaged with the mutant J protein are denser than wild type.

Several hypotheses could explain the observed density difference. In order to compensate for the mutant protein's reduced charge; more J protein may be needed for packaging. If the volume of the mutant particle remains unaltered, additional J protein

would replace water, yielding a greater density. Although J protein stoichiometry is dictated by the capsid's icosahedral symmetry in wild type particles, protein stoichiometry was still assessed via PAGE and the relative amounts of coat (F), spike (G), and J proteins were determined. In a wild type virion each of these proteins is present in 60 copies. As summarized in Table 3, no significant differences in protein ratios were apparent. The variations seen in the F:J ratio is the same as that observed in the F:G ratio. It is possible that mutant particles may have retained a small amount of internal scaffolding protein that may have been below the limits of detection.

The greater density could have been caused by an increase of Cs^+ ions within the mutant capsid. In this model, the positively charged counter ion would supplant the missing basic amino acids in the mutant protein. To address this hypothesis, the density of *J3K->LI* and *su(J)SIF/J3K->LI* particles were compared. The *su(J)SIF* mutation is a nonallele-specific, extragenic, second-site suppressor of charge-altered J proteins, which has been previously characterized and described (Jennings, B. and B. A. Fane. 1997). The *su(J)SIF* suppresses both the small plaque and the temperature-sensitive phenotypes, raising plating efficiencies from 10^{-3} to 0.5 at the restrictive temperatures. An order of magnitude more *J3K->LI* particles was loaded on the same gradient with the double mutant. The position of the *su(F)SIF/J3K->LI* could be ascertained and distinguished from *J3K->LI* particles by titering at 42°C. As seen in Figure 2.2, panel B, they were readily separated by their densities, demonstrating that the suppressor is affecting the density of the capsid, restoring it to a more wild type value. Since both particles are

packaged with the same mutant J protein, the observed density differences are probably not caused by Cs^+ ions or an excess of J protein in the *J 3K->LI* particles.

The extragenic suppressor is a ser -> pro substitution located at amino acid 1 of the coat protein (Jennings, B. and B. A. Fane. 1997). In wild type virion, this serine participates, via the γ O, in a three-way polar interaction (coat-coat-coat) directly atop the threefold axis of symmetry (McKenna, R., *et al.* 1992, 1994). The suppressing substitution most likely alters this interaction. Buoyant density gradients were performed to determine the effect, if any, of this substitution alone in a wild type background (Figure 2.3). Wild type, *su(J)-F S1F/wild type J* , and *J 3K->LI* particles were analyzed in the same gradient. The *su(J)-F S1F/wild type J* is slightly more dense than wild type.

Mutant and wild type particles migrate differently in native gels. The altered densities could be caused by general distortions affecting the entire capsid. If this were the case, alterations in genome-capsid interactions might be expressed on the capsid's external surface. The migration of wild type and mutant virions were analyzed side by side in bi-directional, native agarose gels, which assay for differences in size and net surface charge (Serwer P. and M. E. Pichler. 1978). After electrophoresis, each lane was cut into 2-mm sections with a modified egg-slicer, and particles were eluted and titered. For both wild type and mutant particles, a major population peak was detected migrating toward the positively charged anode, referred to as the negative or major population (Figure 2.4). However, migration rates differed. With longer run times, the negatively

charged particle peaks can be more clearly separated (data not shown). Mutant virions were not more sensitive to DNAse treatment than wild-type virions. Therefore, protruding DNA is probably not responsible for the faster migration rate. There were also positively charged populations in each sample. While these positively charged particles represent a minor portion of the total wild type population (1:1000 ratio), they are quite prominent in the mutant sample (1:3 ratio). As seen in Figure 2.5, the extragenic second-site suppressor restores mutant population ratios toward wild type levels.

Attachment assays as a probe for external capsid alterations: To further explore possible alterations on the outer surface, attachment assays were performed. For these assays, particles were incubated with exponentially growing cells at 37^0C as described in Materials and Methods. At five and ten minutes post infection, aliquots were removed and separated into pellet and supernatant fractions. The level of unattached virion was determined by titering the supernatant. The attachment of wild type particles is three orders of magnitude greater than that of mutant particles (Figure 2.6). The extragenic suppressor appears to correct for defects in host cell recognition, restoring attachment to intermediary efficiency. The level of unattached phage do not reflect the population ratios observed in the native gel migration experiments. Similar experiments were conducted with separated negatively and positively charged mutant and wild type particles (data not shown). The results of those experiments did not differ significantly from the data presented in Figure 2.6, which assayed whole populations. In each instance, wild-type particles exhibited greater attachment efficiencies than mutant particles. While the

positively charged particles of both the mutant and wild-type strains attached more efficiently than their negatively charged counterparts, it is not known whether this is a consequence of nonspecific binding to the negatively charged LPS. These simple assays do not determine whether the mutant particles are defective in DNA ejection, nor can be used to interpret the small plaque phenotypes of the mutants, which may be a consequence of both extracellular and intracellular factors.

Packaging foreign DNA also alters the biophysical properties of capsids. The DNA binding protein connects the genome to the inner surface of the capsid at each asymmetric unit. These 60 interactions allow the remainder of the single-stranded DNA genome to form limited secondary structure by base pairing upon itself within the virion. Hence, the base-pairing properties of the genome may influence the properties of the mature virion. To investigate this, øX174 was packaged with foreign DNA. Two packaging plasmids identical in length to the øX174 genome were constructed. These plasmids contain the øX174 origin of replication, which is both necessary and sufficient for packaging a single-stranded version of the plasmid (Aoyama, A., and M. Hayashi. 1985, Fluit, A. C., *et al.*, 1985), and a gene encoding ampicillin resistance. The two plasmids differed in one segment. This segment is repeated, in either a parallel-parallel or a parallel-antiparallel manner. The parallel-antiparallel configuration may introduce a large hair-pin loop. Particles were packaged *in vivo* by infecting cells harboring the plasmids with wild type øX174. Particles were analyzed by native gel electrophoresis and the gels were processed as described above. Each fraction was titered for phage and

amp^R transducing particles (Figure 2.7). Two population peaks, positively and negatively charged, were detected for both sets of transducing particles (Figure2.7). However, population ratios differ between the two constructs. In addition, the negatively charged populations migrate considerably faster than the internal øX174 control. Therefore to avoid running the transducing particles off the gel, run times were shorter than in the experiments described above. These data suggest that the nucleotide arrangement of the genome can change the biophysical properties of the capsid, perhaps by promoting or inhibiting genome secondary structure.

Discussion

Interactions between the capsid inner surface and the packaged genome. Single-stranded øX174 DNA does not exist as a dense core in the capsid, as is observed in dsDNA bacteriophages (Earnshaw, W. C., and S.R. Casjens. 1980). Instead, it is tethered to the capsid's inner surface by the highly basic DNA binding protein (J) and a group of basic capsid amino acid residues (McKenna, R., *et al.*, 1992, 1994). There are 60 copies of protein J per virion, one associated with each coat protein. In the atomic model, the protein forms an S shaped polypeptide chain devoid of secondary structure. The C-terminus of the protein is tightly associated with a cleft, located near the center of the coat protein. Moving toward the N-terminus, the protein traces a path toward the 5-fold axis of symmetry, crosses over to the adjacent capsid protein, and veers toward the C-terminus of the adjacent J protein. This motif suggests that the DNA binding protein guides the incoming genome into a somewhat ordered conformation. Accordingly, between 8-10% of the genome is ordered in the X-ray structure (McKenna, R., *et al.*, 1992, 1994). Here and in other systems where higher percentages of the genome are ordered; such as Flock house virus (Fisher, A. J., and J. E. Johnson. 1993); Pariacoto virus (Tang, L., *et al.*, 2001), and Satellite tobacco mosaic virus (Larson, S. B., *et al.*, 1998); the genome is icosahedrally ordered via interactions with structural proteins. This phenomenon is thought to contribute to capsid assembly and stability.

Altering the protein components of the tether. To investigate whether genome-capsid interactions affect the final stages of virion morphogenesis and/or the structure of the mature virion, particles packaged with mutant DNA binding proteins were characterized. The mutant particles were significantly more dense than wild type, but the protein composition of the two particles is probably identical. Therefore, the altered density was probably not caused by a gross excess of protein contained in a volumetrically fixed capsid. The effects of possible Cs^+ permeability were more difficult to discern. However, extragenic second-site suppressor procapsids packaged with the mutant DNA binding protein restored particle densities to near wild type values. Therefore a simple model, in which counter ions compensate for the loss of basic amino acids, is not supported by the data. This leaves the intriguing possibility that the dimensions or shape of the mutant particles may be altered.

When suppressor capsids are packaged with wild type J protein, the density values are slightly greater than wild type virion. Since the mutant particles are still more dense than wild type; the suppressor does not act via a compensatory mechanism. This suggests that there is an alternative maturation pathway that minimizes the effect of the genomic tether on the magnitude of capsid collapse.

To investigate whether differences were expressed on the capsid exterior, host cell attachment assays were performed. The particles packaged with the mutant DNA binding protein exhibited dramatically lower attachment efficiencies. As seen in the

density experiments, the presence of the extragenic second-site suppressor restored values toward wild type. Differences in native gel migration, which is a function of size and net surface charge (Serwer P. and M. E. Pichler. 1978), were also observed. While small migration differences were seen between the wild type and mutant particles migrating toward the anode, the most dramatic differences involved the presence of a minor population migrating in the opposite direction. In wild type populations these particles represent a small sub-population (1:1000). However, the ratio was approximately 1:3 in mutant samples. As seen in the other assays, the extragenic suppressor restored the ratio to nearly wild type values.

Altering the nucleic acid component of the tether. Naked øX174 DNA is substantially richer in secondary structure than packaged DNA (Benevides, J. M., *et al.*, 1991). Benevides *et al.*., (1991) hypothesized that the DNA binding protein inhibited the formation of secondary structure. Therefore, it is likely that an interplay between base-pairing and DNA-capsid association occurs. To investigate this hypothesis, two species of øX174 ampicillin transducing particles were generated by packaging single-stranded versions of unit length plasmids. The plasmids differed in the orientation of one cloned section, which was designed to introduce a large hairpin loop. Differences in migration rates and sub-population ratios were observed between the transducing particles and wild type virions.

While this may be one of the first reports of genome-capsid interactions affecting ssDNA viral structure and morphogenesis, the phenomenon has been well documented in ssRNA viruses. Flock house virus (FHV) RNA stabilizes contact regions (Fisher, A. J., and J. E. Johnson. 1993) via nonspecific interactions with coat protein grooves at two-fold axes of symmetry. Deletions of the RNA-interacting residues results in the production of polymorphic structures (Dong, X.F., *et al.*, 1998). Packaging FHV with foreign RNA also leads to altered particles (Bothner, B., *et al.*, 1999). Thus, genome-capsid interactions can effect the fidelity of virion morphogenesis, a function commonly associated with viral scaffolding proteins. A dramatic example of a scaffolding-like function for nucleic acids has been observed in Southern cowpea mosiac virus (SCMV). Deleting the highly basic, RNA-interacting N-terminus of the coat protein results in the production of T=1, as opposed to T=3, capsids (Savithri, H. S. and J. W. Erickson. 1983). Similarly, the nature of the RNA packaged in Brome mosaic virus can determine whether T=3 or 120-subunit capsids are formed (Krol, M. A., *et al.*, 1999).

The role of DNA-capsid interactions in øX174 is obviously not as dramatic. Procapsid morphogenesis does not require the genome (Burch, A. D., *et al.*, 1999, Hamatake, R. K., Aoyama, A. and M. Hayashi. 1985); however, two scaffolding proteins mediate this stage of assembly. In the procapsid there are no discernable pentamer-pentamer interactions. The integrity of the capsid appears to be maintained by the scaffolding proteins. After packaging, the internal scaffolding protein is extruded from the structure and replaced by the DNA binding protein and the tethered genome. This may supplant

scaffolding function in the provirion. The provirion to virion transition is marked by the release of the external scaffolding protein and the completion of the 8.5 Å radial collapse of coat protein pentamers (Dokland, T., *et al.*, 1997, 1999, McKenna, R., *et al.*, 1992, 1994). Genome-capsid interactions may be mediating the magnitude and preserving integrity during the collapse.

Acknowledgements

The authors thank Mr. Bryan L. Jennings for technical assistance. This work was supported by a grant from National Science Foundation grant (B. A. F.).

TABLE 2.1: Genotypes and phenotypes of øX174 *J* mutants in these studies.

Mutant	Genotype	Phenotype
J⁻3K->LI	K->L at residues 2, 4, 5	small plaques, *ts*, *cs*[1]
Su(J)-FS1F/ J⁻3K->LI	K->L at residues 2, 4, 5 Extragenic suppressor (S->F) in residue #1 of capsid protein.	wild type
J⁻K->L ALL	K->L at residues 2, 4, 5, 21, 23, 25	recessive lethal

[1] *ts* and *cs* denote temperature-sensitive and cold sensitive phenotypes, respectively.

TABLE 2.2: Densities of particles generated in *J*⁻ mutant infected cells.

Particle	S value	Particle Density (g/cm^3) No DNAse	DNAse
Wild type virion	114S	1.39	1.39
Procapsid	108S	1.31	1.31
J⁻K->L ALL	70S	1.36	1.32

TABLE 2.3: Protein composition of wild type and *J3K->LI* particles[1].

Proteins[2]	Wild type	*J3K->LI*	variation from wt.
F/G	1.64	1.39	0.15
F/J	3.02	2.72	0.10

[1] Proteins were separated by SDS-PAGE, stained and digitally photographed. Ratios were calculated using band intensities derived via 1D image analysis software (Kodak Digital Science™).

[2] F, G and J, denote the major capsid, spike and DNA binding proteins respectively.

FIGURE LEGENDS

FIG. 2.1. øX174 morphogenesis.

FIG. 2.2. (A) Buoyant densities of wild type and *J3K->L I* particles. Both particles were analyzed in the same gradient. An additional genetic marker, *amB*, was placed in the wild type background. This allowed the particles to be specifically titered on BAF30 pøXB at 42°. The *J3K->L I* mutant is temperature sensitive. The titer of *J3K->L I* was determined on C122 *(sup°)* at 33°C. (B) Buoyant densities of particles packaged with mutant J proteins with and without the *su(J)-FSIF* extragenic second site suppressor. An order of magnitude more of the *J3K->LI* particles, which have a *ts* phenotype, was loaded on the same gradient with the double mutant. The position of the *su(F)SIF/J3K->LI* particles could be ascertained and distinguished from *J3K->LI* by titering at 42°C. Particle titers were normalized to the same order of magnitude for the graph. Symbols: closed circles, wild type; open circles, *J3K->L I* ; squares *su(J)-F SIF/J3K->LI.*

FIG. 2.3. Buoyant densities of wild type, *su(J)-F S1F/wild type J*, and *J3K->L I* particles. All three types of particles were analyzed within the same gradient. An additional genetic marker, *amB*, was placed in the wild type background. This allowed the particles to be specifically titered on BAF30 pøXB at 42°C where The *J3K->L I* mutant is temperature sensitive. An order of magnitude more of the *J3K->LI* and wild type (*amB*) particles were loaded on the gradient than the *su(J)-F S1F/wild type J* particles. The position of the *su(F)SIF/wild type J* particles could be distinguished from the other particles by titering at 42°C on a *sup°* host. Particle titers were normalized to the

same order of magnitude for the graph. Symbols: closed circles, wild type; open circles, closed squares, *J3K->L I* ; open circles, *su(J)-F SIF* packaged with wild type J protein.

FIG. 2.4. (A) Native gel migration of wild type and *J3K->L I* particles. (B) Enlargement of the wild type minor population of positively charged particles. Negative gel section numbers indicate movement toward the (-) electrode, positive gel section numbers indicate movement toward the (+) electrode. Symbols: closed circles, wild type; open circles, *J3K->LI.*

FIG.2.5. Native gel migration of wild type and *su(J)-FSIF/J3K->LI* particles. Negative gel section numbers indicate movement toward the (-) electrode, positive gel section numbers indicate movement toward the (+) electrode. Symbols, closed circles, wild type; open circles, *su(J)-FSIF/J3K->LI* .

FIG. 2.6. Attachment assays. Symbols: closed circles, wild type; closed squares, *J3K->LI*; open circles, *su(J)-FS1F/ J3K->LI* .

FIG 2.7. Native gel migration of wild type øX174 and amp^R transducing particles. The titer of wild type phage has been normalized to the same order of magnitude as the transducing particles. Negative gel section numbers indicate movement toward the (-) electrode, positive gel section numbers indicate movement toward the (+) electrode. Symbols: closed squares, wild type phage, open and closed circles, transducing particles.

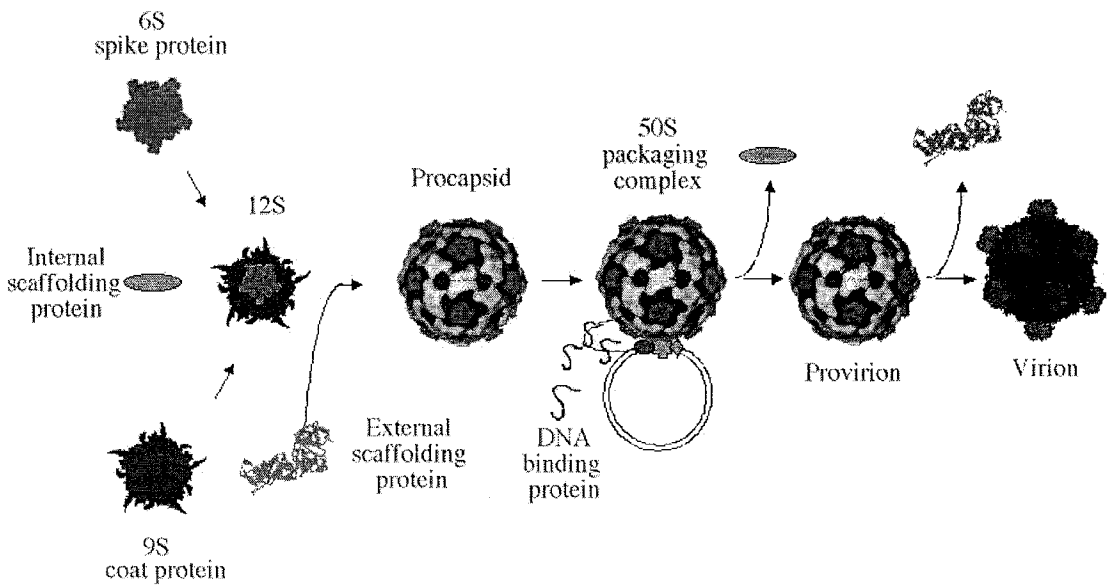
6S
spike protein
12S
Internal
scaffolding
protein
9S
coat protein
External
scaffolding
protein
Procapsid
50S
packaging
complex
DNA
binding
protein
Provirion
Virion

FIG 2.1

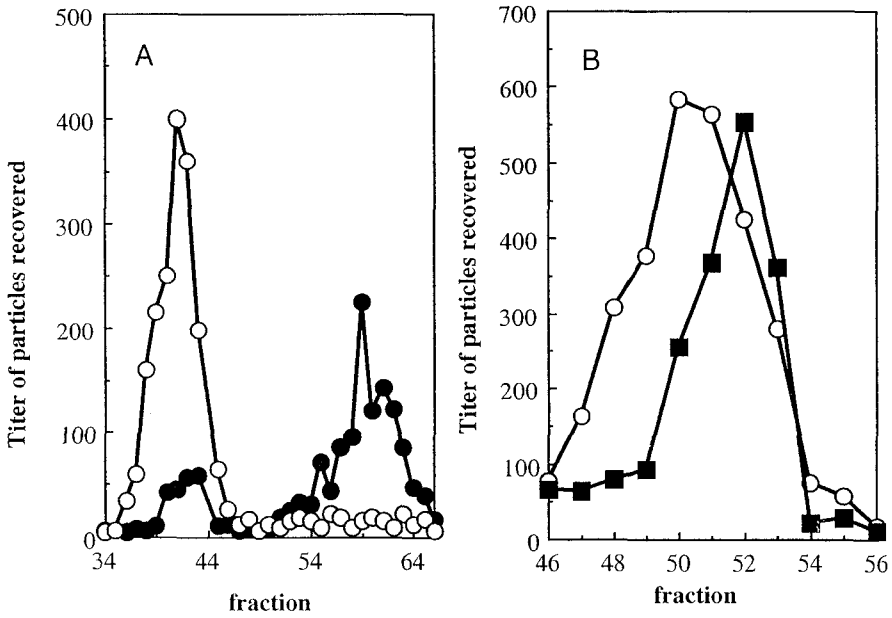
A
B
Titer of particles recovered
fraction
500
400
300
200
100
0
34
44
54
64
700
600
500
400
300
200
100
0
46
48
50
52
54
56

FIG 2.2

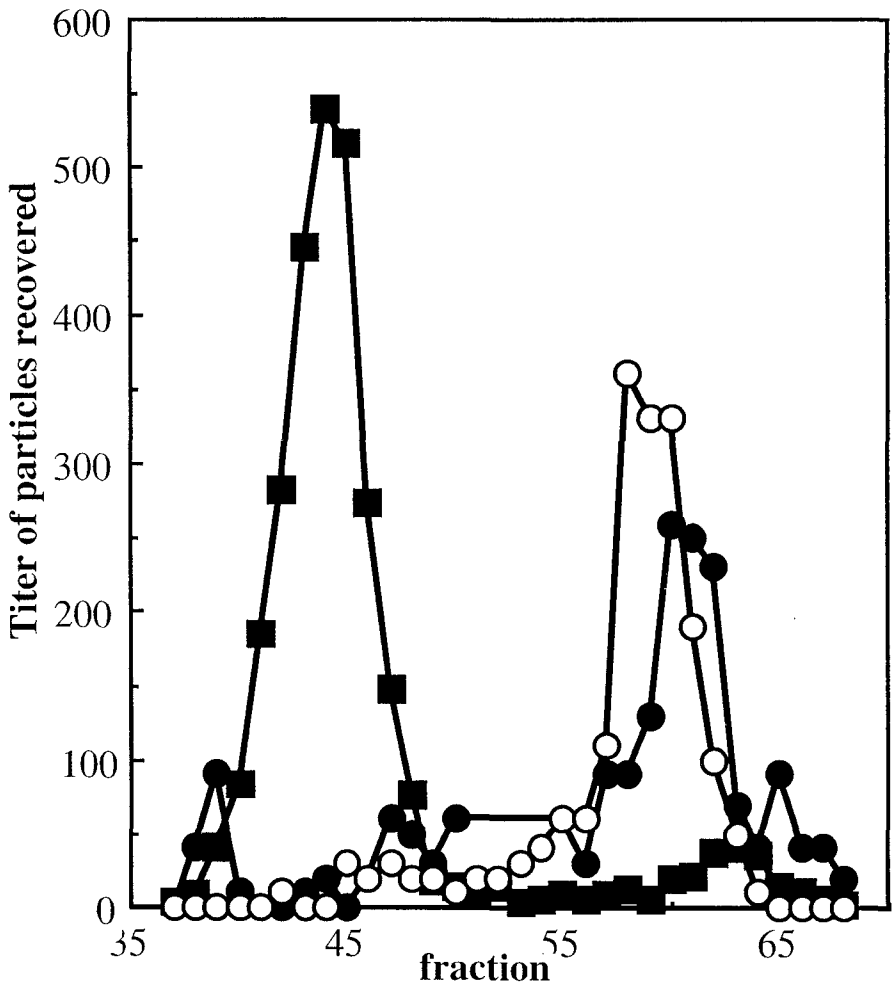
600
500
400
300
200
100
0
Titer of particles recovered
35
45
55
65
fraction

FIG. 2.3

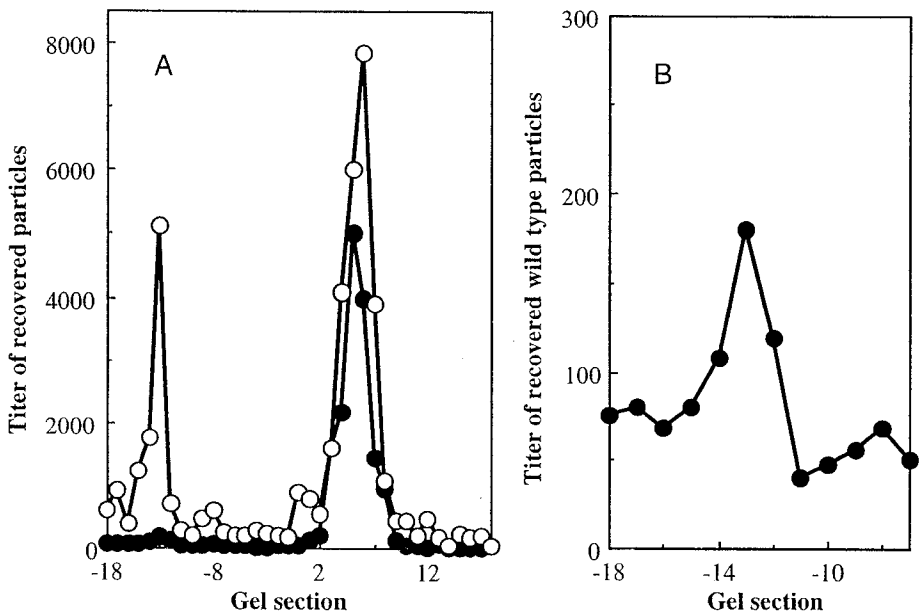
A
8000
6000
4000
2000
0
Titer of recovered particles
-18
-8
2
12
Gel section
B
300
200
100
0
Titer of recovered wild type particles
-18
-14
-10
Gel section

FIG 2.4

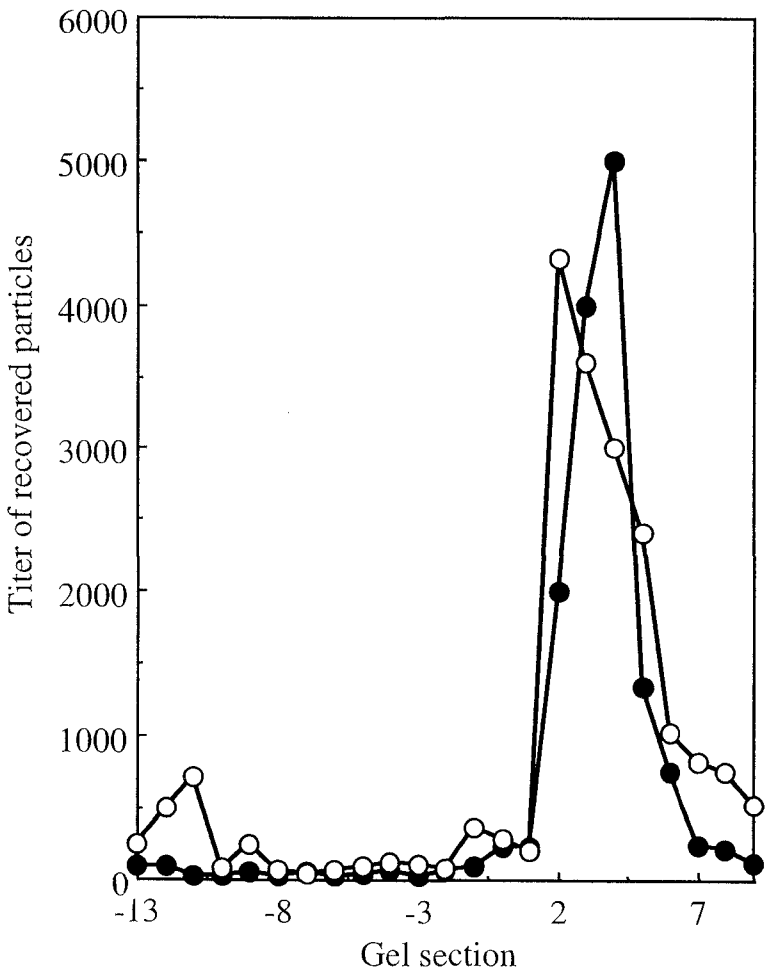
6000
5000
4000
3000
2000
1000
0
Titer of recovered particles
-13
-8
-3
2
7
Gel section

FIG 2.5

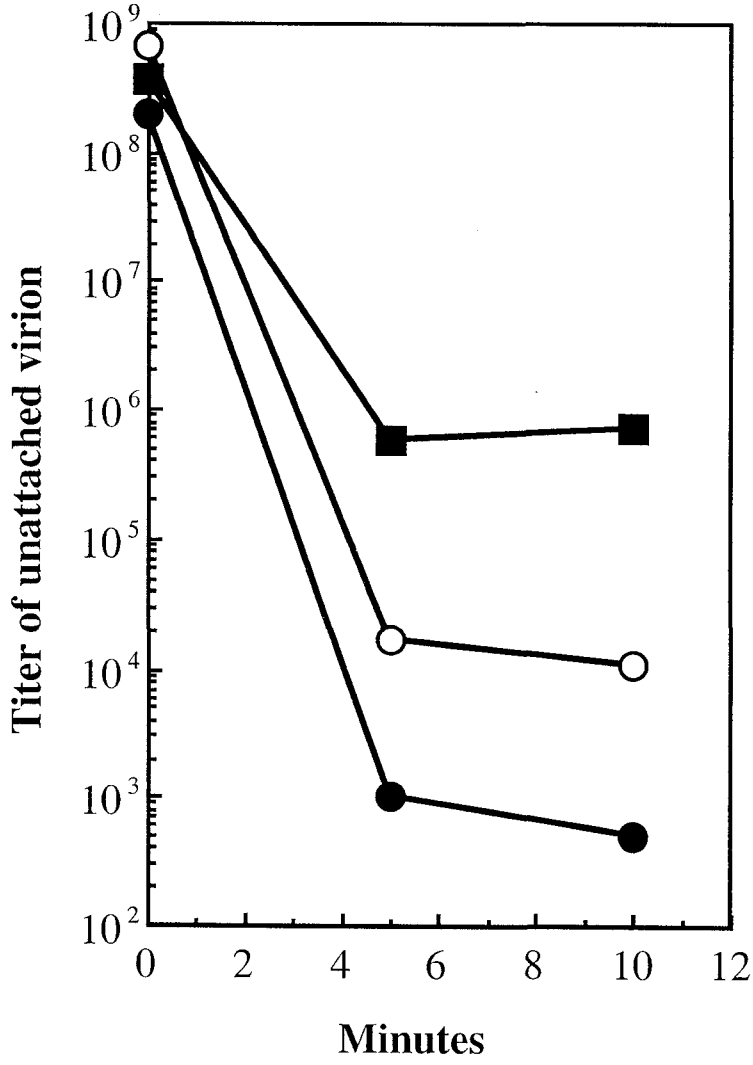
Titer of unattached virion
10^9
10^8
10^7
10^6
10^5
10^4
10^3
10^2
0
2
4
6
8
10
12
Minutes

FIG 2.6

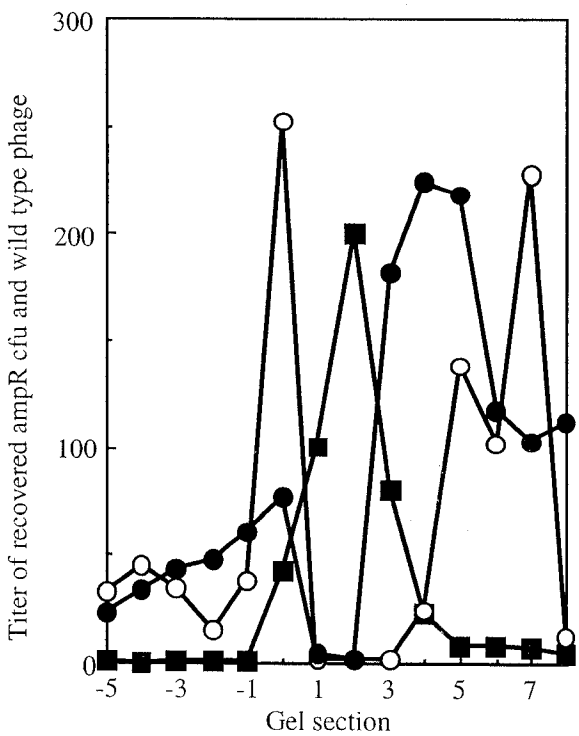
300
200
100
0
Titer of recovered ampR cfu and wild type phage
-5
-3
-1
1
3
5
7
Gel section

FIG. 2.7

CHAPTER 3

GENETIC AND FUNCTIONAL ANALYSES OF THE ØX174 DNA BINDING PROTEIN: THE EFFECTS OF SUBSTITUTIONS FOR AMINO ACID RESIDUES THAT SPATIALLY ORGANIZE THE TWO DNA BINDING DOMAINS.

ABSTRACT

The øX174 DNA binding protein contains two DNA binding domains separated by a proline rich spacer region. The results of previous analyses indicate that the proline residues in this region are critical for function (Jennings, B. and B. A. Fane, 1997). Each DNA binding domain contains a series of basic amino acid residues that bind DNA via simple charge-charge interactions (Jennings, B. and B. A. Fane, 1997). Within each domain is a spatially conserved glycine residue. These glycine and proline residues were mutated and the effects on virion structure were examined. Substitutions for glycine residues yield particles with similar characteristics to mutant particles produced by virions with substitutions for DNA binding residues (Hafenstein, S. and B. A. Fane, 2002). In addition both sets of mutants share a common extragenic second-site suppressor. These results suggest that the defects caused by the mutant proteins are mechanistically similar and that the glycine residues may optimize DNA-protein contacts

mediated by the basic amino acids in the DNA binding domains. However, the defects conferred by substitutions for proline residues appear to be fundamentally different. These observations along with the atomic structure of the øX174 virion (McKenna, R., *et al.*, 1992, 1994), suggest that the proline residues may act to guide both the DNA binding proteins and the associated DNA to the adjacent five-fold related asymmetric unit, thus preventing a chaotic packaging arrangement.

INTRODUCTION

Unlike large icosahedral double stranded (dsDNA) viruses, in which the packaged genome exists as a dense core within the virion (Earnshaw, W.C., and S.R. Casjens. 1980), single-stranded (ss) DNA and ssRNA genomes are often intimately associated with the inner surface of the capsid protein (Agbandje-McKenna, M., *et al.* 1998, Fisher, A. J., and J. E. Johnson. 1993, McKenna, R., *et al.*, 1992, 1994). Altering this association, either by mutating structural proteins or by packaging non-viral nucleic acid, can lead to mature particles with different biophysical characteristics. For example, packaging Flock house virus (FHV) with cellular RNA produces a particle with a crystal structure identical to wild type but with altered solution properties (Bothner, B., *et al.*, 1999). Polymorphic particles result from packaging foreign or incomplete genomes in Brome mosaic virus (BMV) (Krol, M. A., *et al.*, 1999). Altering the nucleic acid binding domain of the coat protein prevents viral assembly in BMV (Rao, A. L. and G. L. Grantham . 1996, Sacher R, and P. Ahlquist. 1989). Similar phenomena have also been observed with the *Microviridae* (Hafenstein, S. and B. A. Fane, 2002).

As illustrated in Figure 3.1, øX174 morphogenesis is dependent on two species of scaffolding proteins and a packaged single-stranded DNA genome (Hafenstein, S. and B. A. Fane, 2002, Hayashi, M., *et al.*, 1988). Together the internal and external scaffolding proteins mediate the assembly of the viral procapsid; into which ssDNA is packaged (Hayashi, M., *et al.*, 1988). After the procapsid is assembled, the single stranded viral

genome is synthesized and packaged, concurrent processes, along with the DNA binding protein (J). The C-terminus of protein J, which is highly conserved within the *Microviridae* associates with a cleft in the coat protein (F) in each asymmetric unit (McKenna, R., *et al.*, 1992, 1994). The binding of the carboxy tail may allow additional interactions between the genome and a cluster of nearby basic residues of F. After the initiation of DNA packaging, the internal scaffolding protein (B) dissociates from the interior of the capsid. During the final stages of øX174 morphogenesis, the external scaffolding protein (D) is released and there is an 8.5 Å radial collapse of coat protein pentamers around the single stranded genome (Dokland, T., *et al.*, 1997, 1999). High-resolution image reconstruction of a *Microviridae* procapsid reveals that there are no capsid pentamer-pentamer contacts in the procapsid (Bernal R. A., *et al.*, 2003). Hence the genome, via its tethering to the inner surface of the coat protein, may play a critical role in maintaining the structural integrity of the capsid upon the dissociation of the external scaffolding protein. Altering the genome's association to the inner capsid, or changing the secondary structure of the packaged genome, alters the biophysical characteristics of the mature virion (Hafenstein, S. and B. A. Fane, 2002). This suggests that the genome-capsid interactions are performing a scaffolding-like function, mediating the final stages of morphogenesis.

The DNA binding protein is a small (37 amino acids in length), highly basic structural protein that binds the single stranded DNA genome through non-specific, charge-charge interactions (Dalphin, M. E., 1989, Jennings, B. and B. A. Fane, 1997). There are two

binding regions, one near the amino terminus and one centrally located in the protein (Figure 3.2). A spacer region rich in proline residues separates the two binding regions in ϕX174 J protein. In order to more fully investigate J protein function during assembly and DNA packaging, the glycine residues within the first and second binding regions and the three proline residues within the spacer region were targeted for analysis. The relative importance of the proline residues has been previously reported (Jennings, B. and B. A. Fane, 1997). The glycine residues were chosen because of their conservation within the DNA binding regions of the *Microviridae* J proteins.

The results of this analysis suggest that the role of the conserved glycine residues may be to optimize the function of the DNA binding motifs. Substitutions for glycines in the binding domain result in biophysically altered particles with properties similar to those observed for particles containing J proteins with substitutions for lysines. Furthermore, the same extragenic second-site suppressors rescue both classes of mutations. On the other hand, the results of biophysical and genetic analyses suggest that the role of the proline residues within the spacer region is fundamentally different.

MATERIALS AND METHODS

Phage plating, stock preparation, media, phage purification, bacterial strains, cloned genes, buoyant density, native gel migration, and attachment assays. The plating protocols, media and stock preparation have all been previously described (Fane, B. A. and M. Hayashi, 1991). *Escherichia coli* C strain C122 (*sup*^{0}) is the wild-type host; BAF5, BAF7 and BAF8 contain a *supE*, *supD*, and *supF* informational suppressor, respectively. BAF30 is a *recA* derivative of C122 (Fane, B. A., Head, S., and M. Hayashi, 1992). Plasmids pøXB and pøXDJ contain IPTG (isopropyl β -D-thiogalactopyranoside)-inducible clones of the øX174 genes designated (Burch, A. D., *et al.*, 1999, Burch, A. D. and B. A. Fane, 2000). The *slyD* host mutation confers resistance to øX174 E-protein-mediated cell lysis (Roof, W. D., *et al.*, 1994). Buoyant density, native gel migration, and attachment assays have been previously described (Hafenstein, S. and B. A. Fane, 2002).

Phage mutants. The øX174 mutants, *J-3K&R->LI*, *J 3K->LII*, and *su (J)-FS1FF* have been previously described (Hafenstein, S. and B. A. Fane, 2002, Jennings, B. and B. A. Fane, 1997). *J* amber mutations were constructed by oligonucleotide-mediated mutagenesis designed to introduce amber codons at the selected sites (Fane, B. A., Head, S., and M. Hayashi, 1992). BAF30 pøXDJ cells were transfected with mutagenized DNA and incubated at 33^0 until plaques appeared. Plaques were stabbed into C122 and pøXDJ seeded lawns. Putative mutants were identified by complementation-dependent growth

then verified by direct DNA sequence analysis. The *su (J)-F S1F* was built directly into the *am (J)G3* and *am(J)G22* backgrounds by oligonucleotide-mediated mutagenesis. Putative double mutants were identified by rescue of the parental *cs* or *ts* phenotype on the *supD* host and retention of the amber phenotype. Genotypes were verified by direct DNA sequence analysis.

Isolation of second site suppressors: The *am(J)G22* mutant was used for the isolation of second-site suppressors. The second-site suppressors were selected for their ability to suppress defects associated with serine insertion at 42^0 and glutamine insertion at 24^0. 5.0 X 10^6 viable phage were plated under restrictive conditions. Revertant plaques were stabbed into three indicator lawns; one seeded with the restrictive host at nonpermissive temperatures, C122 (*sup*^{0}), and BAF30 pøXDJ. Putative suppressor mutants were identified by retention of the *am(J)* phenotype and growth under restrictive conditions. All genotypes were verified by direct DNA sequence analysis.

Recombination rescue experiments : øX174 DNA containing four hundred nucleotides surrounding the *su(J)-F T204I* mutation was amplified via PCR. The DNA was cloned into a non-expression Topo 2.1 vector (Invitrogen) and transformed into the C122 (*sup*^{0}) and BAF7 (*sup D*) cell lines. Rescue frequencies for parental mutants were calculated under restrictive conditions and the presence of both the parental and suppressing mutations in the recombinants were verified via a direct sequence analysis.

RESULTS

Characterization of substitutions for glycine and proline residues. The conserved glycine codons in the two DNA binding regions, G3 and G22, and two proline codons in the spacer region, P14 and P16, were mutated to amber. Despite repeated attempts, a P11 amber mutant was never recovered. Missense proteins were generated by propagating mutants in hosts with tRNA informational suppressors. Serine, glutamine and tyrosine substitutions for G3 appear to be fairly well tolerated conferring, at most, weak cold sensitive (*cs*) phenotypes (Table 3.1). However, substitutions for G22 in the second DNA binding region result in strong *cs* or lethal phenotypes. A similar phenotypic phenomenon was observed in previous studies in which lysine residues in both DNA binding domains were altered (Jennings, B. and B. A. Fane, 1997). Substitutions for proline residues resulted in predominately lethal phenotypes.

Characterization of infectious particles packaged with mutant DNA binding proteins. To further assess the biophysical characteristics of particles containing missense J proteins, G3->Q and G22->Q particles were analyzed by buoyant density centrifugation. In these experiments, mutant particles were analyzed in the same gradient with wild type. Particles were differentially titered as described in the figure legend (Figure 3.3, panel A). As with previously documented particles packaged with charge reduced J proteins (Hafenstein, S. and B. A. Fane, 2002), G22->Q particles are more dense than wild type, suggesting that the nature of the defect in the DNA binding

domains may be similar. Several hypotheses can explain this increased density (see Discussion, and below).

The G3->Q substitution produces two types of packaged particles, one with near wild-type density and another significantly denser. When each particle type was harvested and assayed in a second gradient, the densities remained constant; suggesting that particles did not inter-convert (Figure 3.3, panel B). To determine whether multiple particle types, which may have been below the level of detection in the experiment presented in Figure 3.3, also exist among G22->Q and wild-type populations, the assay was repeated with higher titers. A second population of mutant G22->Q particles less dense than wild type was visualized and a significant minor peak was also seen for wild type virion (Figure 3.4, panel A). The existence of this wild-type sub population suggests that mutant DNA binding proteins cause a ratio shift between extant particles, as opposed to creating entirely novel structures.

Particles packaged with the P14->Y and P16->S proteins, are less dense than wild type (Figure 3.5, panel A, P16->S, data not shown). This is in contrast to serine substitutions for glycine residues, which resulted in particles with increased densities. Although these results suggest that density differences are not the consequence of lower intracellular J protein concentrations caused by informational suppressors, which are known to operate at reduced efficiencies (Winston, F., *et al.*, 1979), this was directly examined by

repeating the assay using a *cs* P16 *missense* mutation (Figure 3.5, panel B). Again the resulting particles were less dense than wild type.

Host cell attachment as an assay for differences on the outer surface of the capsid. Since host cell attachment is a function of the capsid's outer surface, attachment assays were used to explore possible structural differences (Figure 3.6). The attachment efficiency of wild type particles is three orders of magnitude greater than that of the mutant particles with substitutions for proline and glycine residues (Figure 3.6). Similar results were obtained for the other mutants tested, suggesting that alterations to the surface of the capsid are produced by a mutant internal protein.

Second site genetic analyses: To further explore the role of the conserved glycine residues in the DNA binding regions, Second-site suppressors of the missense proteins were isolated. Using *am(J)G22* as the parental strain, second-site suppressors were selected for their ability to suppress defects associated with glutamine substitutions at 24^0 and serine substitutions at 42^0 (Material and Methods). Putative second-site suppressor mutants were identified by the retention of the amber phenotype, J protein complementation dependent growth, and verified by a direct DNA sequence analysis. All second site suppressing mutations were extragenic, conferring amino acid substitutions in the coat protein, F. The T 204 I was independently recovered three times. It was also used in series of marker rescue experiments to verify the identity of the suppressing amino acid (see below).

The su(J)/ *am(J)G22* double mutants were assayed for ability to grow as a function of temperature and missense insertion. Suppressors isolated at 42°C only suppress defects associated with G->S substitutions. Whereas, one of the suppressors isolated at 24^0, *su* (J)-F T204I, suppress *ts* defects and *cs* defects associated with any missense substitution. This suggests that reduced temperatures represent a more restrictive growth condition and selects for suppressors with stronger phenotypes. No suppressors were recovered for *am(J)G3, am(J)P14* and *am(J)P16* due to either leaky phenotypes or high *amber* reversion frequencies.

To determine whether the isolated suppressors were both necessary and sufficient to confer the suppressing phenotype, a series of recombination rescue experiments were performed. Four hundred nucleotides surrounding the *su(J)-F T204I* mutation were cloned into a non expression Topo vector and the plasmid placed into the C122 (sup^0) and BAF7 (*sup D*) cell lines. Rescue frequencies for parental mutants were calculated under restrictive conditions. The *am(J)G22* parent was rescued in BAF7 (*supD*) at 42°C (Table 3.3). The presence of both the parental and suppressing mutations in the recombinants were verified via a direct sequence analysis. Rescue experiments were also performed with the *am(J)P14* mutant and two previously isolated mutants *J-3K&R->LI* and *J-3K->LII* which contain substitutions for lysine residues in the first and second DNA binding regions. No rescue was observed.

Cross-functional second-site suppressors as an assay for common molecular defects: The charge reduced mutants resulting from substitutions for lysine residues and the glycine substitution mutants share common biophysical characteristics. To determine whether this is the consequence of similar molecular defects, a previously characterized extragenic second site suppressor of lysine substitutions, *su(J)-F S1F*, was built directly into the *am(J)G3* and *am(J)G22* backgrounds. In both cases the mutation suppressed defects associated with glycine substitutions (Table 3.4), suggesting the substitutions in the DNA binding region confer similar mechanistic defects. The *su(J)-F S1F* suppressor was previously shown to have no affect on substitutions for proline residues (Jennings, B. and B. A. Fane, 1997). The inability of the *su(J)-F T204* suppressor to rescue the *J3K->LII* mutant is probably due to the relative severity of this particular mutation. Unlike substitutions for glycine residues, the *J3K->LII* substitutions confer a dominant lethal phenotype, for which the *su(J)-F S1F* mutation was originally selected to suppress. The *su(J)-F T204* suppressor, on the other hand, was selected to suppress a much less severe phenotype.

DISCUSSION

Interactions between the viral genome and structural proteins have been shown to be essential to virion assembly in a number of single stranded RNA plant viruses (Lee S. K. and D. L. Hacker, 2001, Rao, A. L. and G. L. Grantham , 1996, Rossmann M. G., *et al.*, 1983, Schmitz, I. and A. L. Rao, 1998) and insect viruses (Dong, X.F., *et al.*, 1998, Wery J. P., *et al.*, 1994). In the dsRNA Infectious bursal disease virus (IBDV) the binding of the two genomic segments by a highly basic region of the C-terminus tail of VP3 appears to be key to the organization of protein and RNA during morphogenesis (Tacken M. G., *et al.*, 2002). In addition, the packaged genome appears to stabilize the mature viral particle in the dsDNA papillomavirus (Fligge, C., *et al.*, 2001) as well as in many of the ss RNA plant viruses (Da Poian, A. T., *et al.*, 2002, Willits, D., *et al.*, 2003). In the *Microviridae*, where the single stranded DNA genome is tethered to the inner surface of the capsid at each asymmetric unit via protein interactions, alterations to either the protein or the DNA component of the tether can change the biophysical properties of the resulting virion (Hafenstein, S. and B. A. Fane, 2002). Clearly genomic material may function as a structural component in virion morphogenesis.

Altered densities: Substitutions for glycine residues may interfere with DNA binding ability of the J protein. G3 and G22 are components of the two highly conserved DNA binding motifs. Substitutions for either of these glycine residues result in particles with buoyant densities greater than wild type, a phenomenon similar to that observed for

charge reduced mutants with decreased DNA binding ability (Hafenstein, S. and B. A. Fane, 2002). Several hypotheses can explain the density differences. Alterations in the number of J proteins found in the final particles could be compensated by internally retained or displaced cesium counter ions. Although the contribution of the Cs^+ ions was assessed to be minimal in previous studies with charged altered mutants, it could not be ruled out in these present studies. However, variation in the amount of protein and counter ions incorporated per virion would result in a density curve visualized as broad peak, beginning near wild type density values and stretching away in a continuous curve toward heavier densities values until particles were no longer viable because detection was a function of viability. But this was not the experimental result. Mutant particles with substitutions for G3 segregated into two distinct and sharp density peaks. Substitutions at G22 result in a density pattern similar to wild type, consisting of a major density population and accompanied by a minor population. These results suggest that the final stages of morphogenesis may not consist of a linear pathway, but several alternate pathways, influenced by the packaged genome, which result in viability.

Substitutions for glycine and proline residues most likely confer mechanistically different defects. Substitutions for glycine residues results in particles with biophysical properties similar to those of the previously reported charge reduced J mutants with substitutions for lysine residues (Hafenstein, S. and B. A. Fane, 2002). Furthermore, the suppressor of the charged reduced mutants also suppresses the defects associated with

missense substitution for both glycine residues, suggesting that the two classes of mutations are mechanistically similar. A set of second-site suppressors of the missense glycine proteins was also isolated and characterized. All but one of the suppressing mutations maps to the two fold axes of F. The exception, F G22 C, is a substitution at the tip of a beta strand, β- B, which might cause the β strand to shift toward the two-fold axis of symmetry (Figure 3.6). None of the F residues interact directly with J residues. Therefore, it is likely that they indirectly alter surface topography restoring infectivity to the packaged particle.

While it seems likely that glycine mutants disrupt the DNA binding capability of J protein, proline mutants appear to be disrupting a different function of protein J. Particles formed with proline-substituted proteins substitutions have unique biophysical properties not shared by other mutant particles. Unlike substitutions lysine residues, where there may be a redundancy of function in the DNA binding regions, and glycine residues which may serve to optimize interactions between lysine residues and the genome's phosphate backbone, proline substitutions are tolerated poorly, with most substitutions conferring lethal phenotypes. In addition, proline substitutions are not rescued by the extragenic suppressors of charge reduced J mutants (Jennings, B. and B. A. Fane, 1997).

While nucleic acid binding domains are characterized by the presence of a high proportion of basic residues, many of the virus systems, which have been shown to have

essential genome-protein interactions, also have proline residues present within the nucleic acid binding domain. FHV has 17 basic residues and 4 proline residues in the N-terminal region (Dong, X.F., *et al.*, 1998). In the N-terminal RNA binding region of SCPMV there is a cluster of 8 basic residues adjacent to three proline residues. Almandine substitution for the proline residues does not effect the binding of the RNA (Lee S. K. and D. L. Hacker, 2001). A strictly conserved proline in the DNA-binding domain of the yeast heat shock transcription factor (HSF) and the enteric bacteria factor for inversion stimulation (FISA) has been shown to be unnecessary to structure, function or stability of the protein (Hardy, J. A. and H. C. Nelson, 2000 , Hobart, S. A.,, *et al.*, 2002). The only biophysical characteristics affected by substitutions for the FISA proline residue are folding kinetics and solubility. This suggests a possible model for function of the conserved proline residues within the DNA binding region of the *Microviridae*. During the packaging reaction, the presence of the proline residues may serve to prevent rapid but random interactions between the DNA and capsid. When the C-terminus of protein J lodges in an internal cleft of the viral capsid protein (F), protein J then moves toward the five-fold axis of symmetry, swinging the bound genome toward the adjacent asymmetric unit, and to the next binding cleft. The proline residues may ensure the proper kinetics of folding and packaging of the genome by guiding the DNA to the adjacent five-fold related asymmetric unit resulting in wild type genomic organization.

ACKNOWLEDGEMENTS

This research was supported by an NSF Grant B. A. F.

TABLE 3.1. Efficiency of plating[1] of amber mutants on hosts with informational tRNA suppressors.

Mutant:	Amino acid substitution: glutamine 24°C	33°C	42°C	serine 24°C	33°C	42°C	tyrosine 24°C	33°C	42°C
am(J)G3	0.2	0.8	0.7	0.03	0.6	0.5	0.7	1.0	1.0
am(J)G22	RF[2]	1.0	1.0	RF	4.0×10^{-3}	3.0×10^{-4}	4.0×10^{-3}	1.0	1.0
am(J)P16	RF	RF	0.01	RF	RF	0.01	RF	1.0	1.0
am(J)P14	RF	RF	RF	RF	RF	RF	9.0×10^{-4}	1.0	1.0

[1] Restrictive titer / permissive titer, as determined on BAF30 pøXDJ.

[2] RF indicates equal to or lower than am^+ reversion frequency.

TABLE 3.2. Efficiency of plating[1] of *su(J)/amG22* mutants on hosts with informational tRNA suppressors.

Mutant[2]	Amino acid substitution: glutamine 24°C	33°C	42°C	serine 24°C	33°C	42°C	tyrosine 24°C	33°C	42°C
Su(J)-F L94I	RF[1]	1.0	1.0	RF	**1.0**	**1.0**[3]	RF	1.0	1.0
Su(J)-F T5A	RF	1.0	1.0	RF	**1.0**	**1.0**	RF	RF	1.0
Su(J)-F Q80H	RF	0.9	1.0	RF	**0.5**	**0.8**	RF	1.0	1.0
Su(J)-F V71F	**1.0**	1.0	1.0	RF	**1.0**	RF	**1.0**	1.0	1.0
Su(J)-F T204I	**1.0**	1.0	1.0	RF	**1.0**	**1.0**	**1.0**	1.0	1.0
Su(J)-F G22C	**1.0**	1.0	RF	RF	**1.0**	RF	**1.0**	1.0	RF

[1] Restrictive titer / permissive titer, as determined on BAF30 pøXDJ. RF indicates equal to or lower than am^+ reversion frequency.

[2] Suppressors are named as follows, "-F" indicates the gene in which the suppressor resides, the major coat protein. "L94I" an leucine to isoleucine substitution for amino acid 94.

[3] Underline text indicates the conditions of isolation. Bold text indicates conditions at which the suppressor mutant is viable but the parent mutant is restricted.

TABLE 3.3 Recombination rescue by a cloned second-site suppressor[1].

	Restrictive plating efficiencies[2]:			
mutant	*supD* host with plasmid	*supD* host no plasmid	*sup°* host with plasmid	*sup°* host[3] no plasmid
am(J)G22	0.1	5.0×10^{-5}		5.0×10^{-5}
am(J)P14	1.0×10^{-4}	1.0×10^{-4}		1.0×10^{-4}
J-3K->LII			5.0×10^{-3}	4.0×10^{-4}
J-3K&R->LI			8.0×10^{-5}	2.0×10^{-4}

[1] Restrictive titer / permissive titer, as determined on BAF30 pøXDJ.

[2] Experiments with amber mutants and *J-3K&R->LI* were performed at 33°C. The experiments with *J-3K->LII* were performed at 42°C.

[3] For amber mutants, this value represents the am^+ reversion frequency. For *J-3K->LII* and *J-3K&R->LI* this value represents the lethal phenotype reversion frequency.

TABLE 3.4. Efficiency of plating[1] of *su(J)-F S1F/am(J)* mutants on hosts with informational tRNA suppressors.

	Amino acid substitution: glutamine			serine			tyrosine		
Mutant	24°C	33°C	42°C	24°C	33°C	42°C	24°C	33°C	42°C
am(J)G3									
	1.0[2]	1.0	1.0	1.0	1.0	1.0	1.0	1.0	1.0
am(J)G22									
	RF	1.0	1.0	RF[3]	**1.0**	**1.0**	RF	1.0	1.0

1 Restrictive titer / permissive titer, as determined on BAF30 pøXDJ.

2 Bold text indicates conditions at which the suppressor mutant is viable but the parent mutant is restricted.

[3] RF indicates equal to or lower than am^+ reversion frequency.

FIGURE LEGENDS

FIG 3.1. øX174 morphogenesis

FIG 3.2. Primary sequence of protein J, the DNA binding protein. The glycine and proline residues, which are the subject of these studies are in bold text. Basic residues are underlined.

FIG 3.3. Buoyant densities of wild type and particles generated with missense proteins. Both particles were analyzed in the same gradient. An additional genetic marker, *amB*, was placed in the wild type background. This allowed the particles to be differentially titered on BAF30 pøXB at 33^{0}C. The titer of the amber J mutants was determined on BAF30 pøXDJ at 33^{0}C. Particle titers were normalized to the same order of magnitude for the graph. Panel A: Symbols: *am(J)G22* with the missense G->Q protein, open square; wild type phage, closed circle; and *am(J)G3* with missense G->Q protein, open circle. Panels B and C: *am(J)G3,* particles packaged with the missense J protein, *G3->Q,* heavy and light peaks were harvested and assayed again with wild type.

FIG 3.4 Reinvestigation of*G22->Q* particles and wild-type and wild type using higher titers. Particles were differentially titered as described in the legend of Figure 3.3. Symbols: wild type, closed circles; and mutant particles, open circles. Panel A: Total particle counts. Panel B: Enlargement to illustrate sub populations.

FIG 3.5. Buoyant density gradients of proline mutants. Symbols: wild type, closed circles; mutant, open circles. Panel A: *am(J)P14->Y, tyrosine insertion* Panel B: *cs(J)P16L*

FIG 3.6. Attachment assays. Symbols: wild type, closed circles; *amJG22 with glutamine* missense protein, open boxes; *cs(J)P16L,* open circles.

FIG 3.7. Location of the second site suppressors of missense G22 proteins.

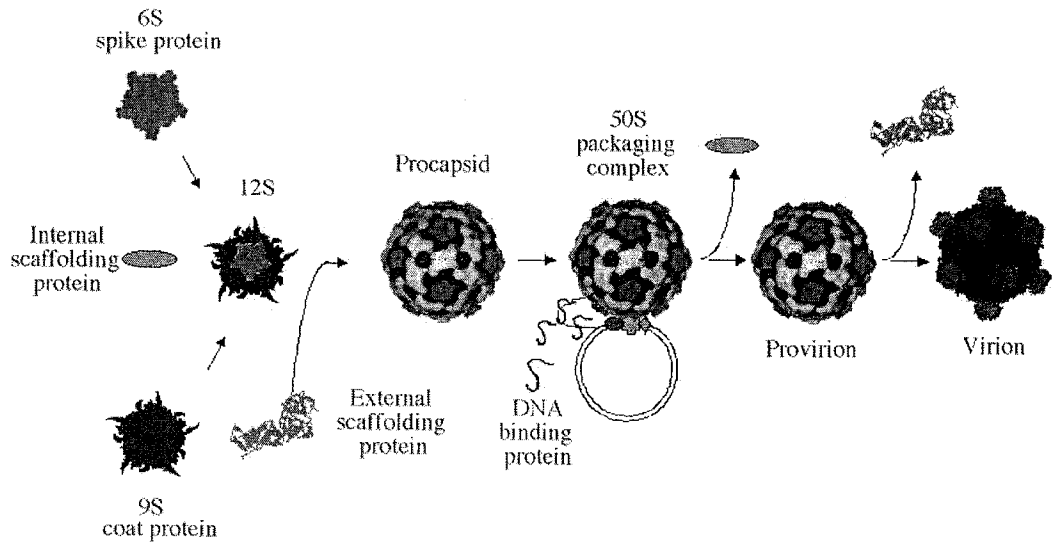
6S
spike protein
12S
Internal
scaffolding
protein
9S
coat protein
External
scaffolding
protein
Procapsid
50S
packaging
complex
DNA
binding
protein
Provirion
Virion

FIG 3.1

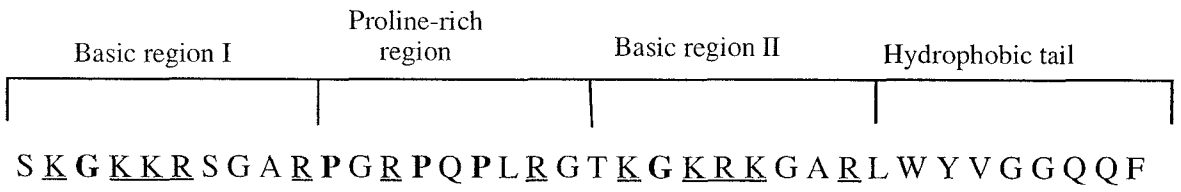
Basic region I
Proline-rich region
Basic region II
Hydrophobic tail
S K G K K R S G A R P G R P Q P L R G T K G K R K G A R L W Y V G G Q Q F

FIG 3.2

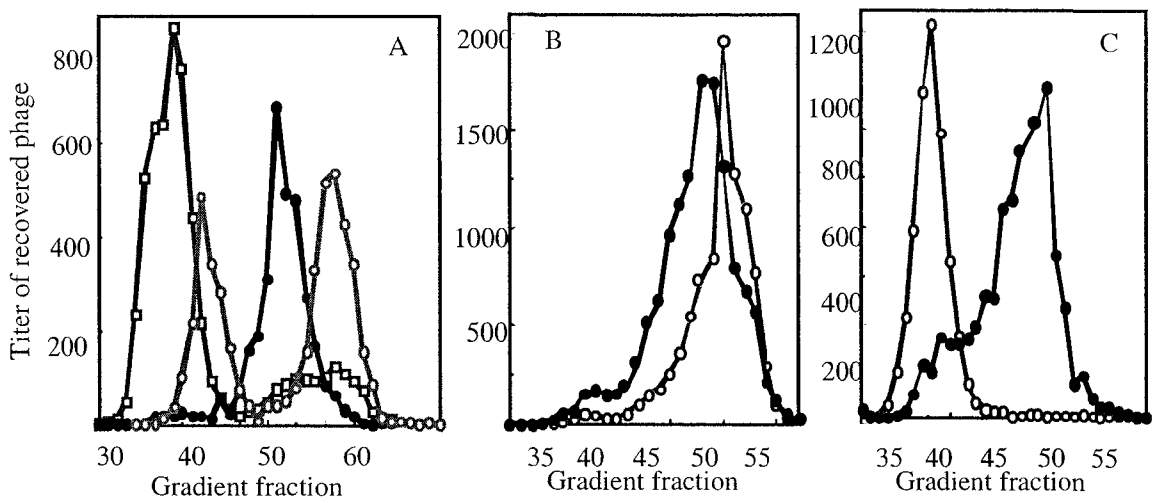
Titer of recovered phage
800
600
400
200
A
30
40
50
60
Gradient fraction
2000
1500
1000
500
B
35
40
45
50
55
Gradient fraction
1200
1000
800
600
400
200
C
35
40
45
50
55
Gradient fraction

FIG 3.3

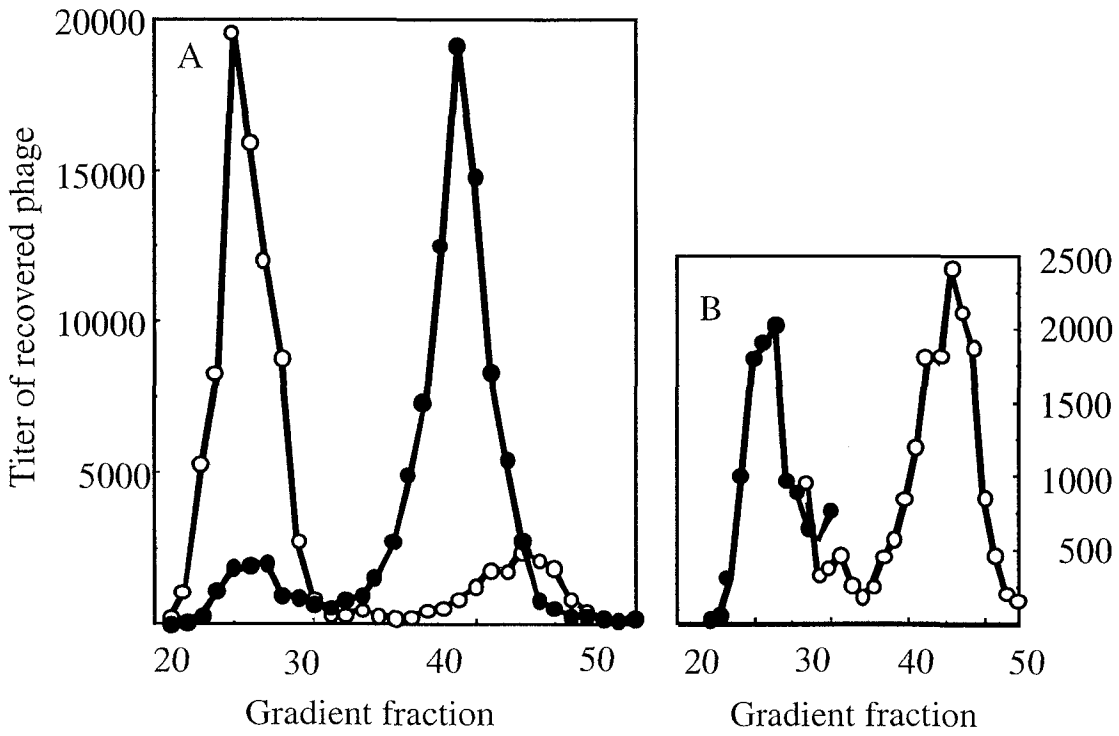
20000
15000
10000
5000
Titer of recovered phage
A
20
30
40
50
Gradient fraction
B
2500
2000
1500
1000
500
20
30
40
50
Gradient fraction

FIG 3.4

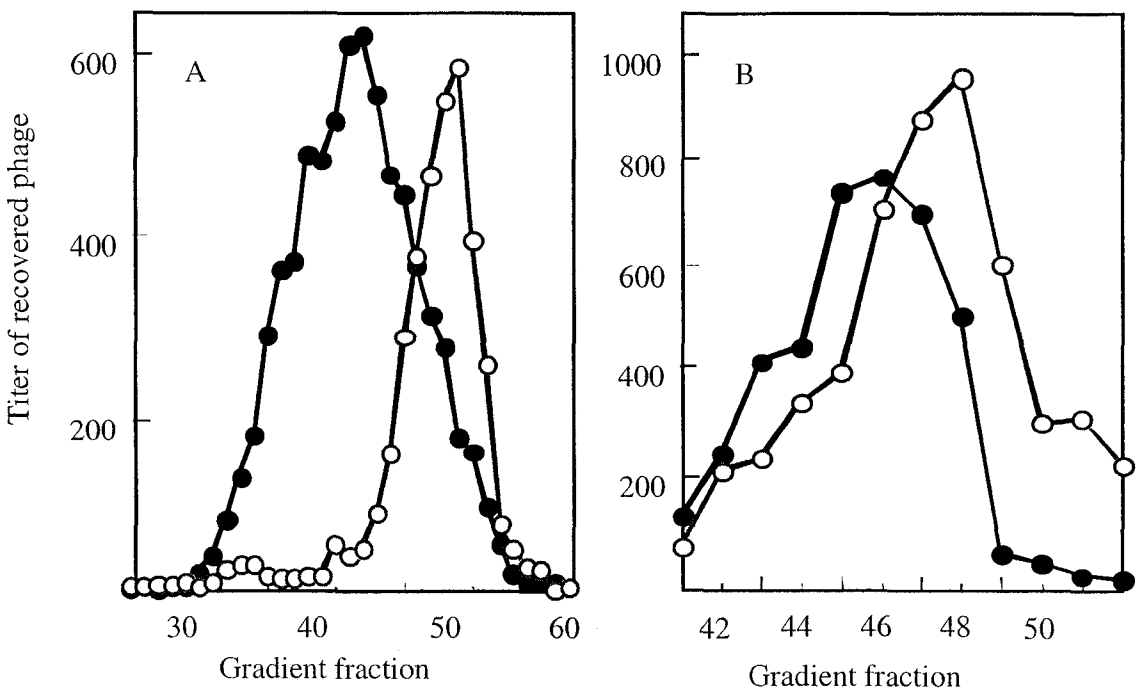
A
B
Titer of recovered phage
600
400
200
1000
800
600
400
200
30
40
50
60
42
44
46
48
50
Gradient fraction
Gradient fraction

FIG 3.5

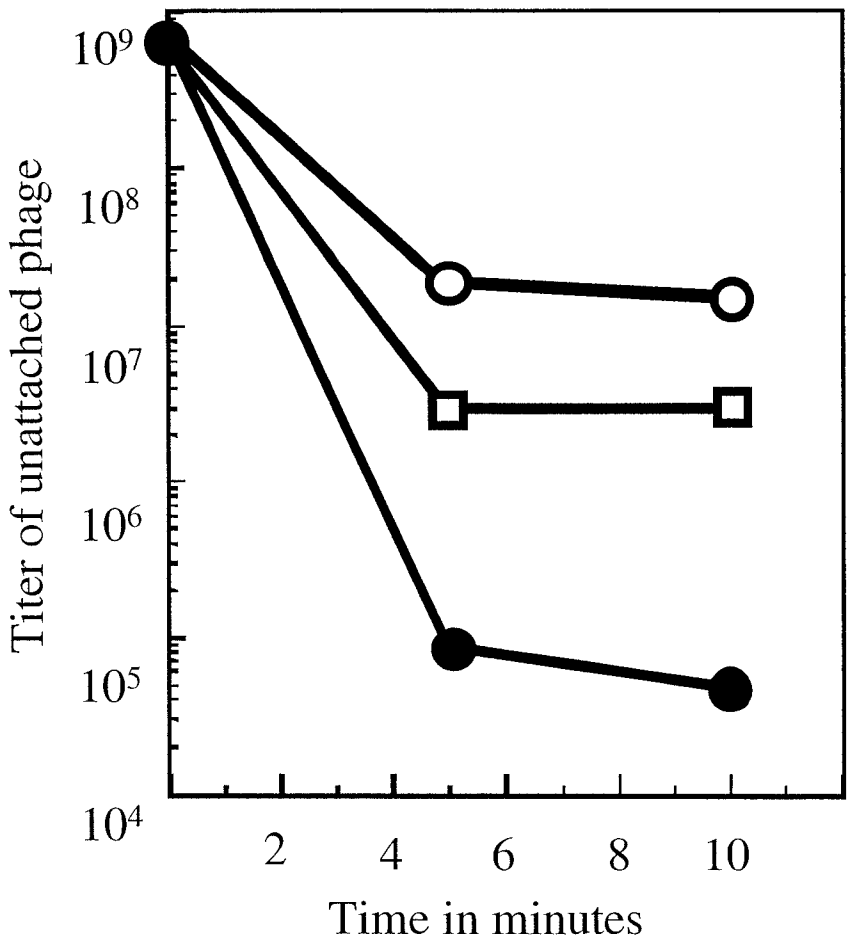
Titer of unattached phage
10^9
10^8
10^7
10^6
10^5
10^4
2
4
6
8
10
Time in minutes

FIG 3.6

FIG 3.7

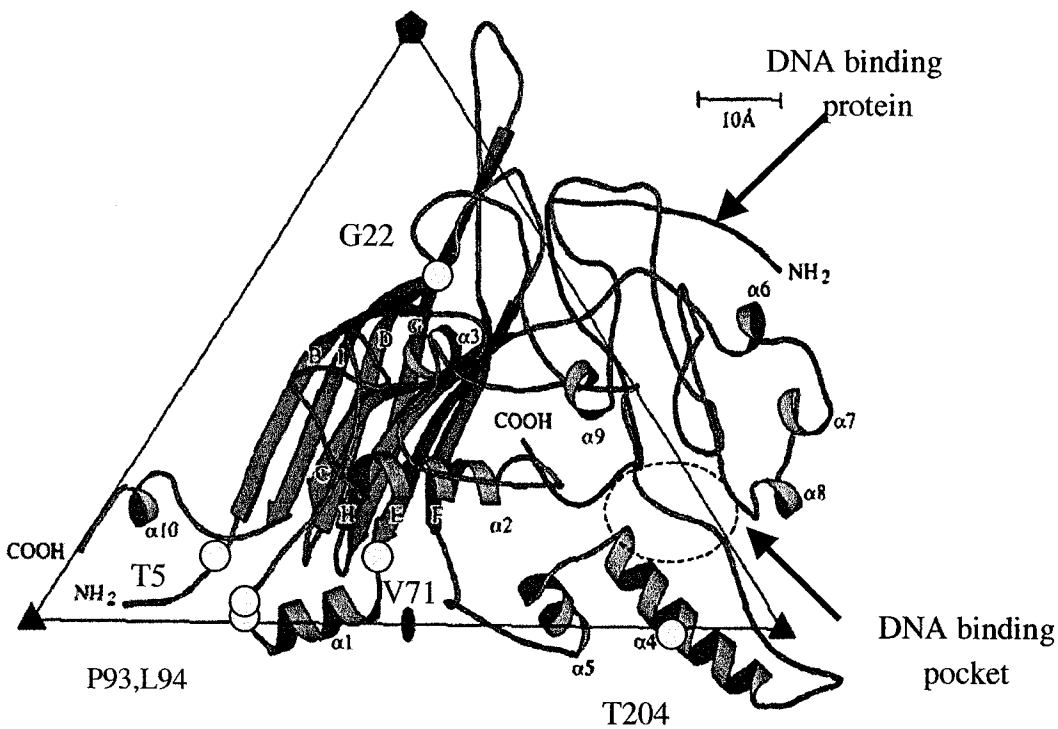
DNA binding
protein
10Å
G22
NH2
α6
α3
COOH
α9
α7
α8
α10
α2
COOH
T5
NH2
V71
α1
α4
α5
P93,L94
T204
DNA binding
pocket

CHAPTER 4

FUNCTION OF A WILD TYPE DNA BINDING PROTEIN WITHIN A FOREIGN ENVIRONMENT RESULTS IN A DIFFERENT ORGANIZATION OF THE GENOME AND ALTERED BIOPHYSICAL PROPERTIES OF THE VIRION: A WORK IN PROGRESS.

ABSTRACT

In the *Microviridae* the organization of the genome is managed by three components: the DNA binding protein, J, the coat protein, F, and the secondary structure of the packaged DNA. These three components form a quaternary structure in the mature virion, which tethers the genome to the inner surface of the capsid. To alter the protein component of the tether without resorting to mutagenesis, the ability to produce chimeric particles was explored. The gene for the DNA binding proteins of *Microviridae* family members G4, α3 and øX174 were cloned and assayed for the ability to cross complement. When successful, endogenous DNA would be packaged into endogenous particles using a foreign and exogenous DNA binding protein. Therefore the resulting chimeric particles are comprised of wild type components with a foreign, yet wild type J protein, as an integral part of the final structure. Since the incorporated J protein is functional in both the chimera and its native environment, comparisons can be made to elucidate packaging and DNA organization, and functions of the DNA binding protein.

INTRODUCTION

Single-stranded øX174 DNA does not exist as a dense core in the capsid, as is observed in dsDNA bacteriophages (Earnshaw and Casjens, 1980). Instead, it is tethered to the capsid's inner surface by interacting with the highly basic DNA binding protein (J) and basic capsid amino acid residues (McKenna *et al.,* 1992, 1994). There are 60 copies of protein J per virion with the C-terminus of the protein tightly associated with a cleft located near the center of the coat protein. Moving toward the N-terminus, the protein traces a path toward the 5-fold axis of symmetry, crosses over to the adjacent capsid protein veering toward the C-terminus of the adjacent J protein (Figure 4.1). This motif suggests that the DNA binding protein guides the incoming genome into a somewhat ordered conformation. Accordingly, between 8-10% of the genome is ordered in the X-ray structure of both øX174 and in α3 (McKenna *et al.,* 1992, 1994; Bernal *et al.,* 2003). Here and in other systems where higher percentages of the genome are ordered within the capsid's icosahedral symmetry such as Flock house virus and Satellite tobacco mosaic virus nucleic acid -structural protein interactions are thought to contribute to both capsid assembly and stability (Fisher and Johnson, 1993; Larson *et al.,* 1998).

The genomic tether in the *Microviridae* has been explored previously by mutating the DNA binding proteins or by packaging foreign DNA genomes. To alter the protein component of the tether without resorting to mutagenesis, the ability to produce chimeric particles was explored. *Microviridae* family members α3, G4 and øX174 share a highly

conserved C-terminus that interacts with the coat protein, F, upon packaging and a variable amino terminal DNA binding domain. The øX174 J protein contains 8 basic residues grouped into two binding motifs that are separated by a spacer region containing three more basic residues and three proline residues. This is a more lengthy and complicated DNA binding domain as compared to G4 or α3. The DNA binding domains for G4 and α3 are shorter, representing half the length of the protein, and less basic, containing 6 and 7 basic residues, respectively. The N-termini function as a non-specific DNA binding domain (Dalphin, 1989; Jennings and Fane, 1997). Although the N-termini show a great deal of amino acid divergence, they are very basic, rich in lysine and arginine residues. The G4 and α3 J protein primary structures seem closely related (70% homology) while significant differences are seen in comparisons to øX174 (Figure 4.2).

When cross complementation can occur, endogenous DNA would be packaged into endogenous particles using a foreign and exogenous DNA binding protein. Therefore the resulting chimeric particles are comprised of wild type components with a foreign, yet wild type J protein, as an integral part of the final structure. Since the incorporated J protein is functional in both the chimera and its native environment, comparisons can be made to elucidate packaging and DNA organization functions of the DNA binding protein. Within its native environment, this protein is fully functional and tested by evolution, however within the chimera its ability to function is constrained by an altered environment and foreign associations that it must make with the capsid protein, F, and the ss DNA genome.

Organization of the genome is managed by three components: The properties of the DNA binding protein, J, the properties of the coat protein, F, and the DNA itself. Altering any one of these components leads to biophysical differences as assayed by native gel, density gradients, or attachment assays (Hafenstein and Fane, 2002). Packaging with mutant charge reduced J proteins results in particles denser than wild type possibly due to weakening the tether of the genome to the inner surface of the capsid, thereby allowing for more genomic secondary structure in the viral core, and ultimately affecting the structure of the mature virion. When α3 particles were packaged with the more extensive øX174 J proteins, the results suggest the genomic attachment was strengthened by substituting a more basic J protein for a less basic protein. The stronger association of the genome may involve more organized DNA visible in the atomic structure. This hypothesis was tested by X-Ray crystallography studies using the α3 chimera in comparison with α3 wild type and øX174 wild type atomic structures. The protein stoichiometry of the wild-type and chimeric α3 particles was also compared. The results of these analyses illustrate that the DNA binding protein affects the order of the genome in the packaged particles and provide insights into protein and virion evolution. While not all questions were answered or hypotheses verified, the results elucidate the limitations of structural analyses and suggests avenues as to how these limitations can be minimized.

MATERIALS AND METHODS

Construction of chimeric particles. To prevent synthesis of α3 J protein, two amber mutations were placed in gene J via oligonucleotide-mediated mutagenesis as described previously in Fane *et al* (1993). In order to produce the high titered stocks required for X-ray crystallography, a third amber mutation was also placed in gene E to prevent the production of the viral lysis protein. The cellular lysis pathway was also blocked by using a lysis deficient *slyD* host (Roof *et al.,* 1994). To produce the chimeric particles, the triple amber mutation was grown in a slyD cell line harboring a clone of the ϕX174 J protein. Yields of 1 mg/ml were typical.

Cesium Chloride buoyant density gradients, attachment assays, native gel electrophoresis, and stoichiometric analyses. These protocols have been previously described in Hafenstein and Fane (2002).

Purification of biologically homogeneous particles. This protocol was modified from Burch and Fane (2003). Relative modifications are described in the text.

RESULTS

Cross complementation of Microviridae DNA binding proteins. The primary sequences of the G4, α3 and øX174 J proteins are illustrated in Figure 4.2. The genes have been cloned, expressed *in vivo* and assayed for cross-complementation (Table 4.1). While all three cloned genes complement G4 and α3 *amJ* mutants, only the øX174 gene complements the øX174 mutant. Hence, more complex and basic J proteins can be substituted for smaller less basic proteins. However, the converse is not true. The results of øX174 packaging studies indicate that the more complex and basic protein is required for particle stability during the packaging reaction. (Fane, Head and Hayashi, 1992). To further examine how the DNA binding protein may influence the biophysical properties of the particles, the packaging arrangement of the DNA, and the structure of the mature virion, α3 particles packaged with the øX174 J protein were produced.

Infectious wild-type α3 and chimeric α particles have different biophysical properties in than wild-type α3. Cesium chloride buoyant density gradients were performed to characterize possible biophysical differences between wild type øX174, α3 wild type, and α3 particles packaged with øX174 J protein. The three different species of virions were assayed in the same buoyant density gradient with additional genetic markers present in both wild type øX174 and α3, which allowed particle types to be differentially titered (see figure legend). Alpha 3 wild type particles are more dense than

øX174 virions, (Figure 4.3) while chimeric particles appear to have a density intermediate between the two. This result argues against the simplest model, in which particle diameters and protein stoichiometry remain constant. In that model, the protein content of the chimeric particle would be greater due to the larger J protein. Additional protein, with a density of 1.3 gm/cm3, would displace water molecules. Hence the chimeric particle should have a greater buoyant density than wild-type, which is clearly not the case. Buoyant density gradients performed with G4 wild type and *G4 amJ* packaged with ϕX174 J protein also resulted in chimeric G4 particles less dense than wild type. However, further biophysical assays were limited to α3 wild type and the α3 chimera in order to use the known atomic structure of ϕX174 (McKenna *et al.,* 1992, 1994) and the recently solved α3 wild type virion structure (Bernal *et al.,* 2003) for comparison.

Distinct sub-populations were present in all three particles analyzed. For both the wild type and the chimeric α3 particles, this minor peak is significantly less dense than the major population. The density difference between major and minor populations is the same magnitude for wild type α3 and the chimera. The buoyant density curve of ϕX174 wild type particles reveals a sub-population of particles present that are substantially more dense than the major population and this minor population of ϕX174 is the same density as the majority of α3 wild type particles.

As further analysis of solution characteristics, the migration of wild type and mutant virions were analyzed side by side in bi-directional, native agarose gels, which assay for differences in size and net surface charge (Serwer and Pichler, 1978). After electrophoresis, the gel was processed as previously described (Hafenstein and Fane, 2002: Chapter 2) and particles were eluted and titered. For both wild types and the chimeric particles a single population peak was detected migrating toward the positively charged anode (Figure 4.4), however, migration rates differed. Alpha 3 wild type particles migrated faster than ϕX174 wild type particles, with the chimera intermediate between the two.

Host cell attachment is a function of the outer surface of the capsid conferred by coat protein surface residues. Attachment assays were performed as previously described (Hafenstein and Fane, 2002) and in Chapter 2. The attachment efficiency is measured by unattached virion titered from the supernatant at progressive time-points. The attachment efficiency of ϕX174, α3 wild type and the chimera all differ widely (Figure 4.5). The chimeric particles attach with efficiency two orders of magnitude greater than the α3 wild type. Given the exact nature of the capsid composition of α3 and the chimera; it is possible that the organization of the DNA, as conferred by the DNA binding protein, is affecting the outer surface topography of the capsid.

The stoichiometry of the minor vertex protein in infectious wild-type and chimeric α3 particles may differ. Although øX174 are related viruses, critical differences

between the two species are apparent. One of these differences is in the incorporation of the minor vertex protein, protein H. Both biochemical and structurally analyses indicate that there are 12 copies of protein H per øX174 wild type virion, one at each vertex (Hayashi *et al.,* 1989; McKenna *et al.,* 1992, 1994). However α3 particles appear to have only 6-8 copies of this protein. Several factors prompted an investigation of the minor vertex protein content of the chimeric particle. 1) The path taken by the øX174 J protein and presumably associated DNA, encircles the five-fold axes of symmetry (McKenna *et al.* 1992, 1994), to a much higher degree than that of the α3 protein (Bernal *et al.*, 2003). Density differences between the wild-type and chimeric α3 particles could be the consequence of H protein content. 2) Determining the amount of H protein within a crystal structure is complicated by its location at the five-fold axes of symmetry, which results in diffuse and unordered density. Quantifying the intensity of diffuse density is more difficult due smaller difference between signal and background. 3) Although the biochemical analyses were also performed on wild-type α3 particles, they were conducted with material from the bulk purifications required for crystallography. Specific infectivities were not calculated, and no biological assays were performed. Hence, the contribution of uninfectious, and perhaps abnormal, particles was not determined.

Wild-type øX174, α3, and chimeric particles were purified as described in Burch and Fane (2003). Briefly, all material with a buoyant density between 1.3 –1.42 gm/cm^3 was purified from infected cells. Material in this density range constitutes unassembled protein (1.3gm/cm^3), assembled empty capsids, procapsids, partially filled capsids (1.32-

1.38 gm/cm^3), and mature virions (1.40 gm/cm^3). This pooled material is then analyzed by rate zonal sedimentation (5- 30% sucrose), which separates as a function of velocity. After fractionation, the OD_{280} and titer of each fraction was determined. In each sample, only one peak was found in the 115S area of the gradient by OD_{280}. The OD profile corresponded to the infectivity profile (data not shown). There was no significant difference in specific infectivity between the three samples. After electrophoresis the gel was scanned and analyzed as described in (Hafenstein and Fane, 2002). The results of the analysis are presented in Table 4.2. Assuming 10-12 copies of protein H in øX174, wild-type α3 particles contain 6-7 copies of this protein per particle. Therefore the results presented in Bernal *et al.* (2003) were verified by this more stringent protocol. Intrinsic error, which was 3.8%, was calculated by comparing coat and major spike protein ratios. The H protein content between the α3 wild-type and chimeric particles differs by 10 %, when F:H intensities are compared, or 13%, when G: H intensities are compared. While the results of these assays are suggestive, they fall short of compelling. The analysis will need to be repeated.

Determination of the wild-type and chimeric α3 crystal structures. The results of these analyses represent a collaborative effort between the Fane and Rossmann laboratories, with one graduate student in each group being the main experimentalists. Due to the collaborative nature, as discussed in the Introduction section of this dissertation, a comparison of the atomic structures of wild type α3 and the chimera structures are briefly summarized here. However, they are interpreted in the Discussion

of this chapter. The atomic structure of the two coat proteins shows no major structural differences in the outer surface of the capsid at 3.5 Å resolution. The F proteins have a root mean square (r.m.s.) deviation of less than 0.3Å when superimposed via the icosahedral symmetry axes. As expected, more J density was visible in the chimera compared to α3 wild type and as shown in Figure 4.6 and the α3 genome is arranged differently in the chimera than in either wild type α3 or wild type øX174 (Figure 4.7). However, the arrangement has some øX174 characteristics.

The binding cleft in F where the C-terminus of J interacts is highly conserved between α3 and øX174. The interactions between J and F proteins in this region are highly conserved between α3 wild type, the chimeric structure, and ϕX174 (Table 4.3). Moving away from the conserved C-terminus toward the divergent amino terminus of protein J there is a disordered region of the protein corresponding to the second DNA binding domain of the øX174 proteins and the mid-region of α3 protein. In α3, this region is the beginning of the one-turn helix comprised of the 11 amino terminal residues. In øX174 and the chimera, the øX174 J protein is devoid of secondary structure. In this area there are a substantial amount of conserved F and J protein interactions. For example, protein J and F residues A60 and D62, respectively (øX174 A59 and D61) are conserved even though the α3 J protein is helical and øX174 J is devoid of secondary structure. This suggests that the path that J proteins takes across the inner surface of F in this area is critical and remains conserved, despite different J protein structures and different F amino acid residues.

Discussion

Changing DNA packaging parameters influence the biophysical characteristics of the particle in solution. Alpha 3 chimeric particles have different biophysical properties than either wild-type α3 or øX174 as assayed by cesium chloride buoyant density centrifugation, native gel electrophoresis, and efficiency of host cell attachment. All three share the same relative infectivity, indicating that there is not a measurable proportion of faulty particles being assembled in the preparation of chimeric particles. Based on previous work, this was not entirely surprisingly. However, it was hoped that the atomic structure of the chimeric particle would more fully explain the basis of these different solution properties.

Packaging α3 with øX174 DNA binding protein seems to induce some øX174-like properties to the structure and organization of α3 DNA. Being able to package α3 virions using the øX174 J protein alters the protein component of the tether without mutagenesis. Weakening the tether by packaging with charge reduced mutant J proteins resulted in particles denser than wild type, possibly allowing more genomic secondary structure to form, and thus creating a greater collapse of coat protein pentamers. Conversely, packaging G4 or α3 with øX174 J protein may suppress secondary structure, producing virions that are less dense than wild type. A stronger association of the genome may result in more organized DNA, visible in the atomic structure. This

hypothesis was tested by comparing the preliminary X-Ray crystallography studies of the chimera to the atomic structure of α3 and to the øX174 structure.

In a comparison of ordered DNA density, the chimera appears more similar to øX174 than α3 wild type. The chimera has DNA density not seen in α3, and the arrangement of ordered nucleotides within the asymmetric unit seems highly conserved with øX174 (Figure 4.6). Viewing previously reported øX174 DNA density from low-resolution data (McKenna *et al.,* 1992) heightens the conservation of DNA organization between the chimera and øX174. The 1992 work assigned 11 nucleotides to the DNA density including the four nucleotides in the binding pocket. The seven other nucleotides are seen in two groups. The first group of three is associated with the end of the C-terminus of J protein. The last group of 4 is above the crook in the C-terminus of J, toward the five fold. This appears to be a common site of ordered DNA, although for all three virion types the arrangement differs.

Although atomic structures exist for all three particles being compared, they were solved over a period of ten years. In that time, the ability to interpret low intensity data, like DNA, has increased dramatically. Hence DNA features in the 1992-1994 øX174 structures may have been missed. With this in mind, the most dramatic difference in the ordered DNA structure may be near the two-fold axis of symmetry where there is density for two nucleotides in the chimeric structure. A reinvestigation of the 1992 data to

reevaluate the low intensity data may indicate that these nucleotides are øX174-like in their arrangement within the chimera.

The N-terminus of the øX174 J protein is not ordered in the chimera crystal structure. Unordered density does not mean that protein, or DNA, is not there, instead it means it is not easily visualized. For density to be ordered the components of the density must sit in nearly the exact same location in each one of the virions' 60 asymmetric units. Unordered density results from material in the same general location at each asymmetric unit, but in different conformations or folds. This leads to a diffuse diffraction pattern, an averaging of as many as 2-60 folds. In the case of the øX174 J protein in the chimera, as the protein crosses into the adjacent five-fold related asymmetric unit, interactions with the α3 coat protein do not tightly constrain its path to its destination, as would interactions with the øX174 coat protein. This is most likely due to the lack of coat-J protein interactions in this region. The coat protein residues that make these interactions in øX174 are not conserved in α3, which has a much smaller J protein that does not cross into the adjacent five-fold asymmetric unit.

Evolutionary implications. Producing the chimera allows an examination of a wild type protein functioning in two different environments. The structural analysis has provided clues as to why øX174 has evolved a more elaborate J while α3 has not. A larger, more basic J protein, with a proline rich spacer region separating two binding motifs, has evolved to package øX174. It has been established that the DNA binding protein

suppresses genomic secondary structure (Benevides *et al*, 1991). When folding the DNA genomes to the lowest free energy as predicted by computer analyses (Santa Lucia, 1998) the øX174 and α3 genomes have the same percentage of secondary structure. However, the α3 genome is 12% larger. This suggests that the øX174 genome folds into a more compact state and a more elaborate J protein may be needed to suppress genomic secondary structure. In addition, a comparison of the electrostatic potentials of the øX174 and α3 capsid inner surfaces indicates that the α3 interior is more basic, suggesting that there are more non-specific coat-DNA interactions in α3 to aid in the use of a less basic J protein for packaging.

Implications on the field of structural biology. In the field of structural biology, the X-ray structure historically has been the gold standard, holding the ultimate answer to every biological question. While this paradigm may have been reasonable thirty years ago, before advances in biotechnology expanded the detail and sophistication to which biological systems could be investigated. Data generated in many laboratories now challenges this belief. Dramatic differences in solution properties are not corresponding to appropriate and expected differences in X-ray structures, here and in other systems. Methodologically, this has led to a reexamination of how crystallographic conditions may influence structures and to a reassessment of the sensitivity of various assays. The electric field in a gel box or the G-force in the centrifuge may be more sensitive in detecting some structural differences. Scientifically, the very concept of the viral particle is changing. Applications in molecular dynamics suggests that the viral capsid is inherently

more flexible than ever realized. Viral particles seem to breathe. There is no one single particle, but a diverse population of conformations, existing in equilibrium with each other. An X-ray structure represents an average of the major population of particles that will associate to form a crystal lattice. Hence, here and in all fields of science, research will always be limited to the study of the most probable events.

There are several hypotheses to explain the lack of structural differences corresponding to differences in biophysical properties in solution. The simplest model would be a difference in diameter, with an expanded capsid causing a less dense virion. The 2.0 % density differences would correspond to a 1.2% difference in radius. But this was not seen in the atomic structure. A more complicated model might be an altered contour that is not ordered, or not present in every asymmetric unit. The central motif of the F protein is an eight-stranded antiparallel β barrel that runs tangential to the viral surface. If a β barrel has been shifted or is bulging outward to accommodate the foreign J protein, or there is an exposure of different side chains not present in every asymmetric unit, the differences will be averaged out in the analysis, and therefore they will not be seen.

The effects of altered protein stoichiometry cannot be discounted. There may be fewer copies of protein H, probably just one, incorporated in the chimera than in α3 wild type. However, this is a preliminary analysis and requires further investigation. Since H protein incorporation is complete prior to packaging a model for alternative H incorporation in

the chimera would have the DNA led by J protein causing a displacement of H protein from the hydrophobic channel formed at the five fold axes of symmetry. The path traced by J within the asymmetric unit shows two conserved interactions between J and F residues in øX174 and the chimera that are in close proximity to the five fold axis of symmetry. These interactions would lead bound DNA in a close circle around the five fold axes of symmetry, a path not seen in α3 wild type. While suggestive, this model would result in a slight variation in protein H content that should not be sufficient as the only factor, but could be contributing to the buoyant density differences, especially of displacement results in some H proteins being only partially extruded. The proteins would remain associated with the capsid, but there partial external location would decrease the buoyant density of the particles.

Because each øX174 J protein contains 13 more residues per copy than α3 J protein, the chimera will contain more J protein than wild type α3, if the wild type ratio of J:F remains the same. But the effect of packaging an additional 845 kDa of protein mass is impossible to gauge. It is not possible at this point to rule out the extra protein mass packaged into the chimeric particles as producing some effect on density of the particle. However, it does not seem likely that the extra length of J protein complexed with DNA and the inner surface of the capsid would be altering the native gel migration or attachment properties of the capsid simply by the presence of sheer mass. Both assays are a function of the outer surface of the capsid. All previous work done on this project

indicates that the J protein functions as an active biological component of the protein-DNA tether which can alter external characteristics of the capsid of the mature virion.

The proline residues in the spacer region of J protein have been proposed to function to organize the DNA. The DNA is organized differently in all three particles and the DNA is known to be a structural element in *Microviridae*. It has been shown that the presence and interaction of the genome with the capsid increases the stability of the virion structure and decreases the dynamics of the capsid. (Da Poian *et al,* 2002) In these studies with comoviruses, the genome apparently stabilizes the virion by reducing the flexibility of the proteins. In the *Microviridae*, despite extensive hydrogen bonding and coat to coat protein interactions, flexibility of the capsid may be affected by the quaternary structure formed by the genome complexed with the coat and DNA binding proteins. Changing the DNA or protein components may lead to altered solution properties because the flexibility and stability of the capsid has changed. This dynamic would not be visualized by X-ray crystallography.

Finally, Das groβe und kleine Bilt

The laws of thermal dynamics have not been disproved. In the case of the *Microviridae*, more than one particle type is present within the species population. Cesium chloride buoyant density centrifugation and simple migration in native gel show the existence of multiple forms of virion particles existing in equilibrium. Even the most

prevalent particle type is represented by variations as evidenced in the broad nature of the peaks seen in the biological assays. As discussed in Hafenstein and Fane (2002) and in Chapter 2, intact virion migration in native agarose gels, for wild type øX174, a major population peak was detected migrating toward the positively charged anode, referred to as the negative or major population (Figure 4.8, panel A). There were also positively charged populations in each sample (Figure 4.8, panel B). While these positively charged particles represent a minor portion of the total wild type population (1:1000 ratio), alterations to the protein or DNA component of the tether result in a shift in population ratios between conformation types.

When population peaks were harvested from a first run wild type øX174 native gel, loaded and electorphoresed in a second native gel; particles again migrated towards both the anode (Figure 4.9, panel A) and the cathode (Figure 4.9, panel B) and the same population ratio was observed. Virion types harvested from native gels appear to interchange in solution, reasserting an equilibrium, and with the next exposure to the electrical field, which most likely hinders conformational changes, all conformations are evidenced. Hence a multitude of structures appear to exist in a complex equilibrium. There is no one particle.

Table 4.1: Cross functional analysis of *Microviridae* J genes.

Mutant	EOP[1] on BAF30 (*recA*) with: pøXJ	pG4J	pα3J	no plasmid
øX174 *amJ*	1.0	1.0×10^{-6}	1.0×10^{-6}	1.0×10^{-6}
G4 *amJ*	1.0	1.0	0.7	2.0×10^{-6}
α3 *amJ*	1.5	1.0	1.0	3.0×10^{-5}

[1] Assay titer / titer on BAF30 (*recA*) harboring plasmid with the same J gene.

Table 4. 2: Protein composition of wild type and chimeric particles[1].

Proteins[2]	ØX174	chimera	α3
F/H	1.18	2.79	2.53
F/G	1.22	1.01	1.05
G/H	0.97	2.75	2.42

[1]Proteins were separated by SDS-PAGE, stained and digitally photographed. Ratios were calculated using band intensities derived via 1D image analysis software (Kodak Digital Science™).

[2]F, H, and G denote the major capsid, pilot protein, and spike proteins respectively.

Table 4.3 Protein J and protein F interactions to 3.6 Å in alpha 3 wild type, α3 packaged with øX174 J protein, and øX174 wild type.

J sequence		Protein J Residues			Residues in protein F making polar contacts with J		
α3	**øX174**	α3	chimera	**øX174**	α3	chimera	**øX174**
	S1						
	K2			K2			$L236_5$, $V237_5$
	G3			G3			$L236_5$, $V237_5$, $M238_5$, **$R239_5$**
	K4			K4			$M238_5$, **$R239_5$**
	K5			K5			$M238_5$, **$R239_5$**
	R6			R6			**$R239_5$**,**$S240_5$**, **$N241_5$**
	S7			S7			**$S240_5$**,$K269_5$, **$S240_5$**, K269, water mediated
	G8			G8			**$L242_5$**,$T267_5$, **$Y268_5$**, $K269_5$
	A9						
	R10		R10	R10		$T268_5$	$T267_5$, $K269_5$, $V46_5$, $T267_5$ water mediated
	P11						
	G12		G12	G12		$T268_5$	$T267_5$ $T267_5$ water mediated
	R13						
	P14		P14	P14		$Q266_5$	$Q265_5$
K1	Q15						
K2	P16		P16	P16	$R412_5$	D62	D61
A4	L17		L17	L17	$L18_5$, $Q410_5$	D62	A59, I60, D61
R5		R5			I61, D62,		
	R18		R18	R18			D61, W243
R6		R6			D62, W244, $R412_5$		
	G19		G19	G19		W244, $R412_5$	**$K407_5$**
S7		S7			$L18_5$, W244, D357		
	T20			T20			$H16_5$, $L17_5$, **$S356$, $K407_5$**, S15 water mediated
P8					$H17_5$, $R412_5$		
	K21		K21	K21		$D14_5$, $R412_5$	$D13_5$, **$K407_5$**
S9							
	G22		G22	G22		$S16_5$, $R412_5$	$D13_5$, $S15_5$, **$K407_5$**, $N409_5$
R10		R10			D14, $S16_5$, H355, D357		
	K23			K23			$D44_5$
R11	R24		R24	R24			**$P11_5$**, $D13_5$, **$Y413_5$**
K12	K25				$D14_5$		
G13	G26						
A14	A27						
R15	R28		R28	R28	$V424_5$	V424	$R420_5$ water mediated
L16	L29		L29	L29	$V424_5$	$V424_5$	**Q349**, R352, **$T419_5$**
W17	W30	W17	W30	W30	N168, I169, I350,	N168, I169, A172	K166, N167, I168, A171, **Q349**
Y18	Y31	Y18	Y31	Y31	L174, $R425_5$	P173, $V424_5$,$R425_5$	P174, F211 R420, water mediated
V19	V32	V19	V32	V32	P139, W140	P139, W140, Y211	P138, W139,
G20	G33	G20	G33	G33	T210, Y211, F212, Q214	Y211, F212, M213, Q214	P138, **D209**, Y210, Q213
G21	G34	G21	G34	G34	P139	P139	P138
S22	Q35	S22			R215		
Q23	Q36	Q23	Q36	Q36	Y135, A138, C164, K167	Y135, A138, C164, K167	A137, K166
F24	F37	F24	F37	F37	F68, Y135, R291	F68, Y135	F67, Y134, F135, **R239**, R290

Subscripts denote symmetry related subunits numbered clockwise
Selection criterion based on a distance of 3.6 Å
In bold are øX174 F protein residues that are not conserved in α3 F protein.
Of the øX174 F protein residues that interact with J protein, 74% are conserved in alpha 3.

FIGURE LEGENDS

FIG 4.1 Coat protein pentamer as viewed at the five fold axis of symmetry with J protein traced in neon green.

FIG 4.2 The primary sequence of the *Microviridae* J proteins. Basic residues are highlighted, proline residues in bold face, and the highly conserved C-terminal residues boxed.

FIG 4.3 Buoyant densities of wild type α3, chimera, and wild type øX174. All three types of particles were analyzed within the same gradient. The chimera was propagated by growing an *α3amJ* mutant on a BAF30*RecA* cell line harboring an inducible clone of the øX174 J gene. An additional genetic marker, *amB*, was placed in the α3 wild type background and the *amD* marker was placed in the øX174 wild type. This allowed the particles to be distinguished by specifically titering on different mutant specific cell lines. Symbols: closed circles, α3 wild type; open circles, chimera; closed squares, øX174 wild type.

FIG 4.4 Native gel migration of α3 wild type, chimera, and øX174. Negative gel section numbers indicate movement toward the (-) electrode, positive gel section numbers

indicate movement toward the (+) electrode. Symbols: closed circles, α3 wild type; open circles, chimera; closed squares, øX174 wild type.

FIG 4.5 The attachment efficiency of ϕX174, α3 wild type and chimera particles. Efficiency was assayed as the titer of unattached virion at progressive time points. Symbols: closed circles, α3 wild type; open circles, chimera; closed squares, øX174 wild type.

FIG 4.6 Electrostatic potential of the inner surface of the virion increases with binding of the øX174 DNA binding protein, J. Dimers of F are shown as viewed from the inside of the virion. Panel A is an F dimer of α3; panel B is α3 chimera showing a dimer of F with ordered øX174 J density traced in red. Panel C, is a dimer of wild type øX174 F; panel D includes øX174 J density as a tracing in red. Data for these figures and the resulting graphics were generated by Ricardo Bernal from Michael G. Rossman Lab, Purdue.

FIG 4.7 Comparable ordered DNA density for α3, chimera, and øX174 wild type particles in an asymmetric unit. The stereo image shows one coat protein with øX174 DNA density in black, α3 in yellow, and the chimera in purple. Protein J is red and F protein is aqua. Data for these figures and the resulting graphics were generated by Ricardo Bernal in Michael G. Rossman Laboratory (Purdue University).

FIG 4.8 Panel A. Bidirectional native gel migration of øX174 wild type. Negative gel section numbers indicate movement toward the (-) electrode, positive gel section numbers indicate movement toward the (+) electrode. The minor, positively charged population peaks at section–13. Panel B inset shows the minor population.

FIG 4.9 Panel A. Bidirectional native gel migration of harvested particles from the major and minor peaks separated from the previous native gel shown in Figure 4.8. The particles that migrated previously as the major population (negatively charged particles) are closed circles. Open circles indicate the migration of particles that were isolated from section –13, the minor peak of positively charged particles in the first run gel shown in figure 4.8. The dashed line is a phage background control.

FIG 4.1


øX174 SKGKKRSGAR PGRPQPLRGT KGKRK GARLWYVGGQQF
α3 KK.ARRS PSRRK GARLWYVGGSQF
G4 KKSIRRS GGKSK GARLWYVGGTQY

FIG 4.2

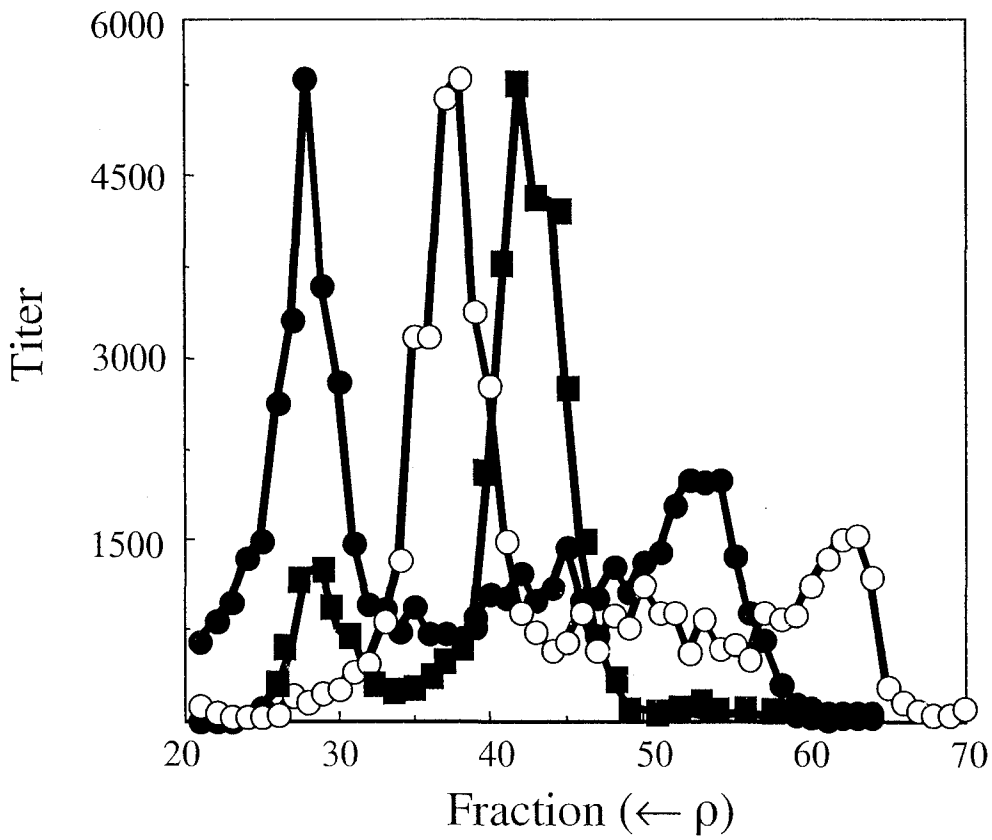

FIG. 4.3

FIG 4.4

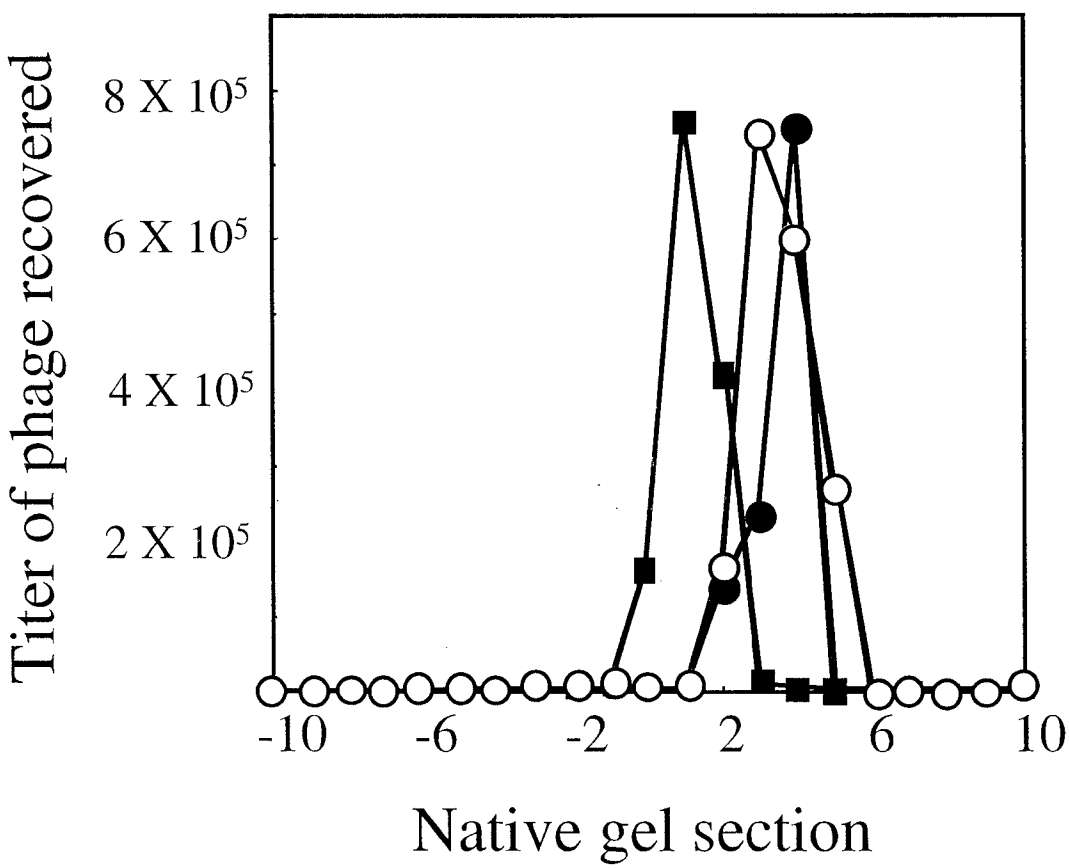
Titer of phage recovered
8 X 10^5
6 X 10^5
4 X 10^5
2 X 10^5
-10
-6
-2
2
6
10
Native gel section

FIG 4.5

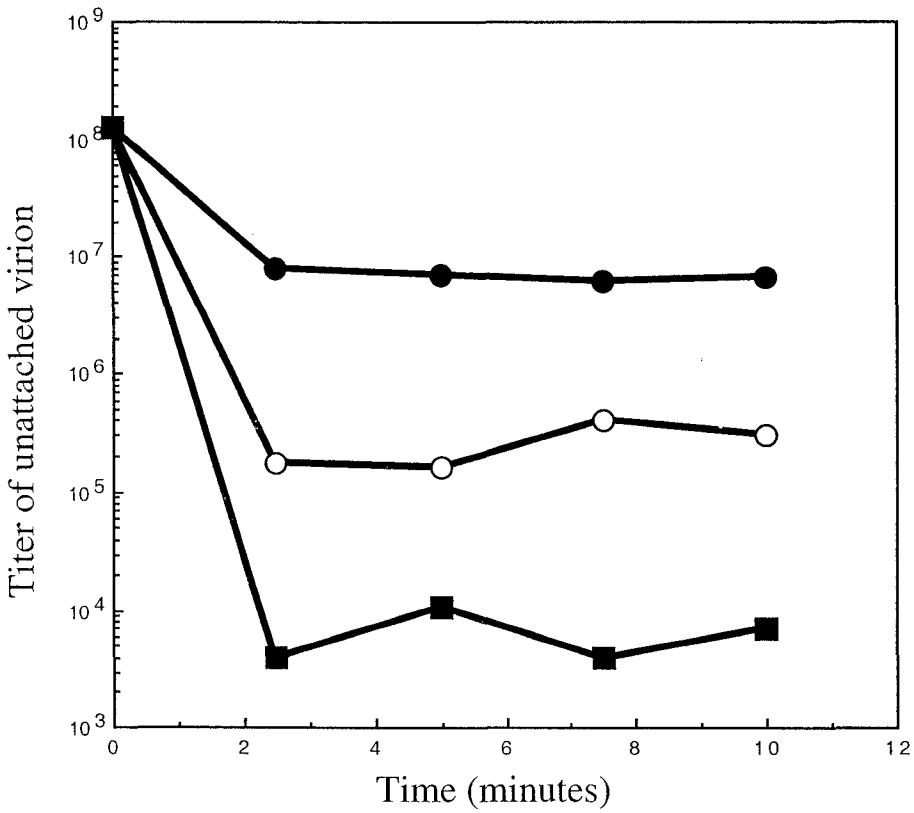
Titer of unattached virion
10^9
10^8
10^7
10^6
10^5
10^4
10^3
0
2
4
6
8
10
12
Time (minutes)

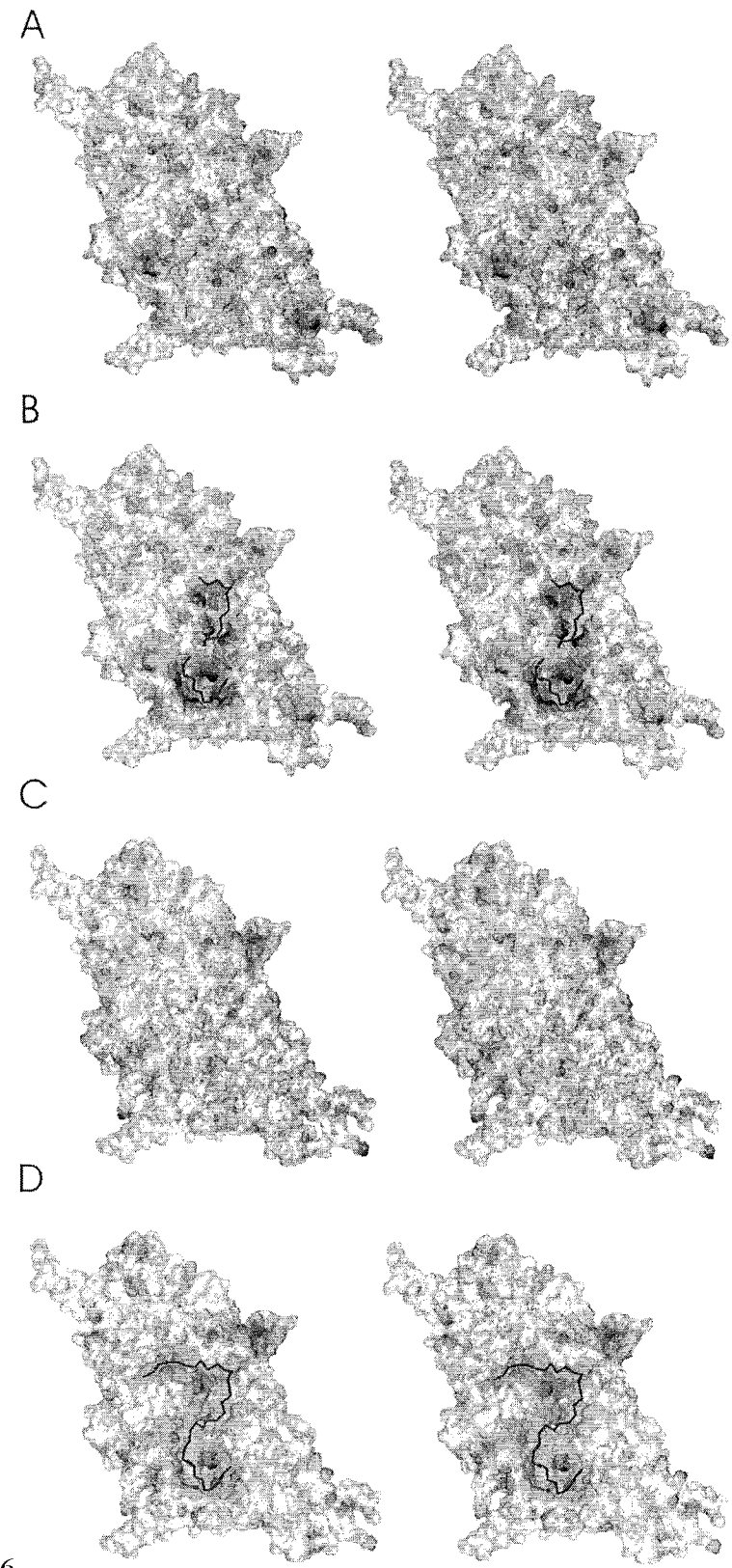

FIG 4.6

FIG 4.7

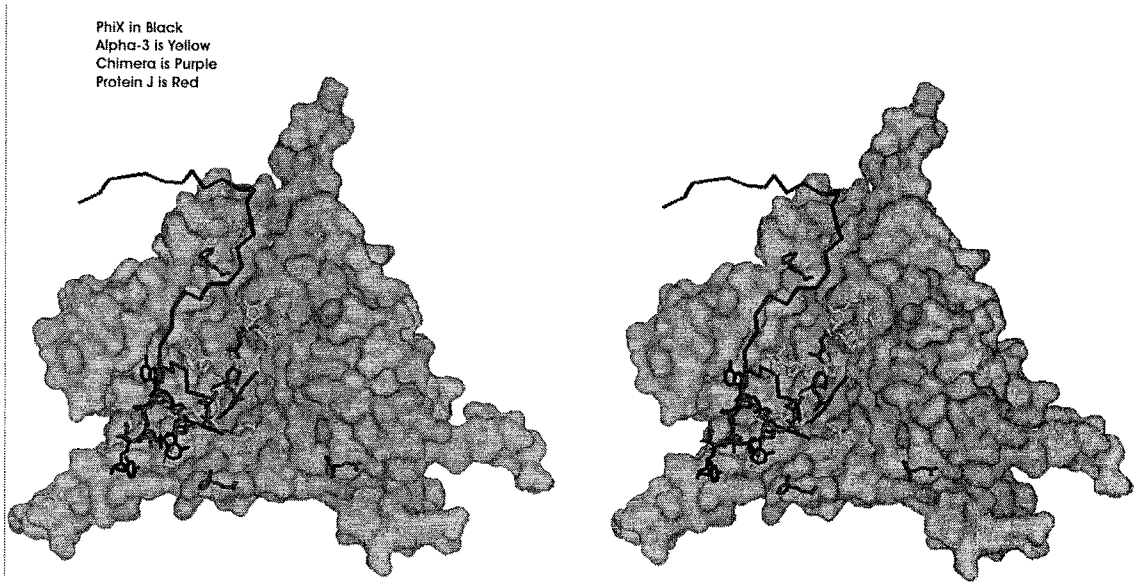
PhiX in Black
Alpha-3 is Yellow
Chimera is Purple
Protein J is Red

FIG. 4.8

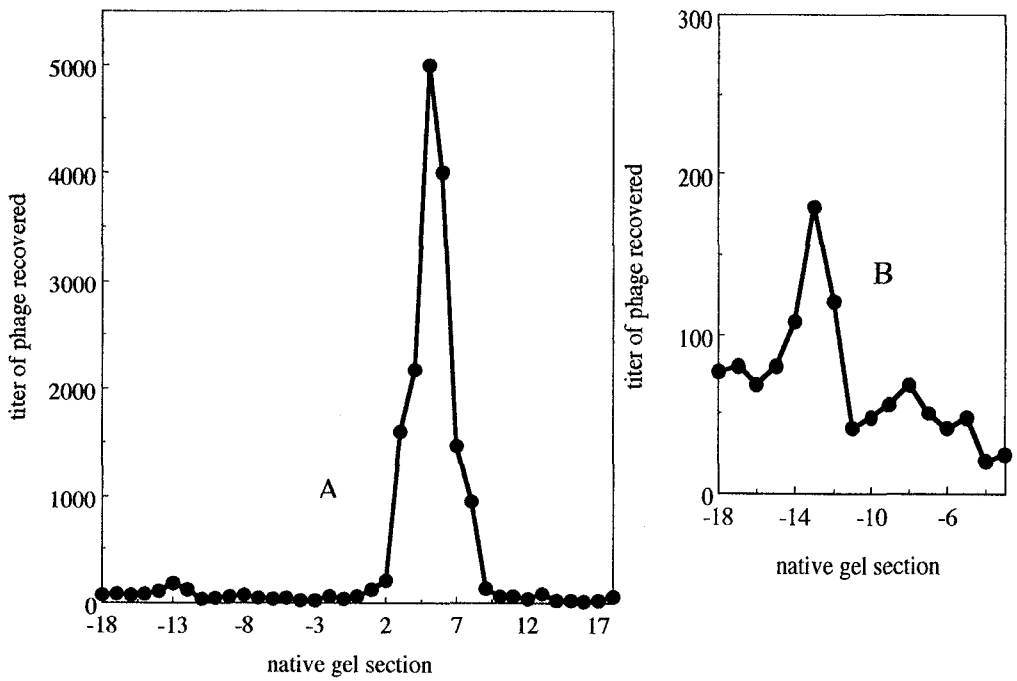
titer of phage recovered
5000
4000
3000
2000
1000
0
A
-18
-13
-8
-3
2
7
12
17
native gel section
titer of phage recovered
300
200
100
0
B
-18
-14
-10
-6
native gel section

FIG. 4.9

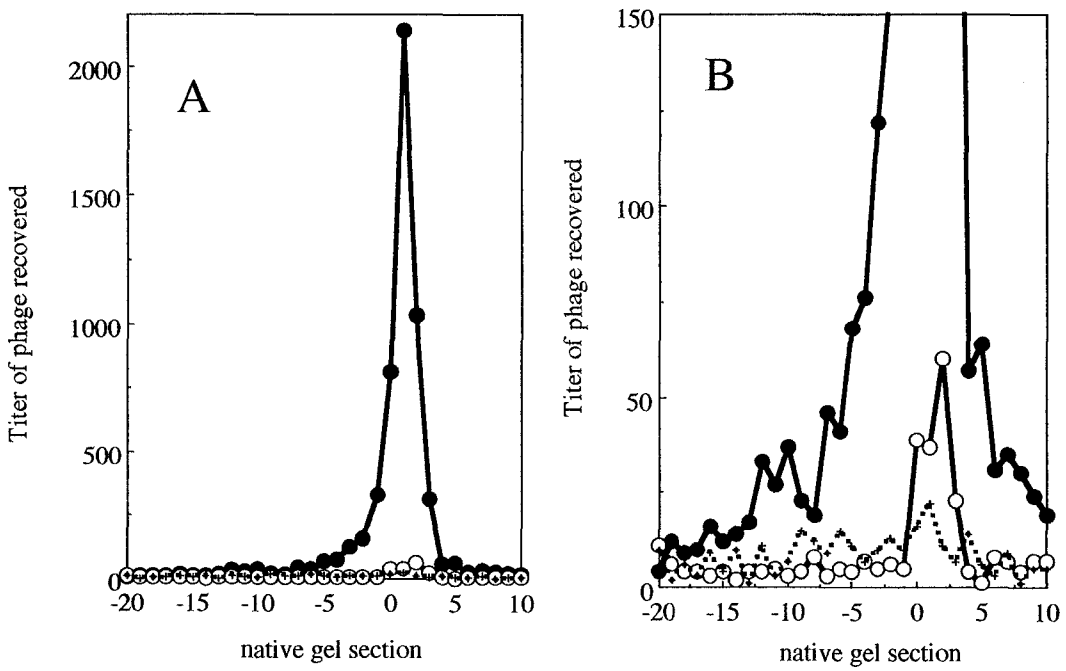
A
2000
1500
1000
500
0
Titer of phage recovered
-20 -15 -10 -5 0 5 10
native gel section
B
150
100
50
0
Titer of phage recovered
-20 -15 -10 -5 0 5 10
native gel section

APPENDIX A:

PhiX174 genome-capsid interactions influence the biophysical properties of the virion: evidence for a scaffolding-like function for the genome during the final stages of morphogenesis

PhiX174 genome-capsid interactions influence the biophysical properties of the virion: evidence for a scaffolding-like function for the genome during the final stages of morphogenesis

Susan Hafenstein and Bentley A. Fane*

Department of Veterinary Sciences and Microbiology, University of Arizona. Tucson , AZ, 85721

Running title: Genome-capsid interactions and virion structure.

*Corresponding author.

Department of Veterinary Sciences and Microbiology

University of Arizona, Building 90

Tucson, Arizona, 85721-0900

Tel: 520-626-6634

Fax: 520 621-6366

ABSTRACT

During the final stages of øX174 morphogenesis, there is an 8.5 Å radial collapse of coat proteins around the packaged genome, which is tethered to capsid's inner surface by the DNA binding protein. Two approaches were taken to determine whether protein-DNA interactions affect the properties of the mature virion, and hence the final stages of morphogenesis. In the first approach, genome-capsid associations were altered with mutant DNA binding proteins. The resulting particles differed from wild type virion in density, native gel migration, and host cell recognition. Differences in native gel migration were especially pronounced. However, no differences in protein stoichiometries were detected. An extragenic second-site suppressor of the mutant DNA binding protein restores all assayed properties to near wild type values. In the second approach, øX174 was packaged with foreign, single-stranded, covalently closed, circular DNA molecules identical in length to the øX174 genome. The resulting particles exhibited native gel migration rates that significantly differed from wild type. The results of these experiments suggest that the structure of the genome and/or its association with the capsid's inner surface may perform a scaffolding-like function during the procapsid to virion transition.

INTRODUCTION

Unlike many double-stranded (ds) DNA viruses which use one scaffolding protein (14, 34), øX174 morphogenesis is dependent on two species (30). Together, these two proteins perform the full spectrum of functions found in one-protein systems. However, after procapsid assembly, the final stages of øX174 morphogenesis differ. In ds DNA systems, procapsids expand during packaging (32, 37, 41) and the genome forms a dense core (18). In contrast, øX174 morphogenesis concludes with the collapse of coat proteins around the single-stranded (ss) genome, which is associated with the inner surface of the capsid (15, 16, 38, 39).

As illustrated in Figure 1, øX174 genome replication is coupled to DNA packaging. The pre-initiation complex, consisting of the host cell *rep* and viral A and C proteins, associates with the procapsid forming the 50S complex (21, 40). The viral A protein binds the origin of replication in replicative form DNA. This is both necessary and sufficient for packaging specificity (4, 26). Upon binding, protein A nicks the origin (47) and forms a covalent ester bond with the DNA (19). After one round of rolling circle synthesis, protein A cuts and ligates the newly generated origin, generating a circular ss molecule (7, 20). This packaging mechanism produces precise genomes of identical length (4).

The highly basic DNA binding protein (J) enters the procapsid along with the ssDNA genome, (27), associating with the genome via charge-charge interactions (33). Once in the procapsid, the C-terminus binds to a coat protein cleft (38, 39). This may facilitate further interactions with a small cluster of adjacent basic capsid amino acids. Accordingly, a portion of the packaged DNA (8-10%) is icosahedrally ordered, tethered to the inner surface (38, 39). This tether constrains the spatial orientation and secondary structure of the remaining nucleotides (5). Morphogenesis completes with the dissociation of the external scaffolding protein and an 8.5 Å radial collapse of capsid pentamers. Whether the tethered genome influences the integrity and/or magnitude of this collapse is addressed in this report.

The interaction of icosahedral capsid proteins with single-stranded genomes is a well-documented phenomenon. Many viral RNA capsid proteins have internally localized basic N-termini extensions that nonspecifically bind genomes (11, 12, 36, 43, 48, 49). The phenomenon has been documented in single-stranded animal viruses as well (1, 10, 25, 46). To investigate the functions of the øX174 genome tether, both the protein and nucleic acid components were altered. The protein component was altered by mutations in the DNA binding protein. The DNA component was altered by packaging foreign, unit-length, single-stranded, circular DNA molecules. In both instances, the altered particles were infectious but exhibited different biophysical properties.

MATERIALS AND METHODS

Phage plating, stock preparation, media, DNA purification, bacterial strains, and plasmids. Plating protocols, media, and stock preparation have been previously described (22). *E. coli* C strains: C122 (*sup*^{0}) is the wild type host; BAF 5 contains a *supE* mutation (22). BAF 30 is a *rec* A- derivative of C122 (23). Plasmids pøXB and pøXDJ contain IPTG inducible clones of the denoted øX174 genes (8,9). The *sly* D host mutation confers resistance to øX174 E-protein mediated lysis (42). The *gro89* host mutation blocks DNA packaging (21).

Phage mutants. The øX174 J mutants, *J3K->LI*, *JK->ALL*, and *J3K->LII/su(J)-FS1F* have been previously described (33). The *su(J)-FS1F* mutation was placed into the *J3K->LI* background by oligonucleotide mediated mutagenesis (24). Progeny that had acquired the *su(J)-FS1F* mutation were identified by selecting against the temperature sensitive phenotype of the *J3K->LI* parent. Two rounds of oligonucleotide mutagenesis were performed to place the *su(J)-FS1F* mutation in the wild type background. Genotypes of all strains were verified by direct DNA sequence analysis.

Buoyant density gradients. For small-scale experiments in which two or three different particles were analyzed within the same gradient, 10^5-10^6 particles were mixed into a 1.4 g/cm^3 CsCl solution and spun for 47.5 hr at 23,000 rpm in an SW51 rotor (Beckmann). Gradients were divided into 80-85 fractions. The location of infectious particles was

determined by a plaque assay. For large-scale preparations of *JK->ALL* 70S particles, 100 ml of *slyD* cells (2.0 X 10^8 cells/ml) were infected (MOI=5) at 33°C and incubated for two hours. To generate wild type procapsids, *gro89* cells were infected with lysis deficient øX174 *am(E)W4*. Infected cells were harvested, resuspended in 10 ml BE buffer, and lysed with T4 lysozyme. Cellular debris was eliminated by centrifugation. The supernatant was layered atop CsCl step gradients and spun as previously described (22). Exogenous virions (1.0 X 10^6) were added to gradients as a density marker. Procapsid and 70S particle bands were clearly visible after centrifugation. Fractions were titered to determine the location of the wild type marker phage.

Native agarose gel electrophoresis. To examine particles by native gel electrophoresis, 10 µl samples, containing 1.0 X10^8 pfu, were mixed with 6 X gel loading buffer (0.25% bromophenol blue, 0.25% xylene cyanol FF, 30% glycerol). Samples were bi-directionally electrophoresed through 0.8% (w/v) agarose TBE gels (TBE: 45 mM tris-borate; 1.0 mM EDTA) for 10 hours at 24 volts/cm^2. After electrophoresis, lanes were cut into 2.0-mm horizontal sections with a modified egg-slicer. Particles were eluted from the gel by vortexing in 0.1 ml HFB buffer. The location of infectious particles was determined by a plaque assay.

Attachment assays. *E. coli* C122 cells were grown to a concentration of 1.0 X 10^8 cells/ml and concentrated 5-fold in growth media (1.0 % tryptone, 0.5% KCL). $MgCl_2$ and $CaCl_2$ were added to a concentration of 10 mM and 5.0 mM, respectively.

Approximately 1.0 X10^8 phage were added to 1.0 ml of cells and incubated at 37^0 C for specified time intervals (see figures). At sampling times, attached phage were removed by centrifugation. Supernatants were titered to determine the level of unattached virions.

Construction of *amp*^{R} packaging plasmids and transducing particles. øX174 DNA containing the øX174 origin of replication was amplified. The 5' PCR primer was designed to introduce an *Nco* I site into the fragment that was then initially cloned into TOPO 2.1 vector (Invitrogen). The TOPO vector was digested with *Nco* I and *EcoR* I (adjacent to cloning site), and the fragment was placed into PSE420 (Invitrogen) digested with the same enzymes (PORI). To bring the size of PORI up to 5386 base pairs, additional material was cloned behind the øX174 origin. These DNA sequences were obtained by amplifying pSE420 DNA between bases 3302 and 3776. This PCR fragment was first placed into a TOP0 2.1 and the orientation of the insert was determined. Depending on orientation, plasmids were cut with *Bam* HI and *Xba* I, or *Not* I and *Sac* I; then cloned into PORI that had been prepared with *Bam* HI and *Nhe* I, or *Not* I and *Sac* I. Plasmids were transformed into BAF 30 *recA* cells. Transducing particles were produced by infecting cells harboring the packaging plasmids with wild type øX174. The presence of the origin of replication in the plasmid is both necessary and sufficient for packaging a single-stranded version of the vector (4, 26). Lysates contain both virion and transducing particles. The titer of transducing particles was determined by infecting 1.0 X 10^8 *slyD* cells at an MOI of 0.1 and subsequent plating on ampicillin (100 μg/ml) plates. The low MOI and *slyD* cells were used to prevent co-infections and a second round of infection by

progeny virions, respectively. The ratio of progeny virions to *amp*^{R} transducing particles was approximately 50:1 in both infections. This represents typical values for these types of experiments (21).

RESULTS

Complete genome encapsidation is not required for the completion of genome biosynthesis. *Microviridae* genome biosynthesis and DNA packaging are concurrent processes (27). Previous work with the øX174 *J* mutants used in these studies demonstrated that mature packaged particle formation was a function of the number of charged residues of the protein (33). For example mutant J proteins with only nine basic amino acid residues (wild-type contains 12) could produce packaged particles with wild-type S values, 114S. However, several other biophysical properties differ (see below). Mutant proteins with only six basic residues produce particles that sediment at 70S (33). Analyzing the nature of the DNA associated with the 70S particles (partial v complete genomes), its susceptibility to DNAse, and the density of the 70S particles would determine if genome biosynthesis terminates with a cessation in packaging, or whether these two processes can be partly uncoupled *in vivo*.

The mutant genotypes and phenotypes used in these studies are summarized in Table 1. DNA associate with *JK->L ALL* 70S particles was extracted and analyzed by electrophoresis (data not shown). It was identical to virion DNA, indicating that single-

stranded DNA biosynthesis went to completion. The density of the particles was determined to 1.36 gm/cm^3 (Table 2) by buoyant density centrifugation, midway between the densities of the 114S virion (1.39 gm/cm^3) and the 108S procapsid (1.31 gm/cm^3) used as standards. These data indicate that the mutant J protein had no effect on genome biosynthesis, but the genome was not fully packaged. To test this hypothesis, particle densities were re-determined after DNAse treatment (2). While the densities of the virion and empty procapsid were not affected, the density of the 70S particle was reduced (Table 2).

Further characterization of infectious particles packaged with mutant DNA binding proteins. Unlike mutant J proteins with less than six basic residues, proteins with nine basic residues, *J3K->LI,* produce infectious particles with wild-type S values. However, the mutant has a small plaque phenotype and is both temperature and cold sensitive. Particles packaged with the *J3K->LI* and wild-type *J protein* were characterized by buoyant density centrifugation. The results of these analyses along with stoichiometric studies (see below) could determine whether the genomic DNA is fully encapsidated, more mutant J protein is needed for packaging, or other possibilities. For these experiments particles packaged with wild type J protein contained an amber mutation in gene B. Since particles could be independently titered (see figure legend), it was possible to characterize both types of virion within the same gradient. As seen in Figure 2, panel A, particles packaged with the mutant J protein are denser than wild type.

Several hypotheses could explain the observed density difference. In order to compensate for the mutant protein's reduced charge; more J protein may be needed for packaging. If the volume of the mutant particle remains unaltered, additional J protein would replace water, yielding a greater density. Although J protein stoichiometry is dictated by the capsid's icosahedral symmetry in wild type particles, protein stoichiometry was still assessed via PAGE and the relative amounts of coat (F), spike (G), and J proteins were determined. In a wild type virion each of these proteins is present in 60 copies. As summarized in Table 3, no significant differences in protein ratios were apparent. The variations seen in the F:J ratio is the same as that observed in the F:G ratio. It is possible that mutant particles may have retained a small amount of internal scaffolding protein that may have been below the limits of detection.

The greater density could have been caused by an increase of Cs^+ ions within the mutant capsid. In this model, the positively charged counter ion would supplant the missing basic amino acids in the mutant protein. To address this hypothesis, the density of *J-3K->LI* and *su(J)SIF/J-3K->LI* particles were compared. The *su(J)SIF* mutation is a nonallele-specific, extragenic, second-site suppressor of charge-altered J proteins, which has been previously characterized and described (33). The *su(J)SIF* suppresses both the small plaque and the temperature-sensitive phenotypes, raising plating efficiencies from 10^{-3} to 0.5 at the restrictive temperatures. An order of magnitude more *J-3K->LI* particles

was loaded on the same gradient with the double mutant. The position of the *su(F)SIF/J⁻ 3K->LI* could be ascertained and distinguished from *J⁻3K->LI* particles by titering at 42°C. As seen in Figure 2, panel B, they were readily separated by their densities, demonstrating that the suppressor is affecting the density of the capsid, restoring it to a more wild type value. Since both particles are packaged with the same mutant J protein, the observed density differences are probably not caused by Cs^+ ions or an excess of J protein in the *J⁻3K->LI* particles.

The extragenic suppressor is a ser -> pro substitution located at amino acid 1 of the coat protein (33). In wild type virion, this serine participates, via the γ O, in a three-way polar interaction (coat-coat-coat) directly atop the threefold axis of symmetry (38,39). The suppressing substitution most likely alters this interaction. Buoyant density gradients were performed to determine the effect, if any, of this substitution alone in a wild type background (Figure 3). Wild type, *su(J)-F S1F/wild type J* , and *J⁻3K->LI* particles were analyzed in the same gradient. The *su(J)-F S1F/wild type J* is slightly more dense than wild type.

Mutant and wild type particles migrate differently in native gels. The altered densities could be caused by general distortions affecting the entire capsid. If this were the case, alterations in genome-capsid interactions might be expressed on the capsid's external surface. The migration of wild type and mutant virions were analyzed side by side in bi-directional, native agarose gels, which assay for differences in size and net

surface charge (45). After electrophoresis, each lane was cut into 2-mm sections with a modified egg-slicer, and particles were eluted and titered. For both wild type and mutant particles, a major population peak was detected migrating toward the positively charged anode, referred to as the negative or major population (Figure 4). However, migration rates differed. With longer run times, the negatively charged particle peaks can be more clearly separated (data not shown). Mutant virions were not more sensitive to DNAse treatment than wild-type virions. Therefore, protruding DNA is probably not responsible for the faster migration rate. There were also positively charged populations in each sample. While these positively charged particles represent a minor portion of the total wild type population (1:1000 ratio), they are quite prominent in the mutant sample (1:3 ratio). As seen in Figure 5, the extragenic second-site suppressor restores mutant population ratios toward wild type levels.

Attachment assays as a probe for external capsid alterations: To further explore possible alterations on the outer surface, attachment assays were performed. For these assays, particles were incubated with exponentially growing cells at 37^{0}C as described in Materials and Methods. At five and ten minutes post infection, aliquots were removed and separated into pellet and supernatant fractions. The level of unattached virion was determined by titering the supernatant. The attachment of wild type particles is three orders of magnitude greater than that of mutant particles (Figure 6). The extragenic suppressor appears to correct for defects in host cell recognition, restoring attachment to intermediary efficiency. The level of unattached phage do not reflect the population ratios

observed in the native gel migration experiments. Similar experiments were conducted with separated negatively and positively charged mutant and wild type particles (data not shown). The results of those experiments did not differ significantly from the data presented in Figure 7, which assayed whole populations. In each instance, wild-type particles exhibited greater attachment efficiencies than mutant particles. While the positively charged particles of both the mutant and wild-type strains attached more efficiently than their negatively charged counterparts, it is not known whether this is a consequence of nonspecific binding to the negatively charged LPS. These simple assays do not determine whether the mutant particles are defective in DNA ejection, nor can be used to interpret the small plaque phenotypes of the mutants, which may be a consequence of both extracellular and intracellular factors.

Packaging foreign DNA also alters the biophysical properties of capsids. The DNA binding protein connects the genome to the inner surface of the capsid at each asymmetric unit. These 60 interactions allow the remainder of the single-stranded DNA genome to form limited secondary structure by base pairing upon itself within the virion. Hence, the base-pairing properties of the genome may influence the properties of the mature virion. To investigate this, øX174 was packaged with foreign DNA. Two packaging plasmids identical in length to the øX174 genome were constructed. These plasmids contain the øX174 origin of replication, which is both necessary and sufficient for packaging a single-stranded version of the plasmid (4, 26), and a gene encoding

ampicillin resistance. The two plasmids differed in one segment. This segment is repeated, in either a parallel-parallel or a parallel-antiparallel manner. The parallel-antiparallel configuration may introduce a large hair-pin loop. Particles were packaged *in vivo* by infecting cells harboring the plasmids with wild type øX174. Particles were analyzed by native gel electrophoresis and the gels were processed as described above. Each fraction was titered for phage and amp^R transducing particles (Figure 7). Two population peaks, positively and negatively charged, were detected for both sets of transducing particles (Figure 7). However, population ratios differ between the two constructs. In addition, the negatively charged populations migrate considerably faster than the internal øX174 control. Therefore to avoid running the transducing particles off the gel, run times were shorter than in the experiments described above. These data suggest that the nucleotide arrangement of the genome can change the biophysical properties of the capsid, perhaps by promoting or inhibiting genome secondary structure.

DISCUSSION

Interactions between the capsid inner surface and the packaged genome. Single-stranded øX174 DNA does not exist as a dense core in the capsid, as is observed in dsDNA bacteriophages (18). Instead, it is tethered to the capsid's inner surface by the highly basic DNA binding protein (J) and a group of basic capsid amino acid residues (38,39). There are 60 copies of protein J per virion, one associated with each coat protein. In the atomic model, the protein forms an S shaped polypeptide chain devoid of secondary structure. The C-terminus of the protein is tightly associated with a cleft,

located near the center of the coat protein. Moving toward the N-terminus, the protein traces a path toward the 5-fold axis of symmetry, crosses over to the adjacent capsid protein, and veers toward the C-terminus of the adjacent J protein. This motif suggests that the DNA binding protein guides the incoming genome into a somewhat ordered conformation. Accordingly, between 8-10% of the genome is ordered in the X-ray structure (38,39). Here and in other systems where higher percentages of the genome are ordered; such as Flock house virus (25); Pariacoto virus (46), and Satellite tobacco mosaic virus (36); the genome is icosahedrally ordered via interactions with structural proteins. This phenomenon is thought to contribute to capsid assembly and stability.

Altering the protein components of the tether. To investigate whether genome-capsid interactions affect the final stages of virion morphogenesis and/or the structure of the mature virion, particles packaged with mutant DNA binding proteins were characterized. The mutant particles were significantly more dense than wild type, but the protein composition of the two particles is probably identical. Therefore, the altered density was probably not caused by a gross excess of protein contained in a volumetrically fixed capsid. The effects of possible Cs^+ permeability were more difficult to discern. However, extragenic second-site suppressor procapsids packaged with the mutant DNA binding protein restored particle densities to near wild type values. Therefore a simple model, in which counter ions compensate for the loss of basic amino acids, is not supported by the data. This leaves the intriguing possibility that the dimensions or shape of the mutant particles may be altered.

When suppressor capsids are packaged with wild type J protein, the density values are slightly greater than wild type virion. Since the mutant particles are still more dense than wild type; the suppressor does not act via a compensatory mechanism. This suggests that there is an alternative maturation pathway that minimizes the effect of the genomic tether on the magnitude of capsid collapse.

To investigate whether differences were expressed on the capsid exterior, host cell attachment assays were performed. The particles packaged with the mutant DNA binding protein exhibited dramatically lower attachment efficiencies. As seen in the density experiments, the presence of the extragenic second-site suppressor restored values toward wild type. Differences in native gel migration, which is a function of size and net surface charge (45), were also observed. While small migration differences were seen between the wild type and mutant particles migrating toward the anode, the most dramatic differences involved the presence of a minor population migrating in the opposite direction. In wild type populations these particles represent a small sub-population (1:1000). However, the ratio was approximately 1:3 in mutant samples. As seen in the other assays, the extragenic suppressor restored the ratio to nearly wild type values.

Altering the nucleic acid component of the tether. Naked øX174 DNA is substantially richer in secondary structure than packaged DNA (5). Benevides *et al.*, (1991) hypothesized that the DNA binding protein inhibited the formation of secondary structure. Therefore, it is likely that an interplay between base-pairing and DNA-capsid association occurs. To investigate this hypothesis, two species of øX174 ampicillin transducing particles were generated by packaging single-stranded versions of unit length plasmids. The plasmids differed in the orientation of one cloned section, which was designed to introduce a large hairpin loop. Differences in migration rates and sub-population ratios were observed between the transducing particles and wild type virions.

While this may be one of the first reports of genome-capsid interactions affecting ssDNA viral structure and morphogenesis, the phenomenon has been well documented in ssRNA viruses. Flock house virus (FHV) RNA stabilizes contact regions (25) via nonspecific interactions with coat protein grooves at two-fold axes of symmetry. Deletions of the RNA-interacting residues results in the production of polymorphic structures (17). Packaging FHV with foreign RNA also leads to altered particles (6). Thus, genome-capsid interactions can effect the fidelity of virion morphogenesis, a function commonly associated with viral scaffolding proteins. A dramatic example of a scaffolding-like function for nucleic acids has been observed in Southern cowpea mosiac virus (SCMV). Deleting the highly basic, RNA-interacting N-terminus of the coat protein results in the production of T=1, as opposed to T=3, capsids (44). Similarly, the nature of the RNA

packaged in Brome mosaic virus can determine whether T=3 or 120-subunit capsids are formed (35).

The role of DNA-capsid interactions in øX174 is obviously not as dramatic. Procapsid morphogenesis does not require the genome (8, 28); however, two scaffolding proteins mediate this stage of assembly. In the procapsid there are no discernable pentamer-pentamer interactions. The integrity of the capsid appears to be maintained by the scaffolding proteins. After packaging, the internal scaffolding protein is extruded from the structure and replaced by the DNA binding protein and the tethered genome. This may supplant scaffolding function in the provirion. The provirion to virion transition is marked by the release of the external scaffolding protein and the completion of the 8.5 Å radial collapse of coat protein pentamers (15,16 38,39). Genome-capsid interactions may be mediating the magnitude and preserving integrity during the collapse.

Acknowledgements

The authors thank Mr. Bryan L. Jennings for technical assistance. This work was supported by a grant from National Science Foundation grant (B. A. F.).

REFERENCES

1. Agbandje-McKenna, M., Llamas-Saiz, A. L., Wang, F., Tattersall, P., and M. G. Rossman, 1998. Functional implications of the structure of the murine parvovirus, minute virus of mice. Structure **6:** 1369-1381.

2. Aoyama, A., Hamatake, R. K., and M. Hayashi. 1981. Morphogenesis of phi X174: in vitro synthesis of infectious phage from purified viral components. Proc. Natl. Acad. Sci. USA **78:** 7285-9.

3. Aoyama, A., Hamatake, R. K., and M. Hayashi. 1983. In vitro synthesis of bacteriophage øX174 by purified components. Proc. Natl. Acad. Sci. USA **80:** 4195-4199.

4. Aoyama, A., and M. Hayashi. 1985. In vitro packaging of plasmid DNAs into ϕX174 bacteriophage capsid. Nature **297:** 704-707.

5. Benevides, J. M., Stow, P. L., Ilag, L. L., Incardona, N. L., and G. J. Thomas, Jr. 1991. Differences in secondary structure between packaged and unpackaged single-stranded DNA of bacteriophage øX174 determined by Raman spectroscopy: A model for øX174 DNA packaging. Biochem. **30:** 4855-4862.

6. Bothner, B., Schneemann, A., Marshall, D., Reddy, V., Johnson, J. E., and G. Siuzdak. 1999. Crystallographically identical virus capsids display different properties in solution. Nature Struct. Biol. **6:** 114-116.

7. Brown, D. R., Roth, M. J., Reinberg, D. and J. Hurwitz. 1984. Analysis of bacteriophage øX174 gene A protein mediated termination and reinitiation of øX174 DNA synthesis. I. Characterization of the termination and reinitiation reactions. J. Biol. Chem. **259:** 10545-10555.

8. Burch, A. D., Ta, J., and B. A. Fane. 1999. Cross-functional analysis of the *Microviridae* internal scaffolding protein. J. Mol. Biol. **286**: 95-104.

9. Burch, A. D. and B. A. Fane. 2000. Foreign and chimeric external scaffolding proteins as inhibitors of *Microviridae* morphogenesis. J. Virol. **74:** 9347-9352.

10. Chapman, M. S. and M. G. Rossmann. 1995. Single-stranded DNA-protein interactions in canine parvovirus. Structure **3:**151-62.

11. Chen, Z.G., Stauffacher, C., Li, Y., Schmidt, T., Bomu, W., Kamer, G., Shanks, M., Lomonossoff, G., and J. E. Johnson. 1989. Protein-RNA interactions in an icosahedral virus at 3.0 A resolution. Science **245:** 154-9.

12. Choi, Y. G. and A. L. N. Rao, 2000b. Packaging of tobacco mosaic virus subgenomic RNAs by Brome mosaic virus coat protein exhibits RNA controlled polymorphism. Virology **275:** 249-257.

13. Dalphin, M. E. 1989. Bacteriophage øX174: Crosslinking studies of the virion and prohead and biophysical characterization of the gene J protein. Doctoral thesis, University of California, San Diego.

14. Desai, P., Watkins, S.C., and S. Person. 1994. The size and symmetry of B capsids of herpes simplex virus type 1 are determined by the gene products of the UL26 open reading frame. J. Virol. **68:** 5365-74.

15. Dokland, T., Bernal, R. A., Burch, A., Pletnev, S., Fane, B. A., and M. G. Rossmann. 1999. The role of scaffolding proteins in the assembly of the small single-stranded DNA virus øX174. J. Mol. Biol. **288:** 595-608.

16. Dokland, T., McKenna, R., Ilag, L. L., Bowen, B. R., Incardona, N. L., Fane , B. A. and M. G. Rossmann. 1997. Structure of a viral assembly intermediate with molecular scaffolding. Nature **389**: 308-313.

17. Dong, X.F., Natarajan, P., Tihova, M., Johnson, J.E., and A. Schneemann. 1998. Particle polymorphism caused by deletion of a peptide molecular switch in a quasi-equivalent icosahedral virus. J. Virol. **72:** 6024-33.

18. Earnshaw, W. C., and S.R. Casjens. 1980. DNA packaging by the double-stranded DNA bacteriophages. Cell 21: 319-331.

19. Eisenberg, S., and A. Kornberg. 1979. Purification and characterization of phiX174 gene A protein. A multifunctional enzyme of duplex DNA replication. J. Biol. Chem. **254:** 5328-32.

20. Eisenberg, S., Griffith, J., and A. Kornberg. 1977. øX174 cistron A protein is a multifunctional enzyme in DNA replication. Proc. Natl. Acad. Sci. USA **74:** 3198-3202.

21. Ekechukwu, M. C., Oberste, D. J., and B. A. Fane. 1995. Host and ϕX174 Mutations Affecting the Morphogenesis or Stabilization of the 50s Complex, a Single-Stranded DNA synthesizing Intermediate. Genetics **140:** 1167-1174.

22. Fane, B. A. and M. Hayashi. 1991. Second-site suppressors of a cold-sensitive prohead accessory protein of bacteriophage øX174. Genetics **128:** 663-671.

23. Fane, B. A., Head, S., and M. Hayashi. 1992. The functional relationship between the J proteins of bacteriophages øX174 and G4 during phage morphogenesis. J. Bacteriol. **174:** 2717-2719.

24. Fane, B. A., Shien, S., and M. Hayashi. 1993. Second-site suppressors of a cold sensitive external scaffolding protein of bacteriophage øX174. Genetics **134:** 1003-1011.

25. Fisher, A. J., and J. E. Johnson. 1993. Ordered duplex RNA controls capsid architecture in an icosahedral animal virus. Nature **361:** 176–179.

26. Fluit, A. C., Baas, P. D., and H. S. Jansz. 1985. The complete 30-base pair origin region of bacteriophage øX174 in a plasmid is both required and sufficient for *in vivo* rolling circle DNA replication. Eur. J. Biochem. **149:** 579-584.

27. Fujisawa, H. and M. Hayashi. 1976. Viral DNA- synthesizing intermediate complex isolated during assembly of Bacteriophage øX174. J. Virol. **19:** 409-415.

28. Hamatake, R. K., Aoyama, A. and M. Hayashi. 1985. The *J* gene of øX174: *In vitro* analysis of J protein function. J. Virol. **54:** 345-350.

29. Hamatake, R. K., Buckley, K. J. and M. Hayashi. 1988. The *J* gene of øX174: Isolation and characterization of a J gene mutant. Mol. Gen. Genet. **211:** 72-77.

30. Hayashi, M., Aoyama A., Richardson D. L., and M. N. Hayashi. 1988. Biology of the bacteriophage øX174. pp. 1-71. In: The Bacteriophages, Vol. 2, Edited by R. Calendar. Plenum Publishing Corporation, New York.

31. Ilag, L. L., Olson, N. H., Dokland, T., Music, C. L., Cheng, R. H., Brown, Z., McKenna, R., Rossman, M. G., Baker, T. S., and N. L. Incardona. 1995. Bacteriophage øX174 procapsid: Purification and structure at 25 Å resolution. Structure **3:** 353-363.

32. Jardine, P. J., and D. H. Combs, 1998. Capsid expansion follows the initiation of DNA packaging in bacteriophage T4. J. Mol. Biol. **284:** 661-672

33. Jennings, B. and B. A. Fane. 1997. Genetic analysis of the øX174 DNA binding protein. Virology **227:** 370-377.

34. King, J., and S. Casjens. 1974. Catalytic head assembling protein in virus morphogenesis. Nature **251:** 112-9.

35. Krol, M. A., Olson, N. H., Tate, J., Johnson, J.E., Baker, T. S., and P. Ahlquist. 1999. RNA-controlled polymorphism in the *in vivo* assembly of 180-subunit and 120-subunit virions from a single capsid protein. Proc. Natl. Acad. Sci. USA **96:** 13650-13655.

36. Larson, S. B., Day, J., Greenwood, A., and A. McPherson. 1998. Refined structure of Satellite Tobacco mosaic virus at 1.8 Å resolution. J. Mol. Biol. **277:** 37-59.

37. Lata, R., Conway, J. F., Cheng, N., Duda, R. L., Hendrix, R. W., Wikoff, W. R., Johnson, J. E., Tsuruta, H., and A. C. Steven. 2000. Maturation dynamics of a viral capsid: visualization of transitional intermediate states. Cell **100:** 253-63.

38. McKenna, R., Olson, N. H., Chipman, P. R., Baker, T. S., Booth, T. F., Christensen, H., Aasted, B., Fox, J. M., Bloom, M. E., Wolfinbarger, J. B. and M. Agbandje-McKenna. 1992. Atomic structure of single-stranded DNA bacteriophage ϕX174 and its functional implications. Nature **355:** 137-143.

39. McKenna, R., Ilag, L. L., and M. G. Rossman. 1994. Analysis of the single-stranded DNA bacteriophage øX174 at a resolution of 3.0 Å. J. Mol. Biol. **237:** 517-543.

40. Mukai, R., Hamatake, R. K., and M. Hayashi. 1979. Isolation of the bacteriophage øX174 prohead. Proc. Natl. Acad. Sci. USA **76:** 4877-4881.

41. Prasad, B. V., Prevelige, P. E., Marietta, E., Chen, R. O., Thomas, D., King, J., and W. Chiu. 1993. Three-dimensional transformation of capsids associated with genome packaging in a bacterial virus. J. Mol. Biol. **231:** 65-74.

42. Roof, W. D., Horne, S. M., Young, K. D., and R. Young. 1994. slyD, a host gene required for phi X174 lysis, is related to the FK506-binding protein family of peptidyl-prolyl cis-trans-isomerases. J. Biol. Chem. **269:** 2902-10.

43. Rossmann, M. G. and J. E. Johnson. 1989. Icosahedral RNA virus structure. Ann. Rev. Biochem. **58:** 533-573.

44. Savithri, H. S. and J. W. Erickson. 1983. The self-assembly of the cowpea strain of southern bean mosaic virus: formation of T = 1 and T = 3 nucleoprotein particles. Virology **126:** 328-335.

45. Serwer P. and M. E. Pichler. 1978. Electrophoresis of bacteriophage T7 and T7 capsids in agarose gels. J. Virol. **28:** 917-928.

46. Tang, L., Johnson, K. N., Ball, L. A., Lin, T., Yeager, M., and J.E. Johnson. 2001. The structure of pariacoto virus reveals a dodecahedral cage of duplex RNA. Nature Struct. Biol. **8:** 77 – 83.

47. Van Mansfeld, A. D., Baas, P. D., and H. S. Jansz. 1984. Gene A protein of bacteriophage øX174 is a highly specific single-stranded DNA nuclease and binds via a tyrosyl residue to DNA after cleavage. Adv. Exp. Med. Biol. **197:** 221-230.

48. Vriend, G., Verduin, B. J., and M. A. Hemminga. 1986. Role of the N-terminal part of the coat protein in the assembly of cowpea chlorotic mottle virus. A 500 MHz proton nuclear magnetic resonance study and structural calculations. J. Mol. Biol. **191:** 453-60.

49. Wikoff, W. R., Tsai, C. J., Wang, G., Baker, T. S., and J. E. Johnson. 1997. The structure of cucumber mosaic virus: cryoelectron microscopy, X-ray crystallography, and sequence analysis. Virology **232:** 91-97.

TABLE 1: Genotypes and phenotypes of øX174 *J* mutants in these studies.

Mutant	Genotype	Phenotype
J⁻3K->LI	K->L at residues 2, 4, 5	small plaques, *ts*, *cs*[1]
Su(J)-FS1F/ J⁻3K->LI	K->L at residues 2, 4, 5 Extragenic suppressor (S->F) in residue #1 of capsid protein.	wild type
J⁻K->L ALL	K->L at residues 2, 4, 5, 21, 23, 25	recessive lethal

[1] *ts* and *cs* denote temperature-sensitive and cold sensitive phenotypes, respectively.

TABLE 2: Densities of particles generated in *J*⁻ mutant infected cells.

Particle	S value	Particle Density (g/cm^3) No DNAse	DNAse
Wild type virion	114S	1.39	1.39
Procapsid	108S	1.31	1.31
J⁻K->L ALL	70S	1.36	1.32

TABLE 3: Protein composition of wild type and *J3K->LI* particles[1].

Proteins[2]	Wild type	*J3K->LI*	variation from wt.
F/G	1.64	1.39	0.15
F/J	3.02	2.72	0.10

[1] Proteins were separated by SDS-PAGE, stained and digitally photographed. Ratios were calculated using band intensities derived via 1D image analysis software (Kodak Digital Science™).

[2] F, G and J, denote the major capsid, spike and DNA binding proteins respective.

FIG. 1. øX174 morphogenesis.

FIG. 2. (A) Buoyant densities of wild type and *J3K->L I* particles. Both particles were analyzed in the same gradient. An additional genetic marker, *amB*, was placed in the wild type background. This allowed the particles to be specifically titered on BAF30 pøXB at 42°. The *J3K->L I* mutant is temperature sensitive. The titer of *J3K->L I* was determined on C122 *(sup°)* at 33°C. (B) Buoyant densities of particles packaged with mutant J proteins with and without the *su(J)-FSIF* extragenic second site suppressor. An order of magnitude more of the *J3K->LI* particles, which have a *ts* phenotype, was loaded on the same gradient with the double mutant. The position of the *su(F)SIF/J3K->LI* particles could be ascertained and distinguished from *J3K->LI* by titering at 42°C. Particle titers were normalized to the same order of magnitude for the graph. Symbols: closed circles, wild type; open circles, *J3K->L I* ; squares *su(J)-F SIF/J3K->LI.*

FIG. 3. Buoyant densities of wild type, *su(J)-F S1F/wild type J*, and *J3K->L I* particles. All three types of particles were analyzed within the same gradient. An additional genetic marker, *amB*, was placed in the wild type background. This allowed the particles to be specifically titered on BAF30 pøXB at 42°C where The *J3K->L I* mutant is temperature sensitive. An order of magnitude more of the *J3K->LI* and wild type (*amB*) particles were loaded on the gradient than the *su(J)-F S1F/wild type J* particles. The position of the *su(F)SIF/wild type J* particles could be distinguished from the other particles by titering at 42°C on a *sup°* host. Particle titers were normalized to the same order of magnitude for

the graph. Symbols: closed circles, wild type; open circles, closed squares, *J-3K->L I* ; open circles, *su(J)-F SIF* packaged with wild type J protein.

FIG. 4. (A) Native gel migration of wild type and*J-3K->L I* particles. (B) Enlargement of the wild type minor population of positively charged particles. Negative gel section numbers indicate movement toward the (-) electrode, positive gel section numbers indicate movement toward the (+) electrode. Symbols: closed circles, wild type; open circles, *J-3K->LI.*

FIG. 5. Native gel migration of wild type and *su(J)-FSIF/J-3K->LI* particles. Negative gel section numbers indicate movement toward the (-) electrode, positive gel section numbers indicate movement toward the (+) electrode. Symbols, closed circles, wild type; open circles, *su(J)-FSIF/J3K->LI* .

FIG. 6. Attachment assays. Symbols: closed circles, wild type; closed squares, *J-3K->LI*; open circles, *su(J)-FS1F/ J-3K->LI* .

FIG 7. Native gel migration of wild type øX174 and amp^R transducing particles. The titer of wild type phage has been normalized to the same order of magnitude as the transducing particles. Negative gel section numbers indicate movement toward the (-) electrode, positive gel section numbers indicate movement toward the (+) electrode. Symbols: closed squares, wild type phage, open and closed circles, transducing particles.

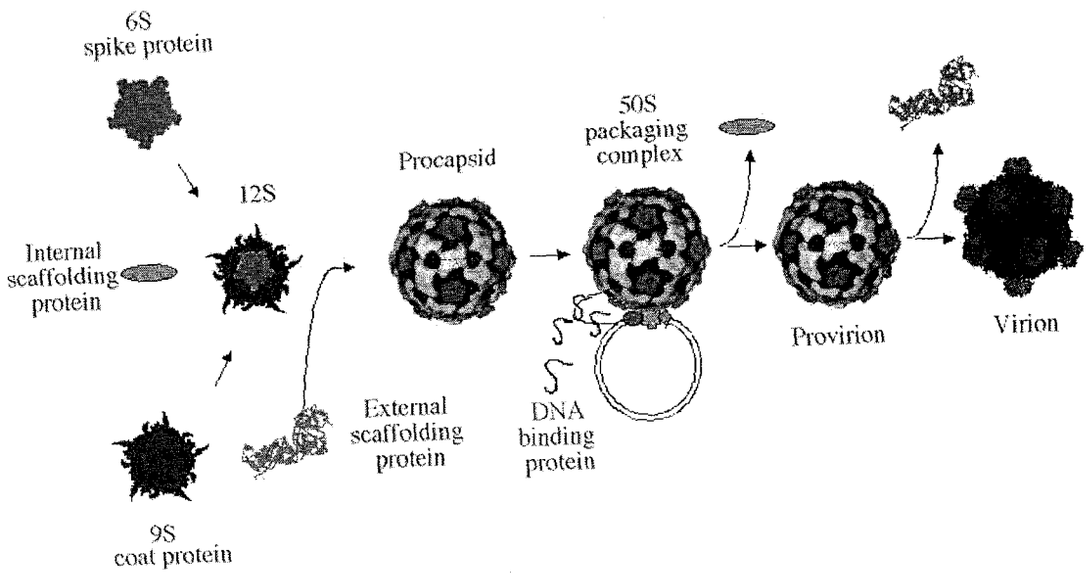
6S
spike protein
12S
Internal
scaffolding
protein
9S
coat protein
External
scaffolding
protein
Procapsid
50S
packaging
complex
DNA
binding
protein
Provirion
Virion

FIG 1

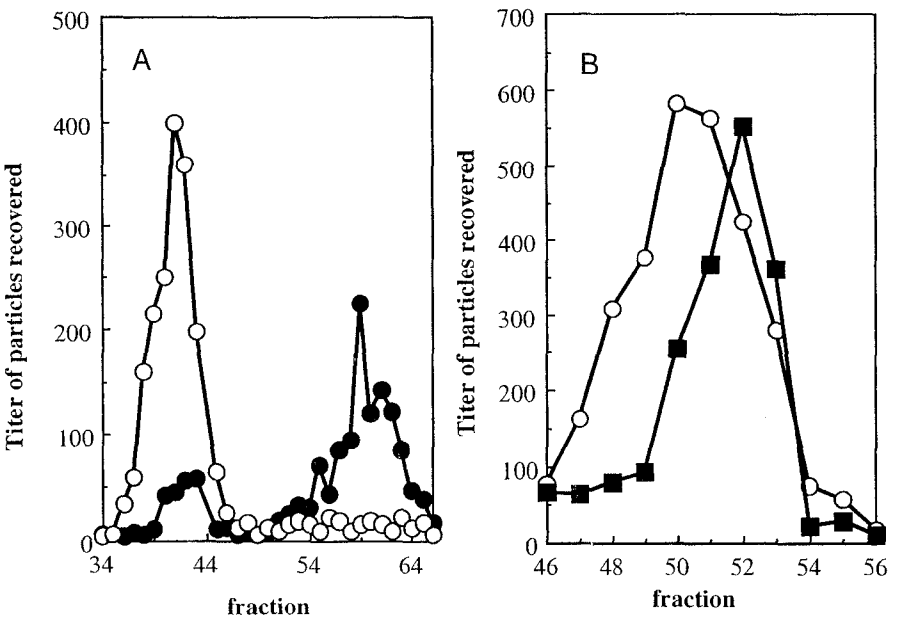
A
B
Titer of particles recovered
fraction
500
400
300
200
100
0
34
44
54
64
700
600
500
400
300
200
100
0
46
48
50
52
54
56

FIG 2

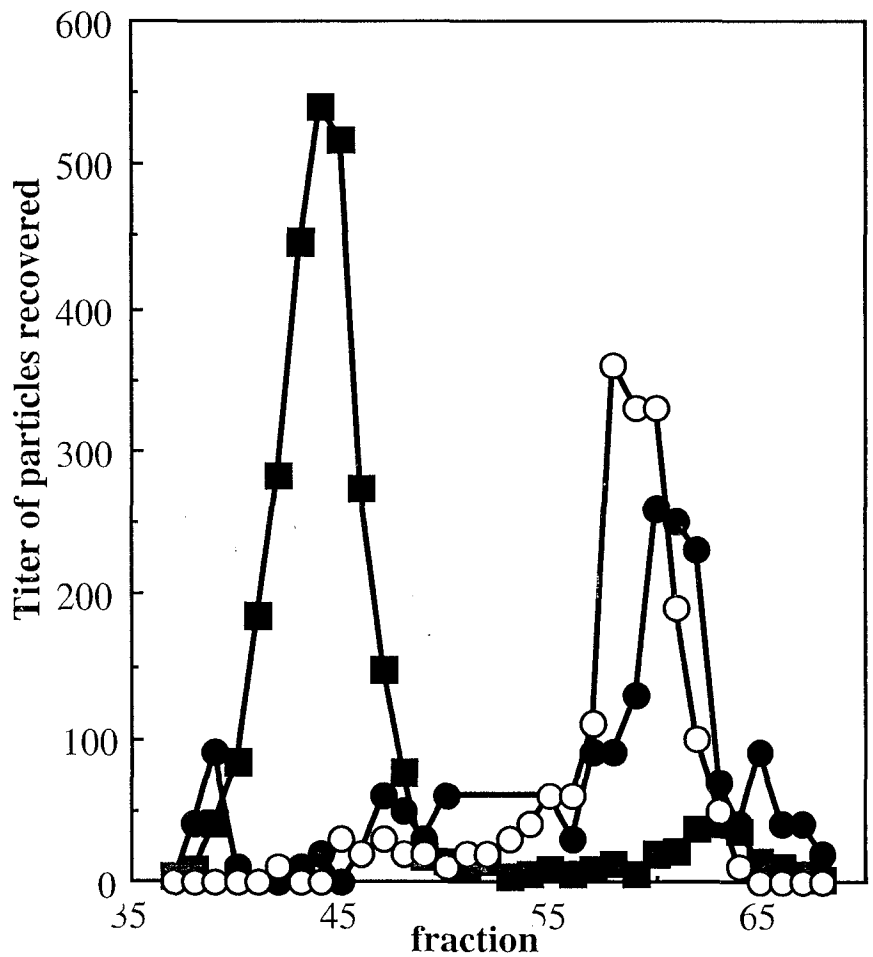
600
500
400
300
200
100
0
Titer of particles recovered
35
45
55
65
fraction

FIG. 3

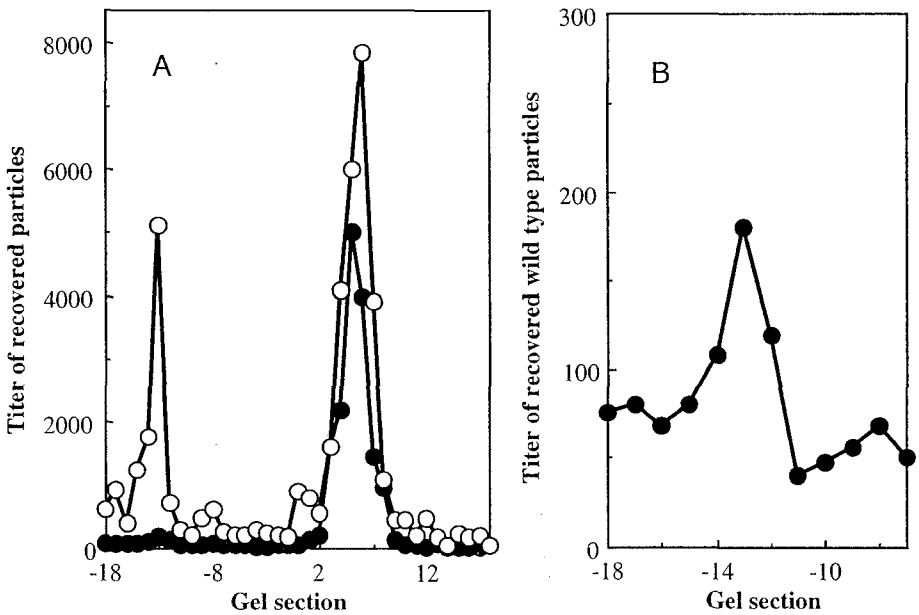
A
8000
6000
4000
2000
0
Titer of recovered particles
-18
-8
2
12
Gel section
B
300
200
100
0
Titer of recovered wild type particles
-18
-14
-10
Gel section

FIG 4

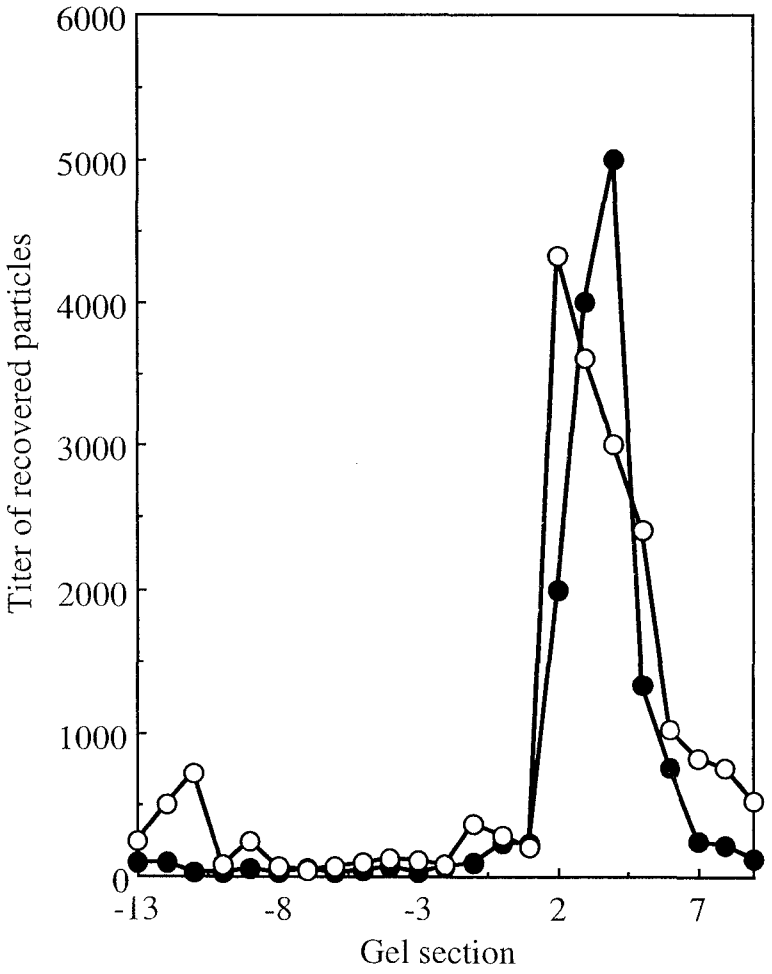
6000
5000
4000
3000
2000
1000
0
Titer of recovered particles
-13
-8
-3
2
7
Gel section

FIG 5

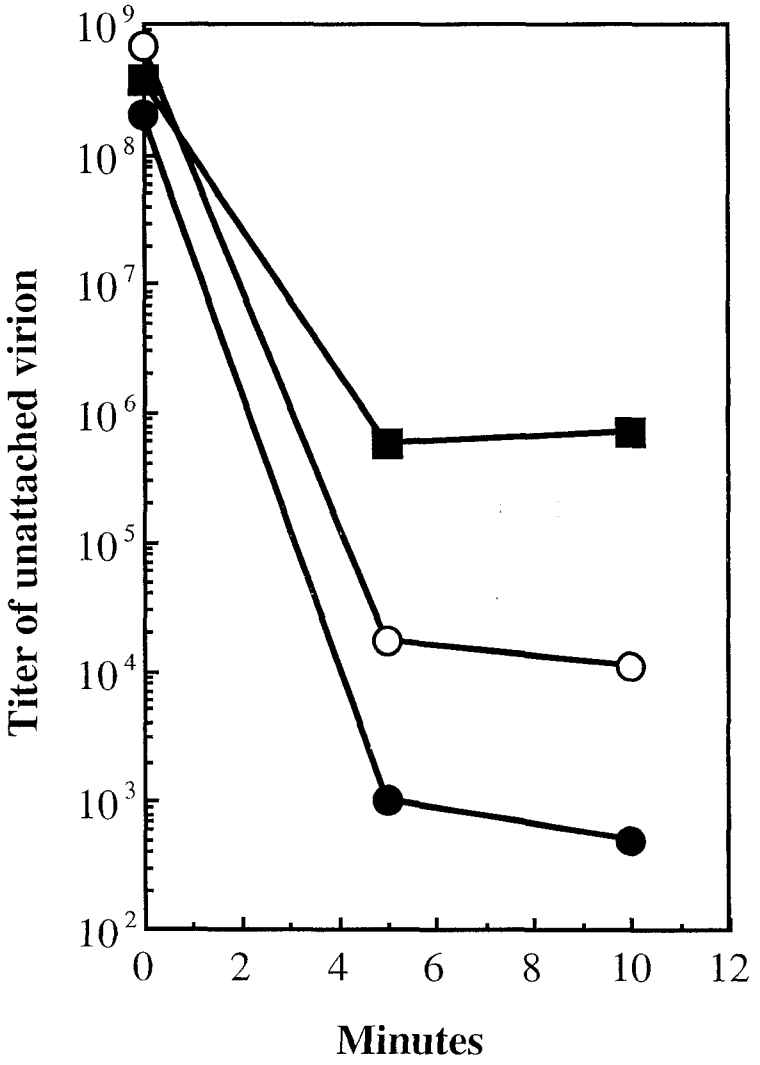
Titer of unattached virion
10^9
10^8
10^7
10^6
10^5
10^4
10^3
10^2
0
2
4
6
8
10
12
Minutes

FIG 6

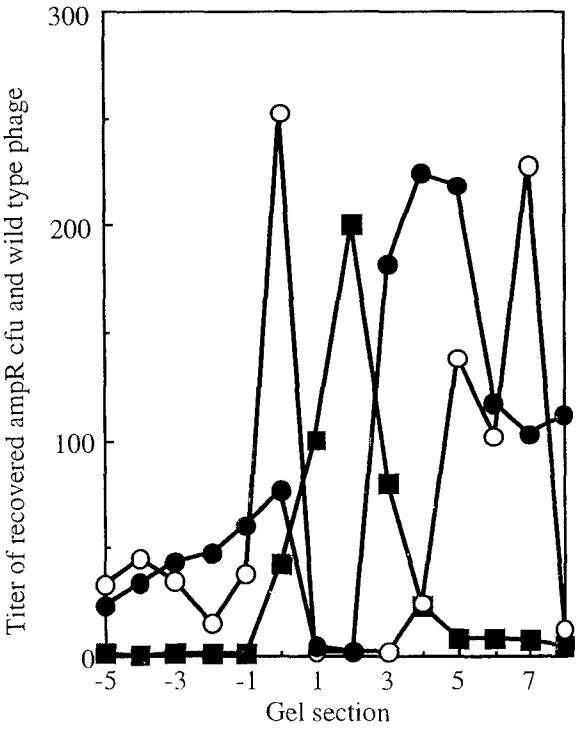
300
200
100
0
Titer of recovered ampR cfu and wild type phage
-5
-3
-1
1
3
5
7
Gel section

FIG. 7

Appendix B:

Structural Studies of Bacteriophage α3 Assembly

Structural Studies of Bacteriophage α3 Assembly

Ricardo A. Bernal[1], Susan Hafenstein[2], Norman H. Olson[1], Valorie D. Bowman[1], Paul R.Chipman[1], Timothy S. Baker[1], Bentley A. Fane[2], and Michael G. Rossmann[1,*]

Running Title: Bacteriophage α3 Assembly.

1. Department of Biological Sciences, Purdue University, 1392 Lilly Hall, West Lafayette, IN 47907-1392.

2. Department of Veterinary Science and Microbiology, University of Arizona, Building 90, Room 201, Tucson, AZ 85721.

* Corresponding author, mgr@indiana.bio.purdue.edu.

Summary

Bacteriophage α3 is a member of the *Microviridae*, a family of small, single-stranded, icosahedral phages that include ϕX174. These viruses have a ssDNA genome associated with approximately 12 copies of an H pilot protein and 60 copies of a small J DNA binding protein. The surrounding capsid consists of 60 F coat proteins decorated with 12 pentameric spikes of G protein. Assembly proceeds via a 108S empty procapsid that requires the external D and internal B scaffolding proteins for its formation.

The α3 "open" procapsid structural intermediate was determined to 15 Å resolution by cryo-electron microscopy (cryo-EM). Unlike the ϕX174 "closed" procapsid and the infectious virion, the α3 open procapsid has 30 Å wide pores at the three-fold vertices and 20 Å wide gaps between F pentamers as a result of the disordering of two helices in the F capsid protein. The large pores are probably used for DNA entry and internal scaffolding protein exit during DNA packaging. Portions of the B scaffolding protein are located at the five-fold axes under the spike and in the hydrophobic pocket on the inner surface of the capsid. Protein B appears to have autoproteolytic activity that cleaves at a Arg-Phe motif and probably facilitates the removal of the protein through the 30 Å wide pores.

The structure of the α3 mature virion was solved to 3.5 Å resolution by X-ray crystallography and was used to interpret the open procapsid cryo-EM structure. The main differences between the α3 and ϕX174 virion structures are in the spike and the DNA binding proteins. The α3 pentameric spikes have a rotation of 3.5° compared to

those of ϕX174. The α3 DNA binding protein, which is shorter by 13 amino acids at its amino end when compared to the ϕX174 J protein, retains its carboxy-terminal binding site on the internal surface of the capsid protein. The icosahedrally ordered structural component of the ssDNA appears to be substantially increased in α3 compared to ϕX174, allowing the building of about 10% of the ribose-phosphate backbone.

Keywords: Bacteriophage α3; three-dimensional structure; procapsid; morphogenesis; ϕX174.

Introduction

Microviridae are small, icosahedral, (+) single-stranded, circular DNA bacteriophages that include ϕX174, G4, and α3 [1]. The morphogenesis of these phages proceeds through an empty procapsid intermediate (Fig. 1). ϕX174 has been the most studied, with the structures of the procapsid and virion having been determined by cryo-EM and X-ray crystallography [2-4]. However, differences between the cryo-EM and X-ray procapsid structures raise questions regarding the true nature of the biologically significant intermediate. The cryo-EM structure at 26 Å resolution has prominent pores at all the three-fold axes of symmetry ("open" procapsid) through which DNA is presumed to package. In contrast, these pores are blocked by three symmetry-related α helices of protein F in the crystal structure, the "closed" procapsid. This structure is similar to that of the mature virion, except for the presence of the scaffolding proteins, suggesting that the crystallization process in ammonium sulfate may have induced a conformational change mimicking the maturation process.

To address some of these questions, studies were initiated with the related bacteriophage α3, with the aim of obtaining a more stable open procapsid. Bacteriophage α3 has an overall amino acid identity of 59% with ϕX174 [5-7] (Table 1), the most conserved protein being the F capsid protein with an identity of 71% (Fig. 2). The least conserved is the spike protein, which has an identity of only 31%. The α3 virion and procapsid structures reported here are at 3.5 Å and 15.0 Å resolution, respectively, demonstrate that the procapsid to virion transition includes a radial collapse of the capsid

pentamers around the genome. In addition, there are major conformational changes at the two-fold and three-fold axes of symmetry. Furthermore, the improved resolution shows that the density around the five-fold axes is a mixture of the H pilot and B internal scaffolding proteins. This suggests that the *Microviridae* internal scaffolding protein, like that of P22 [8,9] and ø29 (Morais, M., personal communication) may play some role in minor vertex protein incorporation.

Results and Discussion

The mature α3 virion

The structure of the α3 virion was determined to 3.5 Å resolution by X-ray crystallography. The virion is icosahedral with 60 copies each of the F capsid, G spike, and J DNA binding proteins. In addition, there are at most 12 copies of the H pilot protein. As with bacteriophage ϕX174, the main feature of the F capsid protein is an eight-stranded antiparallel β-barrel (Figs. 3 and 4). However, the F β-barrel has two large insertions containing twelve α-helices. The longest of these helices is helix 4, which is positioned near the three-fold axes of symmetry. The spike protein also contains the β-barrel motif but, unlike the capsid protein, it has no large insertions. This antiparallel β-barrel motif is found in many plant and animal viruses, such as tomato bushy stunt virus [10] and human rhinovirus [10-12].

Most of the differences between the ϕX174 and α3 structures are in the spike protein G due to a greater divergence of the primary structures (Fig. 2). The first eight and the last ten residues of this protein extend away from its β-barrel and interact with

other F and G subunits. If the G and F proteins within each pentamer are numbered i = 1 to 5 in a clockwise manner as viewed from outside the virus, the amino terminus of subunit G_i makes three main-chain hydrogen bonds with the neighboring symmetry-related amino terminus of subunit G_{i+1}. These terminal extensions form a β-annulus around the five-fold axes of symmetry and thus contribute to the formation of the pentameric spike (Fig. 5). The carboxy terminus of subunit G_i makes five hydrogen bonds with subunit F_{i+1} and five hydrogen bonds with subunit F_{i+2} (Fig. 6). Thus, a total of 50 hydrogen bonds anchor the pentameric spike to the capsid shell (Table 2).

If the α3 and ϕX174 structures are superimposed by aligning the icosahedral symmetry axes, the root-mean-square (r.m.s.) deviations between equivalent C_α atoms of the F and G proteins are 0.8 and 2.7 Å, respectively. However, separate least-squares structural alignments of the F and G proteins result in respective r.m.s. deviations of only 0.5 and 0.7 Å, (Table 3). The significant reduction in the r.m.s. difference between G pentamer C_α atoms is a consequence of a 3.5° clockwise rotation about the five-fold axes, relative to the icosahedral framework if viewed from the outside (Table 4). This demonstrates that the F, but not the G, proteins maintain their relationship to the icosahedral symmetry axes.

In the transition from the open procapsid to the mature virion, coat and spike protein pentamers undergo a respective 5.2 and 8.1 Å radial collapse around the genome (see below). This process requires the spike proteins to lose contacts with the external scaffolding proteins and establish novel contacts with the underlying capsid proteins. As the pentameric spike moves radially inward, it is forced to rotate counter-clockwise

because the carboxy termini of the G proteins are already associated with the capsid. The rotation of the spike stops when contacts are made with F capsid protein residues. In the case of the α3 virion, Thr75 and Asp76 of each G monomer hydrogen bond to capsid protein residues Tyr159 and Gln402, respectively. Similar, but not identical, contacts occur in ϕX174 and G4 (Fig. 6; Table 5), accounting for the relative rotation of the spikes in these three phages. The rotation of the spikes about the five-fold axes is most likely a consequence of morphogenesis.

The positively-charged J protein enters the assembly pathway during DNA packaging by associating with the genome [13] via charge-charge interactions [14,15]. Biophysical characterization of particles packaged with J protein mutants suggest that protein-DNA interactions play a role in mediating the final stages of assembly [14,15]. *Microviridae* J DNA binding proteins contain a positively-charged amino terminus and a highly conserved hydrophobic carboxy terminus, which binds to a pocket on the interior of the F capsid protein. In ϕX174 there is an additional amino terminal basic 13-residue sequence [5-7] (Fig. 2) that binds to a neighboring five-fold related F_{i-1} capsid protein (Fig 4D). Only the carboxy terminal 13 hydrophobic residues can be structurally equivalenced and are almost completely conserved between the α3, ϕX174, and G4 proteins. The first eleven residues of the α3 J protein (corresponding to the middle region of ϕX174) contain a one-turn helix and have an r.m.s. deviation of 4.8 Å between equivalenced C_α atoms when compared to ϕX174. In contrast, the last 13 amino acids superimpose with an r.m.s. deviation of only 0.5 Å, indicating that the amino termini of these two proteins have a different structure.

ϕX174 may have evolved a more elaborate J protein to compensate for a less basic capsid protein inner surface. When the inner surface charge of the α3 and ϕX174 coat proteins was compared, the α3 protein was found to be slightly more basic. This may also explain *in vivo* complementation studies where G4 could efficiently utilize the ϕX174 J protein, but ϕX174 was not able to use the shorter G4 protein [16]. A similar phenomenon has been recently documented for the ϕX174 and α3 J proteins (Hafenstein, S., data not shown).

The sugar phosphate backbone of ten icosahedrally-ordered nucleotides could be identified in the α3 virion electron density map in the proximity of the positively-charged amino terminus of the J protein. The icosahedrally-ordered α3 DNA corresponds to approximately 10% of the genome. The density for these nucleotides is about one-fourth the height of the protein density, but twice the height of the noise. In contrast, only about four icosahedrally-ordered nucleotides were reported in the ϕX174 virion structure, and these were not directly associated with the J protein [17]. However, it should be noted that the amount of ϕX174 ordered DNA may have been under reported, due to the lack of confidence in interpreting low density features (the interpreted density had a larger peak to noise ratio).

α3 procapsid

The α3 open procapsid is an inherently unstable assembly intermediate that is triggered to progress along the assembly pathway upon DNA packaging. A more stable closed procapsid can be produced by high concentrations of ammonium sulfate (Dokland et al, 1999). However, this closed particle probably represents an off-pathway product.

The α3 open procapsid was purified in the absence of high ionic strength compounds, but could not be crystallized due to rapid dissociation. Therefore, a structure determination was undertaken using cryo-EM, which preserves the particle integrity upon vitrification in liquid ethane. The resulting 15 Å resolution reconstruction (Fig. 7) is considerably more detailed than the homologous 26 Å resolution ϕX174 reconstruction.

The capsid and spike proteins from the α3 virion and the scaffolding proteins from the closed procapsid were fitted into the open procapsid density using the program EMfit [18]. There were no contacts, defined as atoms in opposing subunits being separated by less than 4 Å, between symmetry-related subunits. In comparison, the number of atoms in one F subunit of the virion X-ray structure in contact with other F subunits was 6.3% of the total number of atoms in the protein. Therefore, the pixel size had to be reduced by 5% in order to obtain the same percentage of contacts in the open procapsid.

When capsid protein coordinates were fitted into the procapsid density, all atoms are within positive density except for residues 172 to 231. This region consists of helices 4 and 5, found near the three-fold and two-fold axes of symmetry, respectively (Fig. 4A). Hence, protein F, with helices 4 and 5 removed, was fitted into the density using main-chain and side-chain atoms resulting in a *sumf* [†, 18] value of 52% (Fig. 8A; Table 6). Removal of these two helices created an apparent 20 Å gap surrounding the F pentamers (Fig. 7). Similarly a pentamer of G protein was fitted into the density resulting in a *sumf* value of 47% (Fig. 8B; Table 6). All density covered by the atoms of the F and G

[†] *sumf* is the average density of all the fitted atoms normalized by placing the largest density of the map equal to 100.

proteins was then set to zero leaving the remaining density to be interpreted as D and B scaffolding and H pilot proteins.

ϕX174 D1-D2 and D3-D4 external scaffolding protein dimers were used as models to interpret the open procapsid D scaffolding density. This was justified because a D1-D2 dimer can be superimposed onto a D3-D4 dimer with an r.m.s. deviation of less than 2.5 Å. It has been previously reported that the D proteins may exist as dimers in solution and assemble into tetramers during morphogenesis [4] (Table 6). Fitting individual D proteins was not possible because the density at this resolution is somewhat featureless and the coordinates are placed at locations which will cause monomers to overlap.

After the F, G, and D proteins had been fitted into the cryo-EM density of the open procapsid, the only density remaining above 1_ was inside the F capsid, located at the icosahedral two-fold and five-fold axes of symmetry. This density is presumably the B scaffolding protein. In the X-ray structure of the closed procapsid, the B scaffolding protein was disordered between residues 9-60. An attempt was made to manually fit the structure of the ordered component of B (residues 1-8, 61-120) into the difference density of the open procapsid. However, residues 61-80, which form an α-helix in the closed procapsid x-ray structure, were out of density. Therefore, they were independently fitted into a tube like feature of the cryo-EM map that runs close to the nearest five-fold axis of symmetry (Fig. 8D). A secondary structure analysis of the ϕX174 B protein predicts a long central helix between residues 56 and 77, closely matching the long helix in the closed procapsid structure. The tube-like feature connects to the density around the five-

fold symmetry axes previously associated with protein H. Hence, this five-fold associated density could represent five copies of the missing amino-terminal portion of protein B. However, at 15 Å resolution it was not possible to follow more of the polypeptide chain.

The density feature around the five-fold axes of symmetry occupies 41,000 $Å^3$ and is sufficient to accommodate 5 copies of residues 9-60 of the B protein, which would require 40,700 $Å^3$ (see Methods section). Similar density near the five-fold axes in the closed procapsid structure had been interpreted as one copy of protein H. This is also consistent with the molecular weight of one H protein that would occupy about 42,400 $Å^3$. This, together with the above observation that the amino termini of the B protein are close to the density feature at the five-fold axes suggests that this density may represent either protein B or H. Partial occupancy of B is supported by the reduced height of the carboxy terminal section of protein B relative to the other protein density in the ϕX174 closed procapsid and the α3 open procapsid.

The relative mobility in SDS-PAGE gels of the B protein, derived from ϕX174 and α3, changes with the age of the preparation, suggesting that the B protein is unstable (data not shown) [19]. Furthermore it was observed that purified glutathione S-transferase (GST) -B fusion protein degrades with time, generating fragments of distinct sizes. This observation is consistent with earlier data on B proteolysis [19]. Analysis of the GST-B fusion protein cleavage products indicated that one of three fragments was removed from the protein (Fig. 9). The sizes of these fragments are consistent with a repeating motif in the primary structure. An Arg-Phe sequence repeats at approximately 13 amino acid

intervals from the carboxy terminal end of protein B (Fig. 9). The absence of ordered B protein structure prior to Arg 61 in the closed procapsid may be the result of a cleavage event, which may have allowed the amino terminal portion to diffuse away. In contrast, the open procapsid, which probably represents a true assembly intermediate, appears to contain an undigested B scaffolding protein as observed by SDS poly-acrylamide gel electrophoresis.

In P22 and ϕ29, scaffolding proteins exit intact and recycle in further rounds of assembly [20,21]. However, in most bacteriophages and in the *Herpesviridae*, cleavage of the scaffolding protein facilitates its removal during morphogenesis [22]. Therefore, the autoproteolytic activity of protein B may be a necessary component of morphogenesis, facilitating the escape of suitably sized fragments of protein B through the 30 Å diameter pores located at the three-fold axes of symmetry. During the DNA packaging, protein J displaces the carboxy terminus of protein B [3] by competition for the same hydrophobic binding pocket on the internal surface of the F capsid protein. Since the B protein is intact in the open procapsid, it follows that B protein displacement may activate the protein autoproteolytic activity.

Materials and Methods

Purification and crystallization

Mature virion was generated in *E. coli slyD* cells infected with bacteriophage α3 *am(E)W4*. The host cell *slyD* mutation confers resistance to E protein mediated lysis [23]. Both the host cell and phage mutations were needed to effectively block lysis. Twelve liters of cells at 1.0_10^8cfu/ml were infected at a multiplicity of infection (moi) of 5 at 33°C and allowed to incubate for 6 hours. Infected bacterial pellets were resuspended in 400 mL buffer A (50 mM Tris pH 7.5, 25 mM EDTA, 50 mM NaCl, and 0.1 mM β-mercapto-ethanol) and lysed by the addition of 0.2 g lysozyme. After a one-hour incubation at 20°C, the sample was subjected to three rapid freeze/thaw cycles. After removal of bacterial debris by centrifugation at 16,000g, particles were precipitated by the addition of 8.5% PEG 8000 (wv^{-1}). The phage was further purified in two consecutive 0-40% (wv^{-1}) sucrose gradients. The purified sample was concentrated on 100 kDa cutoff Millipore centrifuge concentrator units and a buffer exchange was performed into buffer B (10 mM Tris pH 7.5, 1 mM EDTA, 300 mM NaCl, 0.1 mM β-mercapto-ethanol, and 0.02% sodium azide). The virion was crystallized by vapor diffusion using sitting drops at 45°C. A 10 μL drop of sample was mixed with an equal volume of reservoir buffer containing 3-5% PEG 8000, 100 mM sodium citrate pH 5.0, 40% glycerol, 0.02% sodium azide, and 0.1% β-mercapto-ethanol.

Bacteriophage α3 procapsids were purified from *E. coli slyD* cells infected with α3 *am(E)W4, am(J)M1, am(J)S7*. The amber mutations in gene J prevent the production of the DNA binding protein arresting morphogenesis after procapsid formation. Two amber mutations were used to prevent reversion during the long incubation periods needed to generate sufficient quantities. Moi and infection conditions were identical to those described above. Purification of the procapsid is essentially the same as for the virion with a few minor modifications. After lysis of the bacterial cells, the procapsid was precipitated by the addition of 7% PEG 8000 (wv^{-1}), followed by centrifugation at 16,000g for 10 minutes at 4°C. The procapsid sample was loaded onto a 5-35% sucrose gradient and centrifuged at 121,000g in a SW28 rotor for 4 h at 4°C. Samples collected from the gradients were centrifuged at 226,000g at 4°C for 2 hours in a Ti50 rotor to pellet the procapsid. Procapsids were resuspended overnight in 100-500 μl buffer containing 10 mM Tris pH 7.5, 1 mM EDTA, 0.1M NaCl.

X-ray data collection and processing

Data were collected at BioCARS beam line 14 BM-c at the Advanced Photon Source. A single frozen crystal was used to collect 180° of data with an oscillation angle of 0.25° on a MAR detector (345 mm diameter) and a crystal-to-detector distance of 535 mm. Images were processed with DENZO [24] and scaled together using the program SNP [25]. The space group of the bacteriophage α3 virion crystals was $P2_1$ with cell dimensions of 290.3, 332.1, 337.7 Å, and $\beta = 94.1°$. The Matthews' coefficient, V_M, is 2.6 $Å^3Da^{-1}$ assuming one particle in the unit cell. Thus, the icosahedral symmetry produces 60-fold

noncrystallographic symmetry (NCS) redundancy. The final R_{merge} was 8.0% for all the data (11.5% in the highest resolution bin) with an average of 3.5 measurements per reflection. The overall completeness was 75% (55% in the highest resolution range) after removal of reflections with less that 4_. Initial orientations of the α3 particles in the unit cell were determined with a self-rotation function using the program GLRF [26,27]. The particle orientation had one of its two-fold axes only 0.65° away from being parallel to the crystallographic 2_1 screw axis. This allowed the particle position in the unit cell to be determined using a self-Patterson function, resulting in a large peak on the Harker section corresponding to (0.2498, 0.2500, 0.2498) in fractions of the cell edges. The virion structure was determined to 3.5 Å resolution by molecular replacement real-space averaging using the ϕX174 virion structure as a phasing model [28] with calculated phases to 3.5 Å resolution. The overall correlation coefficient of the back-transformed map was 0.86 (0.56 at 3.5 Å resolution) and an overall *R* factor of 0.19 (0.29 at 3.5 Å resolution).

X-ray structure refinement

The F, G, and J peptide chains were built into the 3.5 Å resolution electron density map using the program O [29]. The subsequent structure was refined using 5 cycles of simulated annealing followed by 5 cycles of strict NCS conjugate gradient minimization using the program CNS [30]. The ten nucleotides were not included in the refinement because there is density only for the sugar phosphate backbone and not the bases. The final *R* factor is 0.23 (0.28 at 3.5 Å resolution) with all of the residues in the most favored regions of the Ramachandran plot as calculated by the program

PROCHECK [31]. Because of the 60-fold NCS redundancy, there was less than 0.3% difference between $R_{working}$ and R_{free}. The coordinates of the crystallographically-determined virion and the cryo-EM-determined open procapsid structures have been deposited with the Protein Data Bank (PDB) (virion accession code 1M06, open procapsid accession code 1M0F).

Cryo-EM

Cryo-EM micrographs were taken on an FEG200 electron microscope at defocus levels ranging from 1.6 to 3.2 μm under focus. The micrographs were digitized on a SCAI flatbed densitometer. Individual particles were selected, boxed, and normalized using the Purdue program ROBEM. The defocus level was estimated from the averaged Fourier transform of all the boxed particles. Initial particle orientations for a preliminary low-resolution reconstruction were calculated using a 26 Å resolution ϕX174 procapsid reconstruction.

Particle orientations and centers were found using the program EMPFT (Polar Fourier Transform) [32], which uses cross correlation procedures to compare particle images against a database of reference projected views produced from a 3D model map. The program EM3DR was used to merge all images for computing a Fourier Bessel transformation to produce a 3D density map of the particle in a standard orientation. The phases and amplitudes of the calculated reconstruction were corrected using the contrast transfer function (CTF) [33]. The resolution was slowly extended to 10 Å for determining the particle orientations and for map calculation. Of 3,433 boxed particles, 2,378 were

included in the final reconstruction and presumably, the rejected particles were damaged to a greater or lesser extent. The effective resolution of the reconstruction was calculated by dividing the images into two sets and calculating individual reconstructions from each half dataset. The resulting reconstructions were Fourier transformed and cross-correlated. The resolution, determined as the point where the correlation coefficient falls below 0.5 and the mean phase difference becomes less than 45°, was found to be 15 Å (Fig. 10). A possible reason for the inability to obtain better than 15 Å resolution may have been due to the tendency of particles to orient themselves non-randomly (Fig. 11). This led to a reconstruction which was lacking data in certain directions. No tilted grids had been used in the data collection as it had been anticipated the particles would have a random distribution.

Volume determination

The volume that a protein molecule (V) would occupy in solution was calculated from the molecular weight (MW) assuming a specific density (ρ_s) of 1.37 g/cm^3, and Avogadro's number (n) according to the formula [34].

$$V = \frac{MW \leftrightarrow \rho_s}{n} \cong (1.212 \leftrightarrow MW) \text{ Å}^3$$

This was compared to the volume of the feature near the five-fold density, which was determined by counting the number of pixels with a density above a cutoff of 0.4 _ (where the highest noise density was 0.2 _).

Fitting X-ray coordinates into cryo-EM density

X-ray coordinates of the α3 capsid and spike proteins were initially fitted manually into the cryo-EM density. The program EMFIT was used to obtain a more quantitative fit [18]. The criteria of fit used by the program are the average value of the density at all atomic sites in the fitted protein, the lack of atoms in negative density, and the absence of icosahedral symmetry-related atomic clashes. The overall measure of fit as expressed by R_{crit} is a combination of all these into a single best fit criterion. After a protein was fit into cryo-EM map, density within a radius of 4.0 Å around all atomic positions was set to zero before fitting the next protein.

Protein B

A GST_B fusion was created by cloning a BamHI_EcoRI fragment containing the ϕX174 protein B into the pGEX-2T plasmid (Pharmacia Biotech). Transformed BL21 (DE3) cells were incubated at 37°C and allowed to reach an optical density of 1.0 before being cooled to room temperature. Induction of GST-B fusion protein was initiated by the addition of IPTG to a final concentration of 0.1 mM. After 20 minutes, the cells were centrifuged at 7,000g and resuspended in two pellet volumes of lysis buffer (50 mM Tris pH 7.5, 10 mM EDTA, 150 mM NaCl, and 0.1 mM β-mercapto-ethanol, 10μg·mL^{-1} lysozyme). After one-hour incubation at 20°C, the sample was subjected to three rapid freeze/thaw cycles and then centrifuged at 16,000g to remove the bacterial debris. The supernatant was loaded onto a glutathione sepharose 4B column (bed volume of 2 mL). The column was washed with 40 mL of wash buffer (50 mM Tris pH 7.5, 10 mM EDTA,

150 mM NaCl, and 0.1 mM β-mercapto-ethanol) and eluted with wash buffer containing 10mM glutathione.

Acknowledgements

We thank Shuji Kanamaru, Cheryl Towell, and Sharon Wilder for their help in the preparation of this manuscript. We are grateful to Stephen Fuller and Erika Mancini for discussions about the cryo-EM reconstruction and to Chuan Xiao for the use of his parallelized versions of EMPFT, EM3DR, and other programs. We also thank the BioCARS staff of the Advanced Photon Source for providing excellent support for their X-ray data collection facilities. This research was supported by a Biophysics Training Grant fellowship and GAANN fellowship to R.A.B., NIH grant GM33050 to T.S.B., NSF grant MCB-9986266 to M.G.R., and NSF grant MCB-9982284 to B.A.F. Figures were generated using the graphics programs VMD [35], Molscript [36], Bobscript [37], and Raster 3D [38].

References

1. Hayashi, M., Aoyama, A. Richardson, D.L. & Hayashi, M.N. (1988). Biology of the bacteriophage ϕX174. In *The Bacteriophages* (Calendar, R., ed.), pp. 1-71. Plenum Press, New York.

2. Ilag, L. L., Olson, N. H., Dokland, T., Music, C. L., Cheng, R. H., Bowen, Z., McKenna, R., Rossmann, M. G., Baker, T. S. & Incardona, N. L. (1995). DNA packaging intermediates of bacteriophage ϕX174. *Structure* **3**, 353-363.

3. Dokland, T., McKenna, R., Ilag, L. L., Bowman, B. R., Incardona, N. L., Fane, B. A. & Rossmann, M. G. (1997). Structure of a viral procapsid with molecular scaffolding. *Nature* **389**, 308-313.

4. Dokland, T., Bernal, R. A., Burch, A., Pletnev, S., Fane, B. A. & Rossmann, M. G. (1999). The role of scaffolding proteins in the assembly of the small, single-stranded DNA virus ϕX174. *J. Mol. Biol.* **288**, 595-608.

5. Sanger, F., Air, G. M., Barrell, B. G., Brown, N. L., Coulson, A. R., Fiddes, C. A., Hutchison, C. A., Slocombe, P. M. & Smith, M. (1977). Nucleotide sequence of bacteriophage ϕX174 DNA. *Nature* **265**, 687-695.

6. Kodaira, K., Nakano, K., Okada, S. & Taketo, A. (1992). Nucleotide sequence of the genome of the bacteriophage α3: interrelationship of the genome structure and the gene products with those of the phages, ϕX174, G4 and ϕK. *Biochim. Biophys. Acta* **1130**, 277-288.

7. Godson, G. N., Barrell, B. G., Staden, R. & Fiddes, J. C. (1978). Nucleotide sequence of bacteriophage G4 DNA. *Nature* **276**, 236-247.

8. Greene, B. & King, J. (1994). Binding of scaffolding subunits within the P22 procapsid lattice. *Virology* **205**, 188-197.

9. Greene, B. & King, J. (1999). In vitro unfolding/refolding of wild type phage P22 scaffolding protein reveals capsid-binding domain. *J. Biol. Chem.* **274**, 16135-16140.

10. Winkler, F. K., Schutt, C. E., Harrison, S. C. & Bricogne, G. (1977). Tomato bushy stunt virus at 5.5-A resolution. *Nature* **265**, 509-513.

11. Rossmann, M. G., Arnold, E., Erickson, J. W., Frankenberger, E. A., Griffith, J. P., Hecht, H. J., Johnson, J. E., Kamer, G., Luo, M., Mosser, A. G. & et al. (1985). Structure of a human common cold virus and functional relationship to other picornaviruses. *Nature* **317**, 145-153.

12. Rossmann, M. G. & Johnson, J. E. (1989). Icosahedral RNA virus structure. *Annu. Rev. Biochem.* **58**, 533-573.

13. Fujisawa, H. & Hayashi, M. (1976). Viral DNA-synthesizing intermediate complex isolated during assembly of bacteriophage ϕX174. *J. Virol.* **19**, 409-415.

14. Jennings, B. & Fane, B. A. (1997). Genetic analysis of the ϕX174 DNA binding protein. *Virology* **227**, 370-377.

15. Hafenstein, S. & Fane, B. A. (2002). ϕX174 genome-capsid interactions influence the biophysical properties of the virion: evidence for a scaffolding-like function for the genome during the final stages of morphogenesis. *J. Virol.* **76**, 5350-5256.

16. Fane, B. A., Head, S. & Hayashi, M. (1992). Functional relationship between the J proteins of bacteriophages ϕX174 and G4 during phage morphogenesis. *J. Bacteriol.* **174**, 2717-2719.

17. McKenna, R., Ilag, L. L. & Rossmann, M. G. (1994). Analysis of the single-stranded DNA bacteriophage ϕX174, refined at a resolution of 3.0 A. *J. Mol. Biol.* **237**, 517-543.

18. Rossmann, M. G., Bernal, R.A. & Pletnev, S.V. (2002). Combining electron microscopic with X-ray crystallographic structures. *J. Struct. Biol.* **136**, 190-200.

19. Richardson, D. L., Jr., Aoyama, A. & Hayashi, M. (1988). Proteolysis of bacteriophage ϕX174 prohead protein gpB by a protease located in the *Escherichia coli* outer membrane. *J. Bacteriol.* **170**, 5564-5571.

20. King, J. & Casjens, S. (1974). Catalytic head assembling protein in virus morphogenesis. *Nature* **251**, 112-119.

21. Casjens, S. & King, J. (1974). P22 morphogenesis. I: Catalytic scaffolding protein in capsid assembly. *J. Supramol. Struct.* **2**, 202-224.

22. Newcomb, W. W., Trus, B. L., Cheng, N., Steven, A. C., Sheaffer, A. K., Tenney, D. J., Weller, S. K. & Brown, J. C. (2000). Isolation of herpes simplex virus procapsids from cells infected with a protease-deficient mutant virus. *J. Virol.* **74**, 1663-1673.

23. Roof, W. D., Horne, S. M., Young, K. D. & Young, R. (1994). *SlyD*, a host gene required for ϕX174 lysis, is related to the FK506-binding protein family of *peptidyl-prolyl cis-trans-isomerases. J. Biol. Chem.* **269**, 2902-2910.

24. Otwinowski, Z., & Minor, W. (1997). Processing of X-ray diffraction data collected in oscillation mode. *Methods in Enzymology* **276A**, 307-326.

25. Bolotovsky, R., Steller, I. & Rossmann, M.G. (1998). The use of partial reflections for scaling and averaging X-ray area detector data. *J. Appl. Crystallogr.* **31**, 708-717.

26. Rossmann, M. G., & Blow, D.M. (1962). The detection of sub-units within the asymmetric unit. *Acta Crystallogr.* **15**, 15-31.

27. Tong, L. A. & Rossmann, M. G. (1990). The locked rotation function. *Acta Crystallogr. sect. A* **46**, 783-792.

28. Rossmann, M. G. (1990). The molecular replacement method. *Acta Crystallogr. sect. A* **46**, 73-82.

29. Jones, T. A., Zou, J. Y., Cowan, S. W. & Kjeldgaard. (1991). Improved methods for binding protein models in electron density maps and the location of errors in these models. *Acta Crystallogr. sect. A* **47**, 110-119.

30. Brunger, A. T., Adams, P. D., Clore, G. M., DeLano, W. L., Gros, P., Grosse-Kunstleve, R. W., Jiang, J. S., Kuszewski, J., Nilges, M., Pannu, N. S., Read, R. J., Rice, L. M., Simonson, T. & Warren, G. L. (1998). Crystallography & NMR system: A new software suite for macromolecular structure determination. *Acta Crystallogr. sect. D* **54**, 905-921.

31. Collaborative Computational Project Number 4. (1994). The CCP4 Suite: Programs for Protein Crystallography. *Acta Crystallogr. sect. D* **50**, 760-763.

32. Baker, T. S. & Cheng, R. H. (1996). A model-based approach for determining orientations of biological macromolecules imaged by cryoelectron microscopy. *J. Struct. Biol.* **116**, 120-130.

33. Baker, T. S., Olson, N. H. & Fuller, S. D. (1999). Adding the third dimension to virus life cycles: three-dimensional reconstruction of icosahedral viruses from cryo-electron micrographs. *Microbiol. Mol. Biol. Rev.* **63**, 862-922.

34. Harpaz, Y., Gerstein, M. & Chothia, C. (1994). Volume changes on protein folding. *Structure* **2**, 641-649.

35. Humphrey, W., Dalke, A. & Schulten, K. (1996). VMD: visual molecular dynamics. *J. Mol. Graph.* **14**, 27-38.

36. Kraulis, P. J. (1991). MOLSCRIPT: a program to produce both detailed and schematic plots of protein structures. *J. Appl. Crystallogr.* **24**, 946-950.

37. Esnouf, R. M. (1999). Further additions to MolScript version 1.4, including reading and contouring of electron-density maps. *Acta Crystallogr. sect. D* **55**, 938-940.

38. Merritt, E. A. & Bacon, D. J. (1997). Raster3D photorealistic molecular graphics. In *Methods in Enzymology*, Vol. 277, pp. 505-524. Academic Press, San Diego.

39. Fujisawa, H. & Hayashi, M. (1977). Assembly of bacteriophage ϕX174: identification of a virion capsid precursor and proposal of a model for the functions of bacteriophage gene products during morphogenesis. *J. Virol.* **24**, 303-313.

40. Mukai, R., Hamatake, R. K. & Hayashi, M. (1979). Isolation and identification of bacteriophage ϕX174 prohead. *Proc. Natl. Acad. Sci. U. S. A.* **76**, 4877-4881.

41. Siden, E. J. & Hayashi, M. (1974). Role of the gene beta-product in bacteriophage ϕX174 development. *J. Mol. Biol.* **89**, 1-16.

42. Dokland, T., McKenna, R., Sherman, D. M., Bowman, B. R., Bean, W. F. & Rossmann, M. G. (1998). Structure determination of the phiX174 closed procapsid. *Acta Crystallogr. D Biol. Crystallogr.* **54** 878-90.

Figure Legends

Figure 1. *Microviridae* assembly pathway. The first morphogenetic intermediates in the assembly pathway are the 9S and 6S particles, respective pentamers of the F capsid and G spike proteins [1]. The internal and external scaffolding proteins direct the assembly of these pentameric intermediates into an empty protein shell called the procapsid [39-41]. The single-stranded DNA (ssDNA) is concurrently synthesized and packaged along with the basic DNA binding protein J, which displaces the internal scaffolding protein B by competition for the same hydrophobic binding pocket on the internal surface of the F capsid protein [3,4,42]. The resulting particle, or provirion, sheds the external scaffolding protein lattice forming the mature virion.

Figure 2. Amino acid alignment based on the structural superpositions of proteins F, G, and J for bacteriophages α3, ϕX174, and G4. Alpha helices α1 to α10 (/\/\) in F and β-strands βB to βI (⇨) are labeled to be consistent with the nomenclature established for ϕX174. Completely conserved residues are boxed.

Figure 3. Secondary structure assignment for α3 F (upper panel) and G (lower panel) proteins based on the program PROCHECK [31]. Boxes and cylinders represent β-strands and α-helices, respectively. β-strands B, C, D, and E form hydrogen bonds with β-strands I, H, G and F, respectively.

Figure 4. Stereo representation of the bacteriophage α3 structural proteins illustrating the level of conservation between α3, ϕX174, and G4. More conserved areas are shaded blue and less conserved regions are shaded red. Conservation was defined by $\_{}_{i-4,i+4} f(i)$ where *i* is a residue and $f(i) = 1$ if there is complete conservation among the three phages or 0 otherwise. A) Protein F has a highly conserved β-barrel, while surface residues are less conserved. B) The spike protein is the least conserved of all the proteins. C) Superposition of the spike protein from bacteriophage α3 (orange) and ϕX174 (green). The bacteriophage α3 spike protein has a 3.5° anticlockwise rotation about the five-fold axis compared to the spike protein of ϕX174. The amino and carboxy termini of the spike protein extend away from the β-barrel and make extensive contacts with symmetry-related F and G proteins. D) Superposition and conservation of the DNA binding protein J. In blue is the highly conserved carboxy terminal region of α3 and ϕX174. The less conserved sequence and structural amino-terminal regions are colored green for α3 and

red for ϕX174. Note the 13 amino terminal residues in ϕX174 are missing in α3.

Figure 5. Stereo ribbon diagram of the interface between proteins F (right) and G (left). The two protein pentamers have been pulled apart to highlight the contact residues. The amino terminal residues of the spike proteins highlighted in blue only make contact with neighboring spike proteins. The carboxy terminal residues of the G proteins, highlighted in green, make ten hydrogen bonds per monomer with matching residues in the F capsid proteins, also highlighted in green. Two additional hydrogen bonds per monomer between Thr75 and Asp76 of G with Tyr159 and Gln402 of F, respectively, are highlighted in red. These latter residues probably limit the amount of rotation of the spike in the transition from procapsid to mature virus.

Figure 6. Stereo diagram of the G and F contact residues at the interface between the capsid and spike proteins. In gray are residues belonging to the F_1 capsid protein. In red are the residues belonging to the G_1 spike protein. Symmetry-related residues that belong to G_2, G_3, G_4, and G_5 are in yellow, magenta, green, and light blue, respectively. Hydrogen bonds are represented by dotted lines.

Figure 7. Comparison of the ϕX174 and α3 procapsids. The particles illustrated on the left-hand column correspond to the bacteriophage ϕX174 closed procapsid structure calculated to 15 Å resolution from the X-ray atomic coordinates. On the right are shown stereo diagrams of the α3 cryo-EM reconstruction also at 15 Å resolution. The second row is a cross-section that allows a clear view of the interior of the procapsid and the additional density feature around the five-fold axes of symmetry present only in the α3 open procapsid. The third row consists of a particle where all proteins except for F were removed to illustrate the apparent 20 Å wide gaps in the α3 procapsid that are created by the disorder of helices 4 and 5. The fourth row shows the same for the D proteins. The α3 particles in the last two rows were calculated from coordinates that resulted from fitting the X-ray structural components derived from the closed procapsid into the open procapsid cryo-EM density.

Figure 8. Stereo diagrams of the procapsid protein coordinates fitted into the open procapsid density. The surface of the cryo-EM density is contoured at a level of 0.5_ and suitably slabbed to see into the interior of the density. A) Helices 4 and 5 are clearly shown to be out of density after fitting the capsid protein F into the density. B) Protein G was fitted into the density as a pentamer. C) The D external scaffold proteins were fitted as dimers of D1(red)-D2(green) and D3(yellow)-D4(violet). D) The internal scaffolding protein B was manually fitted into the open procapsid cryo-EM structure where its long α-

helix fits into a tube of density that leads toward the uninterpreted density around the five-fold axis of symmetry (yellow). A side view of the open procapsid is shown with the outer surface of the particle on the top and the interior of the particle on the bottom. Proteins F (light blue), G (brown), D1 (red), D2 (green), D3 (yellow), D4 (violet) and B (magenta) were included along with their two-fold-related subunits. Icosahedral five- and two-fold symmetry axes are shown as lines.

Figure 9. Proteolysis of the GST-B fusion protein. A) SDS-PAGE gel of purified GST-B fusion protein after incubation at room temperature. Proteolytic fragments begin to appear one hour post induction. Thus, the incubation time indicated for each lane is calculated from the time of induction and includes the two hours needed for purification. The first lane represents the sample immediately following purification and the sample in the second lane was incubated an additional 24 hours at room temperature. The full length fusion protein is indicated by the label GST-B. Proteolytic fragments are labeled 1, 2, and 3. B) Sequence of the ϕX174 B protein with the possible cleavage sites labeled the same as in the gel. Residues that were ordered in the high resolution structure of the closed procapsid are highlighted in bold. Each of the potential cleavage sites has a common motif composed of an Arg and a Phe, which are underlined.

Figure 10. Fourier cross-correlation for the α3 open procapsid reconstruction data. The data were divided in half and corresponding individual reconstructions were cross-correlated. The correlation (❑) dropped below 0.5, and the average difference between phase angles (○) was greater than 45° at about 15 Å resolution.

Figure 11. Icosahedral asymmetric unit showing the non-random orientation of the individual particles used for the cryo-EM image reconstruction of the α3 open procapsid. Each point represents the orientation of a particle relative to the standard orientation given by the triangular asymmetric unit. The orientations are plotted as polar angles with ϕ as the x-axis and θ as the y-axis. The angle ω is not plotted.

Table 1. Amino acid identity for proteins F and G.

	Protein F (%)	Protein G (%)
α3-ϕX174	72	31
α3-G4	64	30
G4-ϕX174	67	41

Table 2. Polar protein contacts.

Protein G_1 Residues			Residues in F making polar contacts with G_1		
α3	**ϕX174**	**G4**	α3	**ϕX174**	**G4**
	Q3	Q3		$Q254_3$	$Q254_2$
T75	N67	T68	Y159	Y158	M397
D76			Q402		
E179	E167	T171	$R56_2$	$E366_2$	$Q395_2$
Q181	I169	Q174	$D396_2$, $F399_2$	$S396_2$, $R255_2$	$S396_2$, $S255_2$
Q184	Q172	P175	$S256_3$	$R56_3$, $T255_3$, $S396_3$	$R56_3$, $Q398_2$
P185			$R57_3$, $Q403_2$		
K187	K175	K177	$R57_3$, $S256_3$, $L258_3$, $Q400_2$	$R56_2$, $T255_3$, $L257_3$, $Q395_3$	$R56_3$, $S255_3$, $L257_3$, $Q395_2$
Protein J Residues			Residues in protein F making polar contacts with J		
α3	**ϕX174**		α3	**ϕX174**	
	G3			$L236_5$, $V237_5$, $M238_5$	
	K4			$R239_5$	
	K5			$R239_5$	
	R6			$R239_5$	
	S7			$K269_5$	
	G8			$T267_5$, $Y268_5$	
	R10			$T267_5$, $K269_5$	
	G12			$T267_5$	
R5	L17		A60, D62	D61	
R6	R18		W244, D62	D61	
S7	G19		D357, W244	$K407_5$	
	T20			$S356$, $L17_5$	
	K21			$K407_5$	
R10	G22		H355, D357	D13, $S15_5$, $K407_5$, $N409_5$	
	R24			$T413_5$	
W17			K167, A172, I350, N168, I169		
Y18			L174		
V19			P139, W140		
G20	G33		T210, Y211, F212, Q214, P139	Y210, Q213	
G21			P139		
S22			R215		
Q23	Q36		Y135, C164, A138, K167	K166	
F24	F37		Y135, F68, R291	Y134, R290	

Subscripts denote symmetry-related subunits numbered clockwise
Selection criterion based on a distance of 3.0 Å

Table 3. Superposition of C_α coordinates of various virion proteins.

Superposition of proteins*	Number of equivalent C_α atoms	r.m.s.d. (Å) by least-squares refinement	r.m.s.d. (Å) by alignment of icosahedral axes
α3 / ϕX174 all	618	0.65	2.85
α3 / ϕX174 protein F	416	0.49	0.85
α3 / ϕX174 protein G	175	0.71	2.72
" G pentamer	875	0.72	2.72
α3 / ϕX174 protein J	13	0.36	0.53
α3 / G4 all	602	0.68	2.70
α3 / G4 protein F	417	0.76	0.85
α3 / G4 protein G	175	0.79	2.29
" G pentamer	865	0.78	2.29
G4 / ϕX174 all	600	0.47	1.51
G4 / ϕX174 protein F	417	0.40	0.59
G4 / ϕX174 protein G	173	0.65	3.27
" G pentamer	860	0.66	3.27

Table 4. Rotation and translation of G petamer for superposition.

	Rotation (^{0})	Translation (Å)
α3 - ϕX174	3.6	-0.2
α3 – G4	2.3	-0.4
G4 -ϕX174	1.1	0.2

Table 5. Residues that stop the spike rotation.		
	Protein F	Protein G
α3	Y159, Q402	T75, D76
ϕX174	Y158	N67
G4	M397, Q398	T68, N66

Table 6. EMfit results

Object used for fitting	*sumf* (%) before fit	*sumf* (%) after fit	Clash[§] (%)	(-)Density[§] (%)	Rotation* (degrees)	Translation* (Å)
α3 virion F	47.8	51.8	6.1	4.0	1.0	5.2
α3 virion G	27.8	46.8	0.0	1.7	2.5	8.1
ϕX174 virion F	42.2	51.3	12.7	2.8	2.1	5.2
ϕX174 virion G	28.8	47.3	0.0	1.3	1.1	8.2
ϕX174 closed procapsid F	50.9	51.6	2.6	2.6	1.3	2.2
ϕX174 closed procapsid G	24.8	47.5	0.0	1.1	1.8	2.7
ϕX174 closed procapsid D1D2	43.4	45.3	0.0	4.3	1.3	2.1
ϕX174 closed procapsid D3D4	44.6	45.2	1.2	4.5	1.0	1.7

*Anticlockwise rotation and outward radial translation (as determined by the program homology) relate the position of the protein in the native particle and after fitting into procapsid.

[§] Clash is the percentage of symmetry related atoms that are < 3.0 Å apart. Negative (-) density describes the percentage of atoms whose position corresponds to an area of negative density in the cryo-EM map.

Figure 1

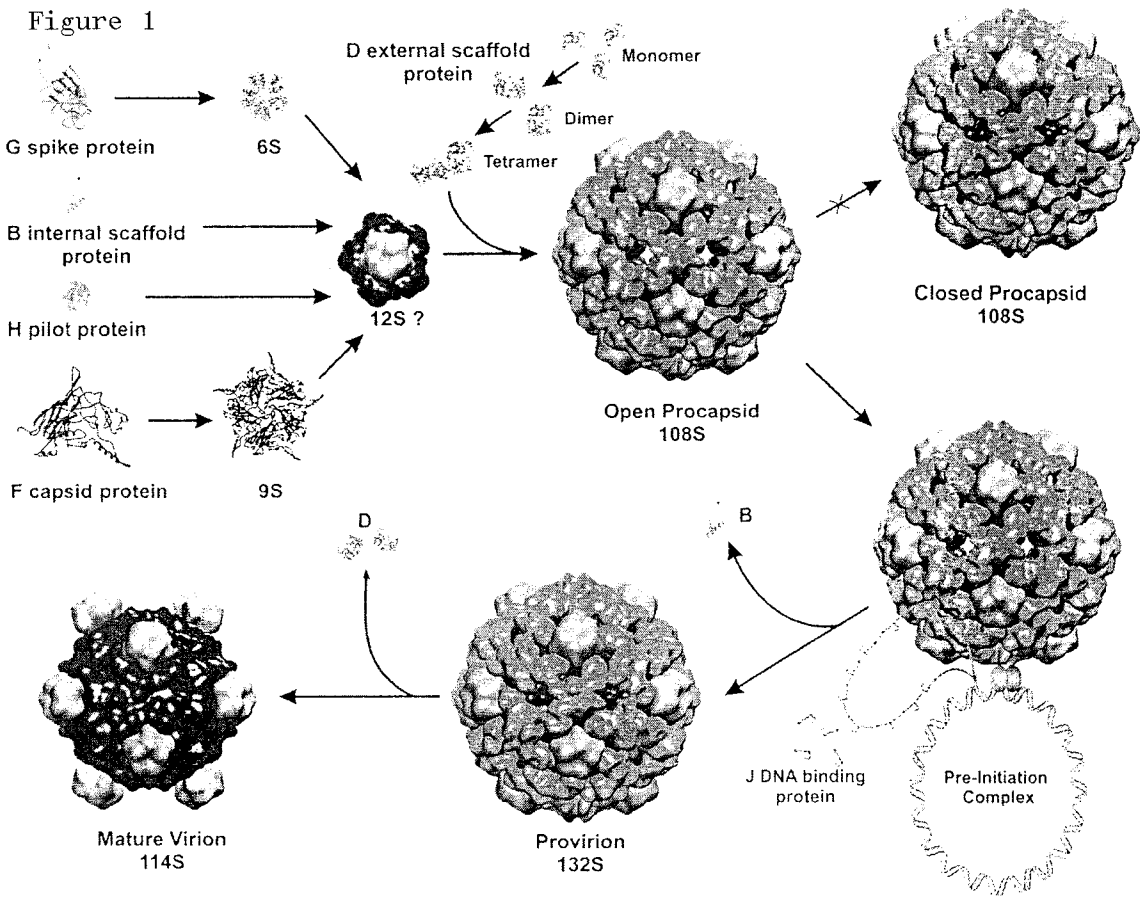
G spike protein
6S
D external scaffold protein
Monomer
Dimer
Tetramer
B internal scaffold protein
H pilot protein
12S ?
F capsid protein
9S
Open Procapsid
108S
Closed Procapsid
108S
B
D
J DNA binding protein
Pre-Initiation Complex
Provirion
132S
Mature Virion
114S

Figure 2

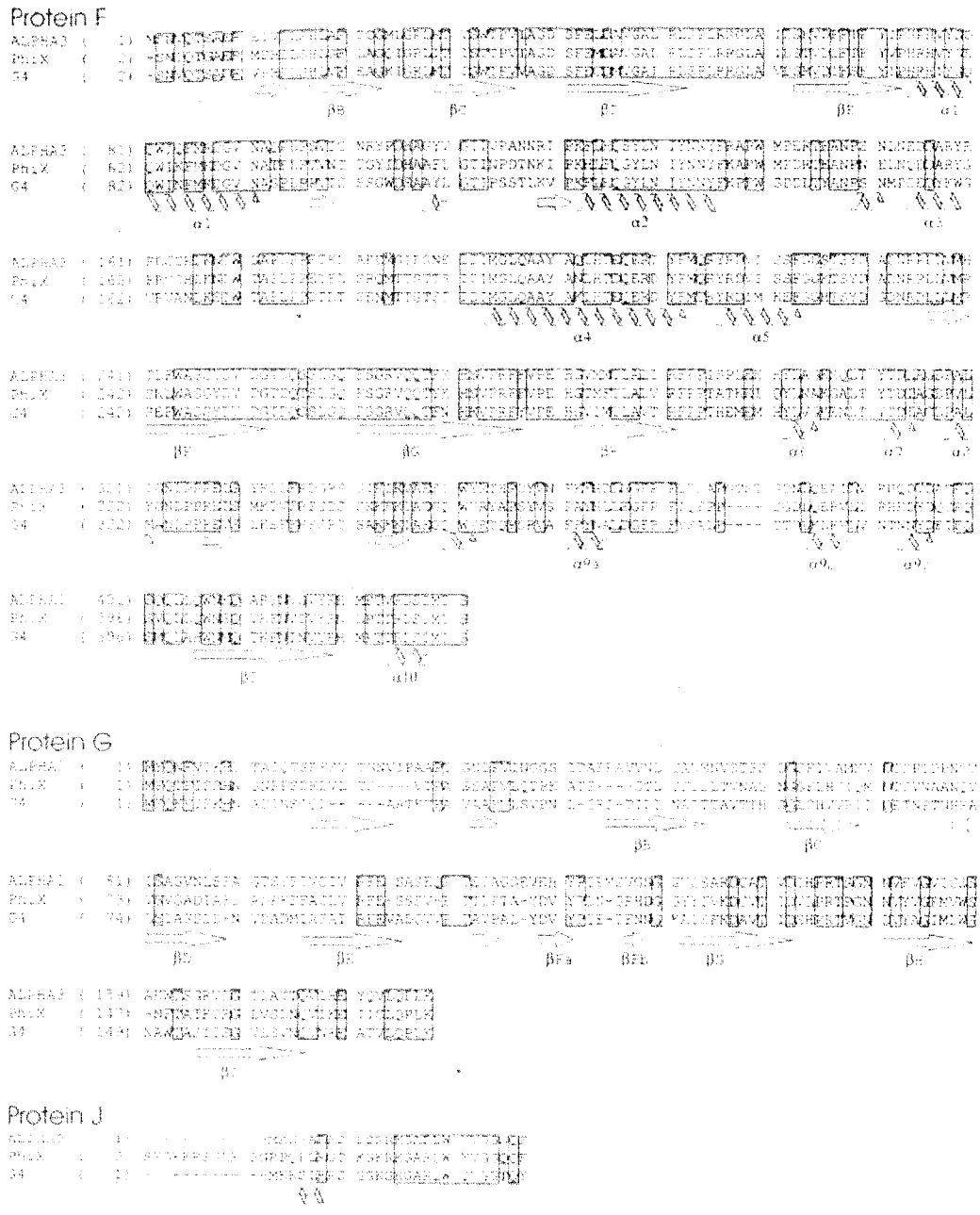

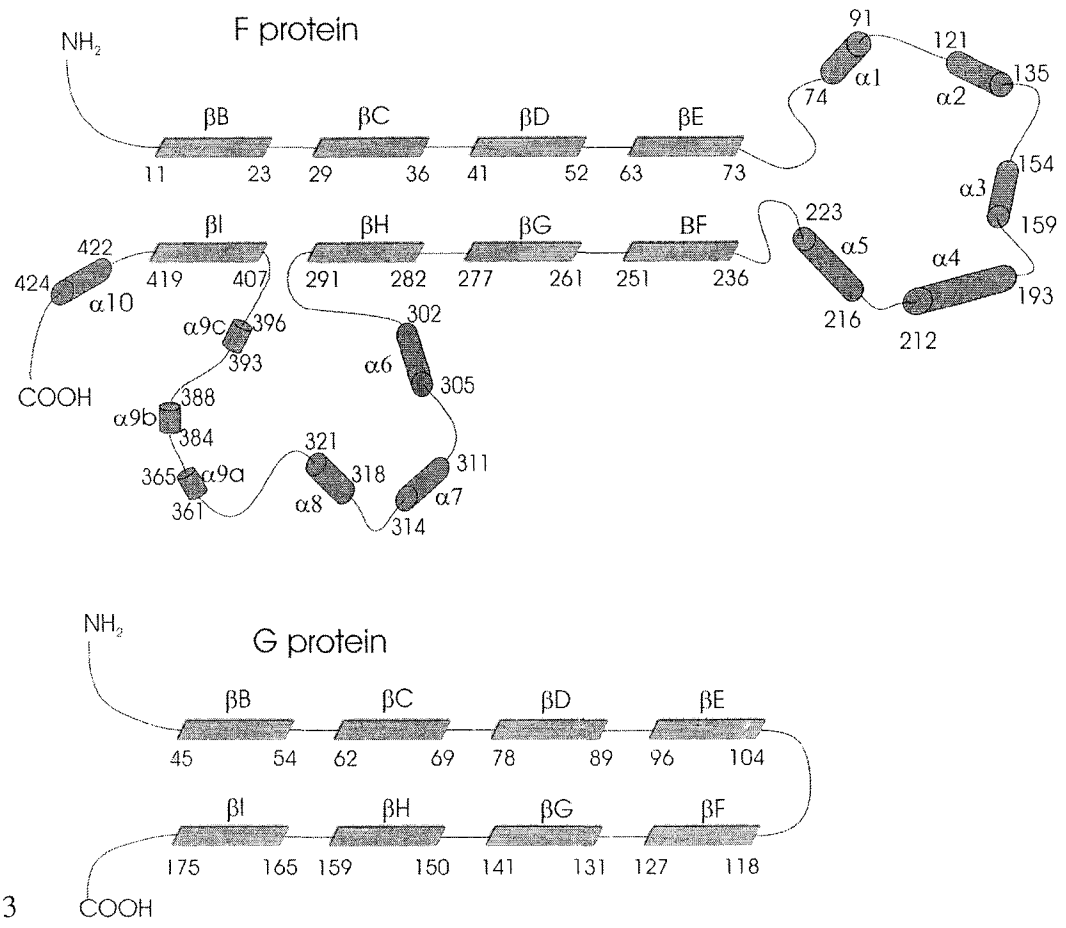
F protein
NH2
βB
βC
βD
βE
11
23
29
36
41
52
63
73
74
91
α1
121
α2
135
154
α3
159
223
α5
α4
193
216
212
βI
βH
βG
BF
422
424
α10
419
407
291
282
277
261
251
236
α9c
396
393
302
α6
305
COOH
388
α9b
384
321
318
311
α8
α7
365
α9a
361
314
G protein
NH2
βB
βC
βD
βE
45
54
62
69
78
89
96
104
βI
βH
βG
βF
175
165
159
150
141
131
127
118
COOH

Figure 3

Figure 4

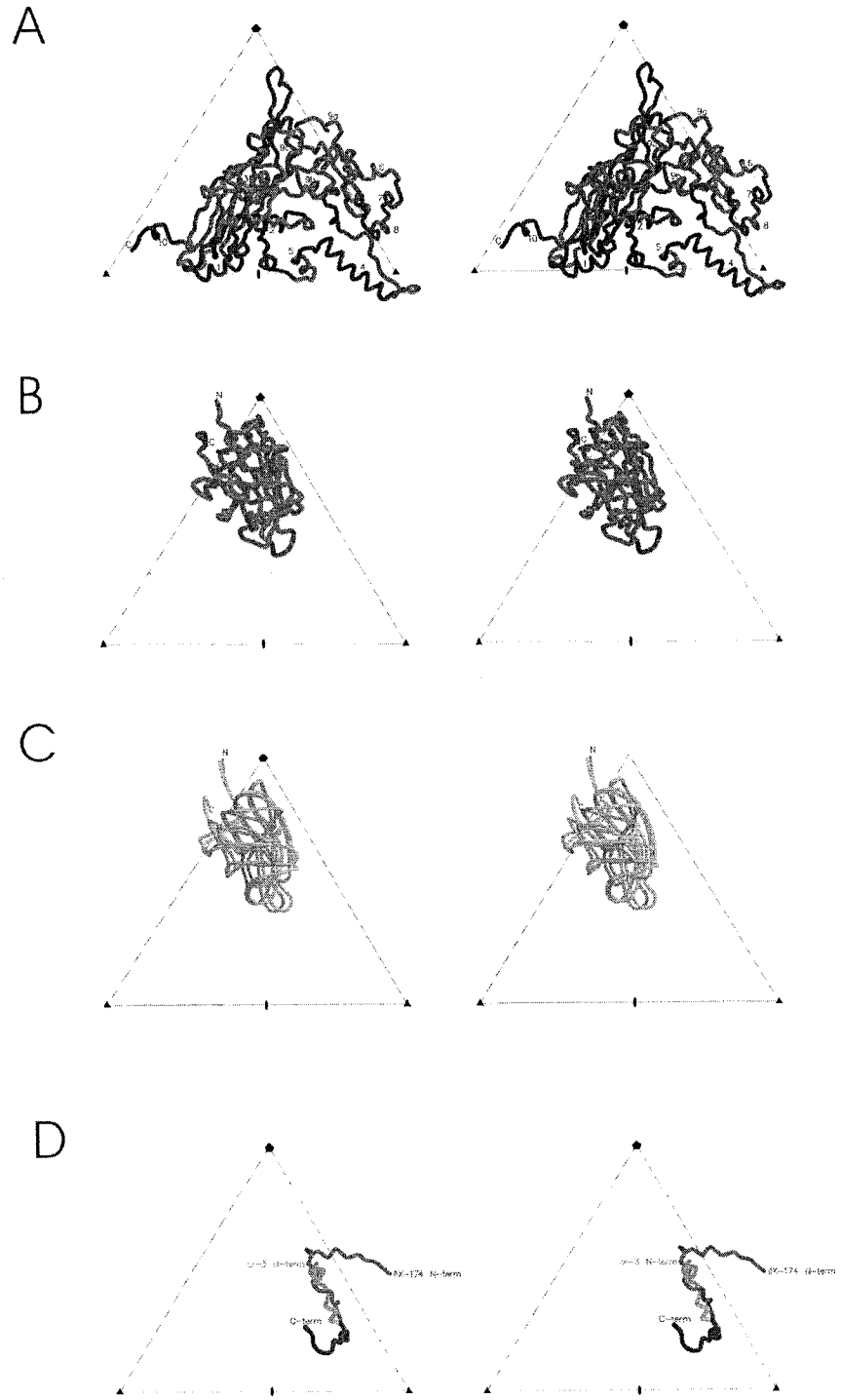

Figure 5

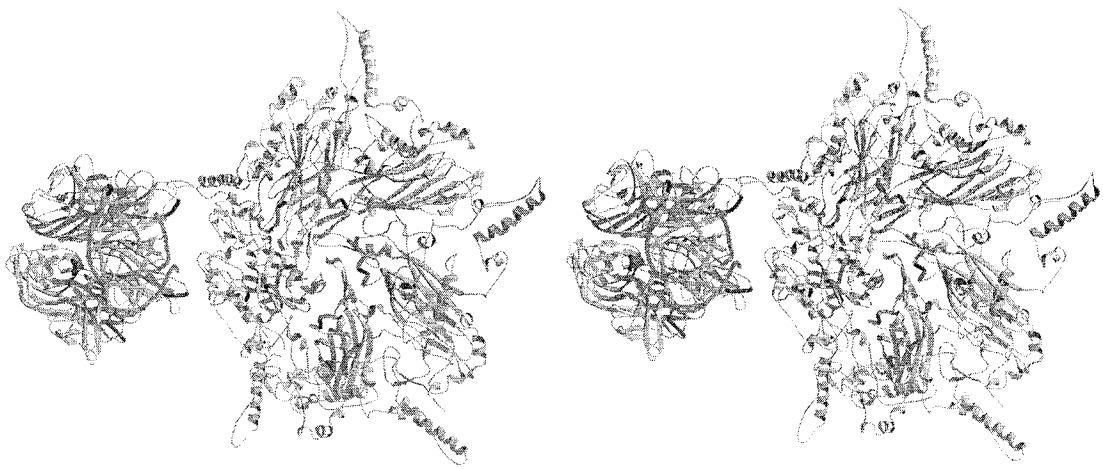

Figure 6

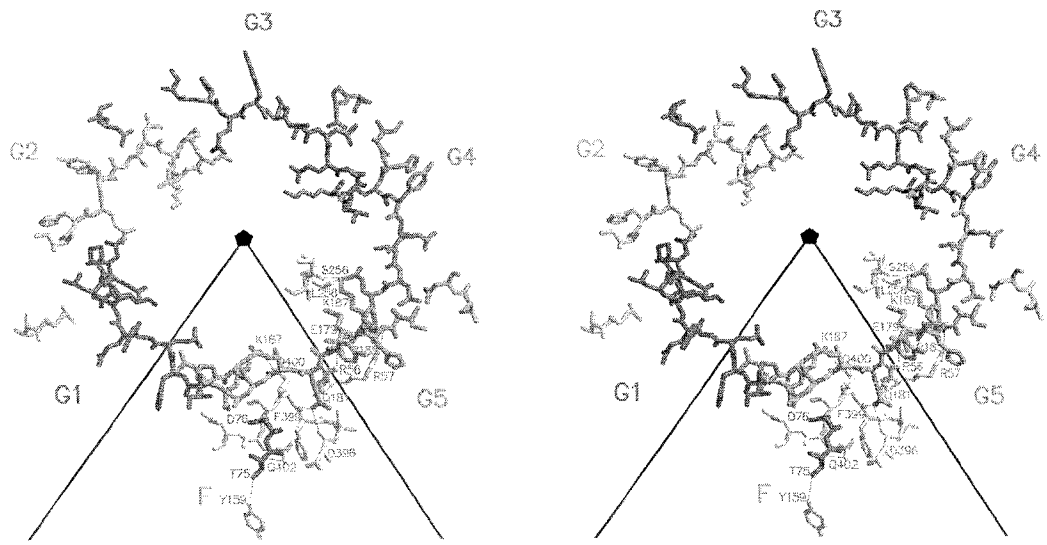

Figure 7

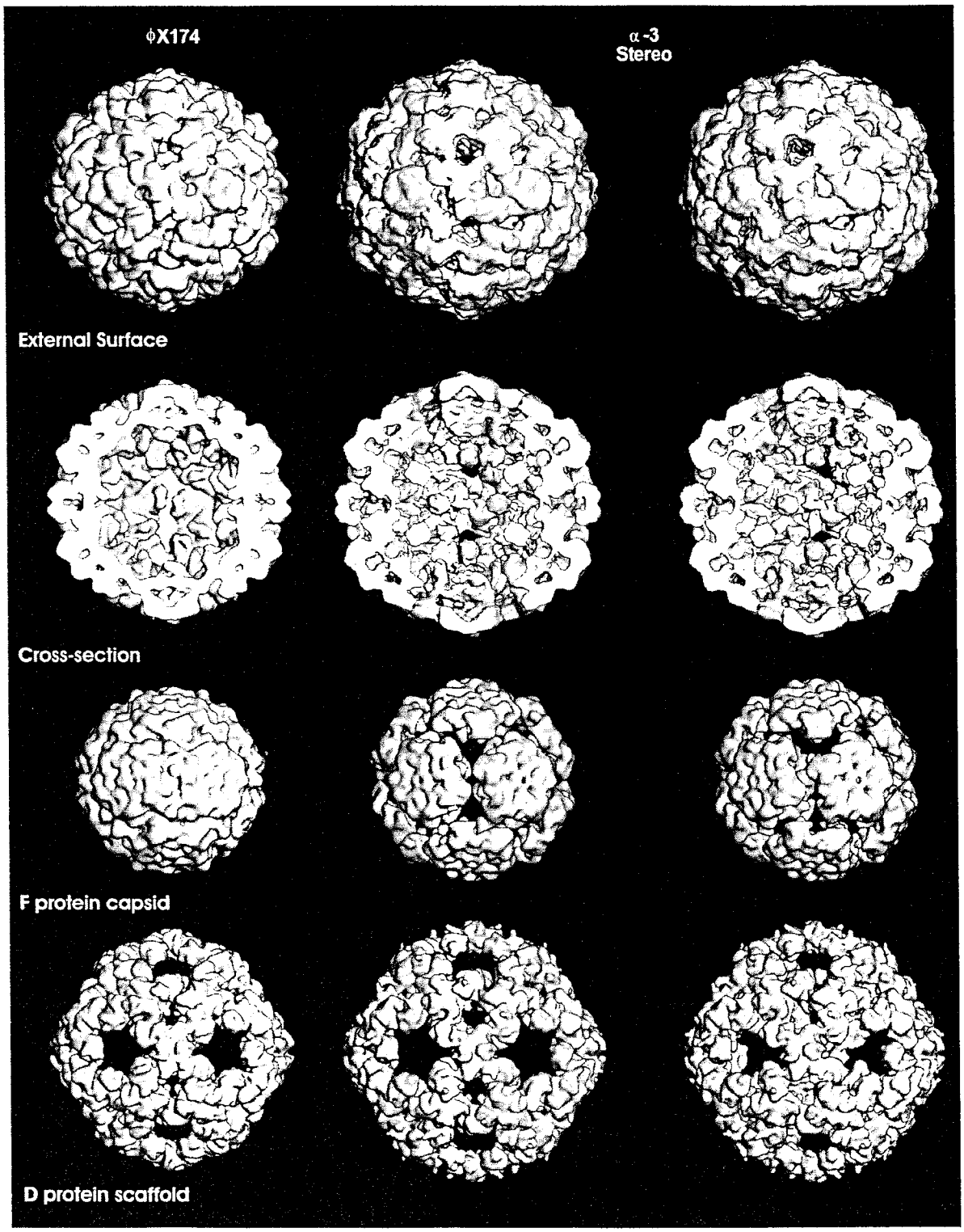
ϕX174
α-3
Stereo
External Surface
Cross-section
F protein capsid
D protein scaffold

Figure 5

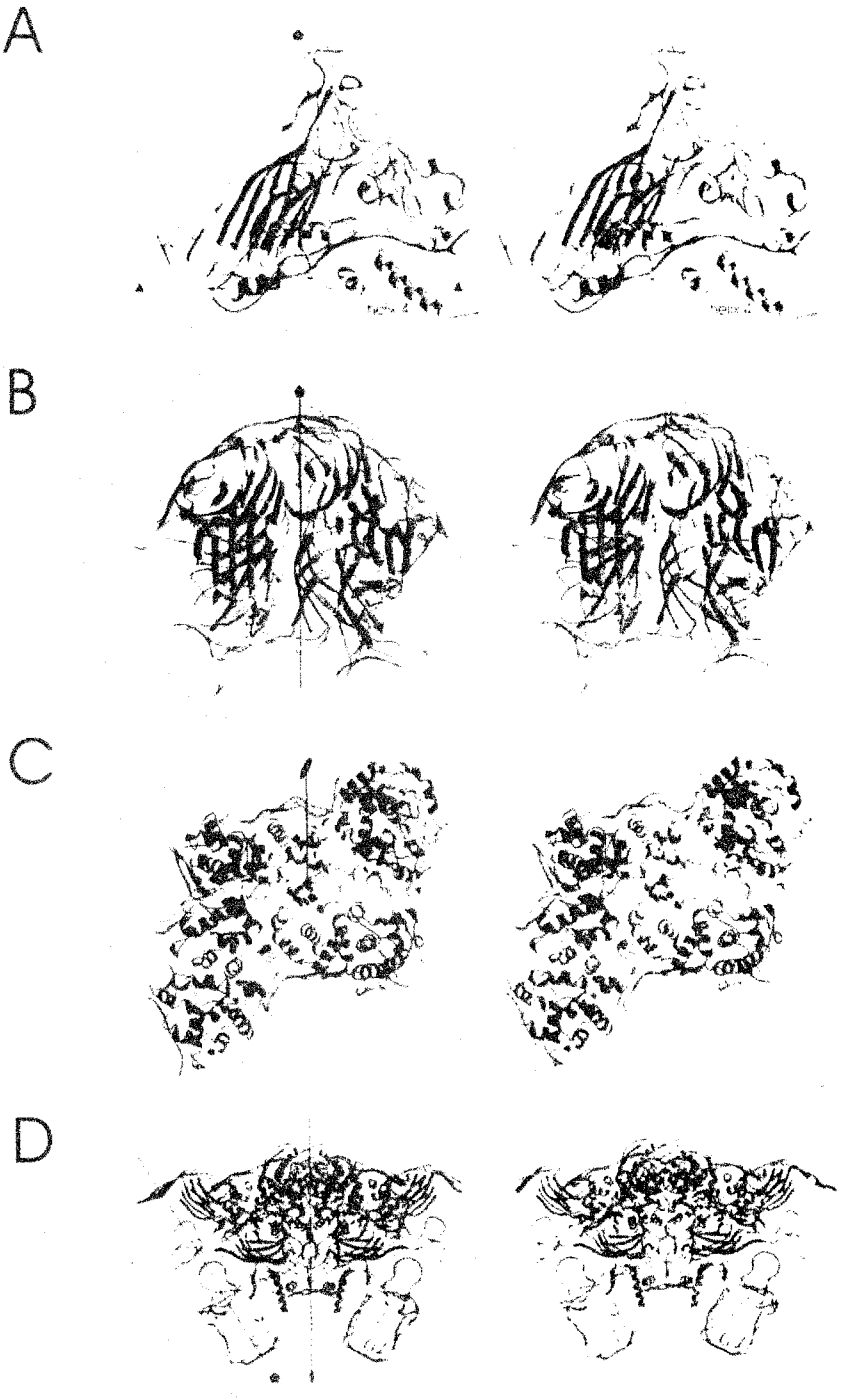

Figure 9

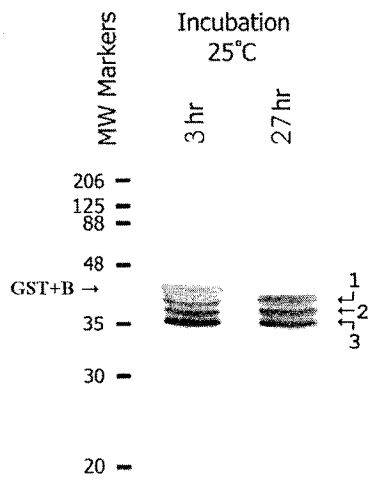

GST-(1) **MEQLTKNQ**AV ATSQEAVQNQ NEPQLRDENA HNDKSVHGVL NPTYQAGLRR DAVQPDIEAE

3* 2 1

(61) **RKKRDEIEAG KSYCSRRFGG ATCDDKSAQI YARFDKNDWR IQPAEFYRFH DAEVNTFGYF**

* Previously reported cleavage site [15].

Figure 10

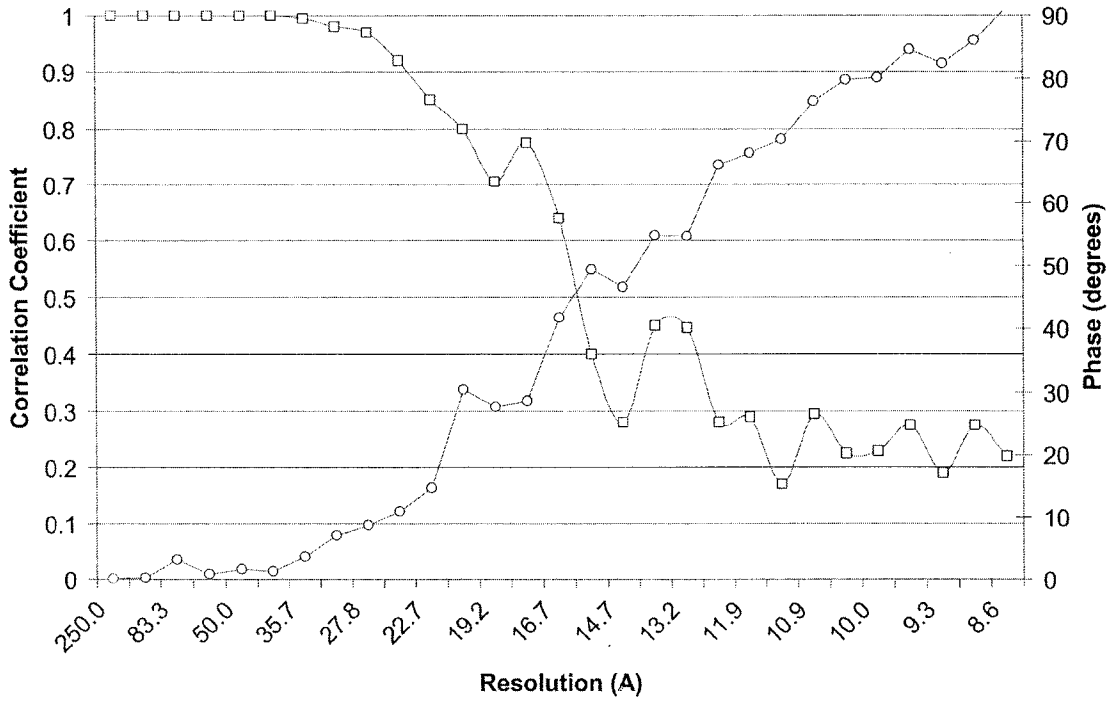
Correlation Coefficient
Phase (degrees)
Resolution (A)
1
0.9
0.8
0.7
0.6
0.5
0.4
0.3
0.2
0.1
0
90
80
70
60
50
40
30
20
10
0
250.0
83.3
50.0
35.7
27.8
22.7
19.2
16.7
14.7
13.2
11.9
10.9
10.0
9.3
8.6

Figure 11

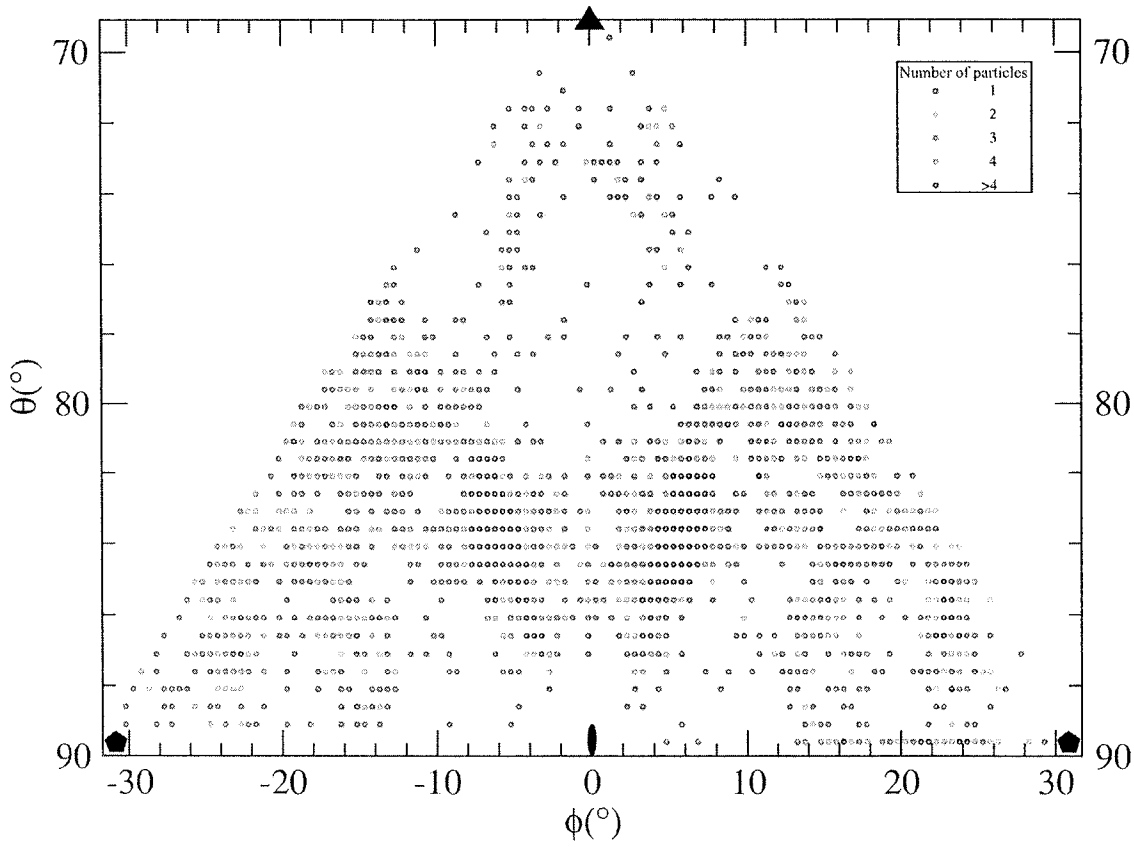

REFERENCES

Agbandje-McKenna, M., Llamas-Saiz, A. L., Wang, F., Tattersall, P., and M. G. Rossman, 1998. Functional implications of the structure of the murine parvovirus minute virus of mice. Structure **6:** 1369-1381.

Alestrom, P., Akusjarui, G., Lager, M., Yeh-kai, L. and U. Pettersson, 1984. Genes encoding the core proteins of Adenovirus type 2. J. Biol. Chem. **259**: 13980-13985.

Anderson, C. W., Young, M. E., and S. J. Flint, 1989. Characterization of the Adenovirus 2 virion protein mu. Virol. **172:** 506-512.

Aoyama, A. and M. Hayashi, 1985. Effects on genome size on bacteriophage phiX174 DNA packaging *in vitro*. J. Biol. Chem. **260:** 11033-11038.

Aoyama, A., and M. Hayashi, 1985. In vitro packaging of plasmid DNAs into phiX174 bacteriophage capsid. Nature **297:** 704-707.

Aoyama, A., Hamatake, R. K., and M. Hayashi, 1981. Morphogenesis of phi X174: in vitro synthesis of infectious phage from purified viral components. Proc. Natl. Acad. Sci. USA **78:** 7285-9.

Aoyama, A., Hamatake, R. K., and M. Hayashi. 1983. In vitro synthesis of bacteriophage øX174 by purified components. Proc. Natl. Acad. Sci. USA **80:** 4195-4199.

Benevides, J. M., Stow, P. L., Ilag, L. L., Incardona, N. L., and G. J. Thomas, Jr., 1991. Differences in secondary structure between packaged and unpackaged single-stranded DNA of bacteriophage øX174 determined by Raman spectroscopy: A model for øX174 DNA packaging. Biochem. **30:** 4855-4862.

Bernal, R. A., Hafenstein, S., Olson, N. H., Bowman, V. D., Chipman, P. R., Baker, T. S., Fane, B. A., and M. G. Rossmann, 2003. Structural studies of bacteriophage α3. J. Mol. Biol. **325**: 11-24

Bink, H. H., Hellendoorn, K., van der Meulen, J., and W. A. Pleij, 2002. Protonation of non-Watson-Crick base pairs and encapsidation of turnip yellow mosaic virus RNA Proc. Natl. Acad. Sci. USA. **99**: 13465-13470

Bothner, B., Schneemann, A., Marshall, D., Reddy, V., Johnson, J. E., and G. Siuzdak, 1999. Crystallographically identical virus capsids display different properties in solution. Nature Struct. Biol. **6:** 114-116.

Bredenbeek, P. J., Frolov, I., Rice, C. M., and S. Schlesinger, 1993. Sindbis Virus expression vectors: Packaging of RNA replicons by using defective helper RNAs. J. Virol **67:** 6439-6446.

Brown, D. R., Roth, M. J., Reinberg, D., and J. Hurwitz, 1984. Analysis of bacteriophage øX174 gene A protein mediated termination and reinitiation of øX174 DNA synthesis. I. Characterization of the termination and reinitiation reactions. J. Biol. Chem. **259:** 10545-10555.

Burch, A. D., Ta, J., and B. A. Fane, 1999. Cross-functional analysis of the *Microviridae* internal scaffolding protein. J. Mol. Biol. **286**: 95-104.

Burch, A. D. and B. A. Fane, 2000. Foreign and chimeric external scaffolding proteins as inhibitors of *Microviridae* morphogenesis. J. Virol. **74:** 9347-9352

Burch, A. D. and B. A. Fane, 2003. Genetic analyses of putative conformation switching and cross-species inhibitory domains in *Microviridae* external scaffolding proteins. Virology *in press.*

Chapman, M. S. and M. G. Rossmann, 1995. Single-stranded DNA-protein interactions in canine parvovirus. Structure **3:**151-62.

Chen, Z.G., Stauffacher, C., Li, Y., Schmidt, T., Bomu, W., Kamer, G., Shanks, M., Lomonossoff, G., and J. E. Johnson, 1989. Protein-RNA interactions in an icosahedral virus at 3.0 A resolution. Science **245:** 154-9.

Choi, Y. G. and A. L. N. Rao, 2000a. Molecular studies on bromovirus capsid protein. Virol. **275**: 207-217

Choi, Y. G. and A. L. N. Rao, 2000b. Packaging of tobacco mosaic virus subgenomic RNAs by Brome mosaic virus coat protein exhibits RNA controlled polymorphism. Virol. **275:** 249-257.

Copeland, T. D., Morgan, M. A., and S. Oroszlan, 1984. Complete amino acid sequence of the basic nucleic acid binding protein of Feline Leukemia Virus. Virol. **133:** 137-145.

Da Poian, A. T., Johnson, J. E., and J. L. Silva, 2002. Protein-RNA interactions and virus stability as probed by the dynamics of tryptophan side chains. J. Biol. Chem. **49:** 47596-602

Dalphin, M. E, 1989. Bacteriophage øX174: Crosslinking studies of the virion and prohead and biophysical characterization of the gene J protein. Doctoral thesis, University of California, San Diego.

Davis, N. L. and R. R. Ruekert, 1972. Properties of a ribonucleoprotein particle isolated from nonidet P-40-treated Rous Sarcome Virus. J. Virol. **10:** 1010-1020.

Desai, P., Watkins, S.C., and S. Person, 1994. The size and symmetry of B capsids of herpes simplex virus type 1 are determined by the gene products of the UL26 open reading frame. J. Virol. **68:** 5365-74.

Dokland, T., R. McKenna, L. L. Ilag, B. R. Bowen, N. L. Incardona, B. A. Fane and M. G. Rossmann, 1997. Structure of a viral assembly intermediate with molecular scaffolding. Nature **389**: 308-313.

Dokland, T., R. A. Bernal, A. Burch, S. Pletnev, B. A. Fane and M. G. Rossmann, 1999 The role of scaffolding proteins in the assembly of the small single-stranded DNA virus øX174. J. Mol. Biol. **288:** 595-608

Dong, X.F., Natarajan, P., Tihova, M., Johnson, J.E., and A. Schneemann, 1998. Particle polymorphism caused by deletion of a peptide molecular switch in a quasi-equivalent icosahedral virus. J. Virol. **72:** 6024-33.

Dubensky, T. W., Driver, D. A., Polo, J. M., Belli, B. A., Latham, E. M., Ibanez, C. E., Chada, S., Brumm, D., Banks, T. A., Mento, S. J., Jolly, D. J., and S. M. W. Chang,

1996. Sindbis virus DNA-based expression vectors: Utility for in vitro and in vivo gene transfer. J. Virol. **70:** 508-519

Earnshaw, W. C., and S.R. Casjens, 1980. DNA packaging by the double-stranded DNA bacteriophages. Cell 21: 319-331.

Eisenberg, S., Griffith, J., and A. Kornberg, 1977. PhiX174 cistron A protein is a multifunctional enzyme in DNA replication. Proc. Natl. Acad. Sci. USA **74:** 3198-3202.

Eisenberg, S. and A. Kornberg, 1979. Purification and characterization of the øX174 cistron A protein. A multifunctional enzyme of duplex DNA. J. Biol. Chem. **254:** 5328-5332.

Ekechukwu, M. C., Oberste, D. J. , and B. A. Fane, 1995. Host and phiX174 mutations which affect the morphogenesis or stabilization of the 50S complex, a single stranded DNA synthesizing intermediate. Genetics **140:** 1167-1174.

Fane, B. A. and M. Hayashi, 1991. Second-site suppressors of a cold-sensitive prohead accessory protein of bacteriophage phiX174. Genetics **128:** 663-671.

Fane, B. A., Head, S., and M. Hayashi, 1992. The functional relationship between the J proteins of bacteriophages phiX174 and G4 during phage morphogenesis. J. Bacteriol. **174:** 2717-2719.

Fane, B. A., Shien, S., and M. Hayashi, 1993. Second-site suppressors of a cold sensitive external scaffolding protein of bacteriophage phiX174. Genetics **134:** 1003-1011.

Fisher, A.J. and J. E. Johnson, 1993. Ordered Duplex RNA Controls Capsid Architecture in an Icosahedral Animal Virus. Nature **361:** 176-179.

Fligge, C., Schafer F., Selinka, H. C., Sapp, C. and M. Sapp, 2001. DNA-induced structural changes in the papillomavirus capsid. J. Virol. **75:** 7727-7731.

Fluit, A. C., Baas, P. D., and H. S. Jansz, 1985. The complete 30-base pair origin region of bacteriophage phiX174 in a plasmid is both required and sufficient for in vivo rolling circle DNA replication. Eur. J. Biochem. **149:** 579-584.

Fox, J. M., Wand, F., Speir, J. A., Olson, N. H., Johnson, J. E., Baker, T. S., and M. J. Young, 1998. Comparison of the native CCMV virion with in vitro assembled CCMV virions by cryoelectron microscopy and image reconstruction. Virol. **244:** 212-8

Fujisawa, H. and M. Hayashi, 1976. Viral DNA- synthesizing intermediate complex isolated during assembly of Bacteriophage phiX174. J. Virol. **19:** 409-415.

Fujisawa, H. and M. Hayashi, 1977. Two infectious forms of bacteriophage phiX174. J. Virol **23:** 439-442.

Godson, G. N., Barrell, B. G., Standen, R. and J. C. Fiddes, 1978. Nucleotide sequence of bacteriophage G4 DNA. Nature **276:** 236-247.

Gorziglia, M. I., Kadan, M. J., Yei, Soonpin, Lim, J., Lee, G. M., Luthra, R., and B. C. Trapnell, 1996. Elimantion of both E1 and E2a from the Adenovirus vector further imporves prospects for *in vivo* human gene therapy. J. Virol. **70**: 4173-4178.

Hafenstein, S. and B. A. Fane, 2002. PhiX174 genome-capsid interactions influence the biophysical properties of the virion: evidence for a scaffolding-like function of the genome during the final stages of morphogenesis. J. Virol. **76:**4350-5356

Hamatake, R. K., Aoyama, A. and M. Hayashi, 1985. The *J* gene of øX174: *In vitro* analysis of J protein function. J. Virol. **54:** 345-350.

Hamatake, R. K., Buckley, K. J. and M. Hayashi, 1988. The *J* gene of øX174: Isolation and characterization of a J gene mutant. Mol. Gen. Genet. **211:** 72-77.

Hardy, J. A. and H. C. Nelson, 2000. Proline in alpha-helical kink is required for folding kinetics but not for kinked structure, function, or stability of heat shock transcription factor. Protein Sci. **9:** 2128-2141.

Hayashi, M. , 1978. Morphogenesis of the isometric phages. pp.531-547. In: The single stranded DNA phages. Ed: D. Denhardt, D. Dressler and D. S. Ray. Cold Spring Harbor Laboratory, NY.

Hayashi, M., Aoyama A., Richardson D. L., and M. N. Hayashi, 1988. Biology of the bacteriophage øX174. pp. 1-71. In: The Bacteriophages, Vol. 2, Edited by R. Calendar. Plenum Publishing Corporation, New York.

Hobart, S. A., Meinhold, D. W., Osuna, R., and W. Colon, 2002. From two-state to three-state: the effect of the P61A mutation on the dynamics and stability of the factor for inversion stimulation results in an altered equilibrium denaturation mechanism. Biochemistry. **41:** 13744-13754.

Ilag, L. L., Olson, N. H., Dokland, T., Music, C. L., Cheng, R. H., Brown, Z., McKenna, R., Rossman, M. G., Baker, T. S., and N. L. Incardona, 1995. Bacteriophage øX174 procapsid: Purification and structure at 25 Å resolution. Structure **3:** 353-363.

Jardine, P. J., and D. H. Combs, 1998. Capsid expansion follows the initiation of DNA packaging in bacteriophage T4. J. Mol. Biol. **284:** 661-672

Jennings, B. and B. A. Fane, 1997. Genetic analysis of the øX174 DNA binding protein. Virol. **227:** 370-377.

King, J., and S. Casjens, 1974. Catalytic head assembling protein in virus morphogenesis. Nature **251:** 112-9.

Kodaira, K., Nakano, K., Okada, S. and A. Taketo, 1992. Nucleotide sequence of the genome of bacteriophage α3: interrelationship of the genome structure and the gene products with those of the phages øX174, G4 and øK. Biochem. Biophysic. Acta. **1130:** 277-288.

Kotin, R. M., 1996. Prospects for the use of adeno-associated virus as a vector for human gene therapy. Hum. Gene Ther. **5:**793-801.

Krol, M. A., Olson, N. H., Tate, J., Johnson, J.E., Baker, T. S., and P. Ahlquist, 1999. RNA-controlled polymorphism in the *in vivo* assembly of 180-subunit and 120-subunit virions from a single capsid protein. Proc. Natl. Acad. Sci. USA **96:** 13650-13655.

Larson, S. B., Koszelak, S., Day, J., Greenwood, A., Dodds, J. A., and A. McPherson, 1993. Double-helical RNA in satellite tobacco mosaic virus. Nature **361:** 179-182

Larson, S. B., Day, J., Greenwood, A., and A. McPherson, 1998. Refined structure of Satellite Tobacco mosaic virus at 1.8 Å resolution. J. Mol. Biol. **277:** 37-59.

Lata, R., Conway, J. F., Cheng, N., Duda, R. L., Hendrix, R. W., Wikoff, W. R., Johnson, J. E., Tsuruta, H., and A. C. Steven, 2000. Maturation dynamics of a viral capsid: visualization of transitional intermediate states. Cell **100:** 253-63.

Lee, S. K. and D. L. Hacker, 2001. In Vitro analysis of an RNA binding site within the N-terminal 30 amino acids of the southern cowpea mosaic virus coat protein. Virol. **286**: 317-327

Lieber, A., He, C. Y., Kirillova, I., and M. A. Kay, 1996. Recombinant Adenoviruses with large deletions generated by Cre-mediated excision exhibit different biological properties compared with first-generation vectors in vitro and in vivo. J. Virol. **70:** 8944-8960.

Lokesh, G. L., Gowri, T. D.S., Satheshkumar, P. S., Murthy, M. R. N., and H. S. Savithri, 2002. A molecular switch in the capsid protein controls the particle polymorphism in an icosahedral virus. Virol. **292**: 211-223

Marshall, D. and A. Schneemann, 2001. Specific packaging of nodaviral RNA2 requires the N-terminus of the capsid protein. Virol. **285**:165-175

McKenna, R. Ilag, L. L., and M. G. Rossmann, 1994. Analysis of the single-stranded DNA bacteriophage øX174 at a resolution of 3.0 A. J. Mol. Biol. **237:** 517-543.

McKenna, R., Xia, Willingmann, P., Ilag, L. L., Krishnaswamy, S., Rossmann, M. G., Olson, N. H., Baker, T. S. and N. L. Incardonna, 1992. Atomic structure of single-stranded DNA bacteriophage øX174 and its functional implications. Nature **355:**137-143.

McKenna, R., Bowen, B. R., Ilag, L. L., Rossmann, M. G. and B. A. Fane, 1996. The atomic structure of the degraded procapsid particle of bacteriophage G4: Induced structural changes in the presence of calcium ions and functional implications. J. Mol. Biol. **256:** 736-750.

Mukai, R., Hamatake, R. K. and M. Hayashi, 1979. Isolation of the bacteriophage øX174 prohead. Proc. Natl. Acad. Sci. **76:** 4877-4881.

Prasad, B. V., Prevelige, P. E., Marietta, E., Chen, R. O., Thomas, D., King, J., and W. Chiu, 1993. Three-dimensional transformation of capsids associated with genome packaging in a bacterial virus. J. Mol. Biol. **231:** 65-74.

Rao, A. L. and G. L. Grantham, 1996. Molecular studies on bromovirus capsid protein. II. Functional analysis of the amino-terminal arginine-rich motif and its role in encapsidation, movement, and pathology. Virology 226: 294-305.

Roof, W. D., Horne, S. M., Young, K. D., and R. Young, 1994. slyD, a host gene required for phi X174 lysis, is related to the FK506-binding protein family of peptidyl-prolyl cis-trans-isomerases. J. Biol. Chem. **269:** 2902-10.

Rossmann M. G., Abad-Zapatero C., Erickson, J. W. and H. S Savithri, 1983. RNA-protein interactions in some small plant viruses. J. Biomol. Struct. Dyn. 1:565-579.

Rossmann, M. G. and J. E. Johnson, 1989. Icosahedral RNA virus structure. Ann. Rev. Biochem. **58:** 533-573.

Russell, D. W. and A. D. Miller, 1996. Foamy Virus Vectors. J. Virol. **70:** 217-222.

Sacher R, and P. Ahlquist, 1989. Effects of deletions in the N-terminal basic arm of brome mosaic virus coat protein on RNA packaging and systemic infection. J. Virol. **63:** 4545-52.

Sanger, F., Coulson, A. R., Friedmann, C. T., Air, G. M., Barrell, B. G., Brown, N. L., Fiddes J. C., Hutchison, C. A. III, Slocombe, P. M., and M. Smith, 1978. The nucleotide sequence of bacteriophage øX174. J. Mol. Biol. **125:** 225-246.

SantaLucia, J.Jr., 1998. A unified view of polymer, dumbbell, and oligonucleotide DNA nearest-neighbor thermodynamics. Proc. Natl. Acad. Sci. USA **95:** 1460-1465.

Savithri, H. S. and J. W. Erickson, 1983. The self-assembly of the cowpea strain of southern bean mosaic virus: formation of T = 1 and T = 3 nucleoprotein particles. Virology **126:** 328-335.

Schmitz, I. and A. L. Rao, 1998. Deletions in the conserved amino-terminal basic arm of cucumber mosaic virus coat protein disrupt virion assembly but do not abolish infectivity and cell-to-cell movement. Virology **248:**323-331.

Serwer P. and M. E. Pichler, 1978. Electrophoresis of bacteriophage T7 and T7 capsids in agarose gels. J. Virol. **28:** 917-928.

Siden, E. J. and M. Hayashi, 1974. Role of the gene B product in bacteriophage øX174 development. J. Mol. Biol. **89**:1-16

Tacken M. G., Peeters B. P., Thomas A. A., Rottier, P. J., and H. J. Boot, 2002. Infectious bursal disease virus capsid protein VP3 interacts both with VP1, the RNA-dependent RNA polymerase, and with viral double-stranded RNA. J Virol. 76:11301-1111.

Tang, L., Johnson, K. N., Ball, L. A., Lin, T., Yeager, M., and J. E. Johnson, 2001. The structure of pariacoto virus reveals a dodecahedral cage of duplex RNA. Nature Struct. Biol. **8:** 77 – 83.

Tonegawa, S and M. Hayashi, 1970. Intermediates in the assembly of øX174 J. Mol. Biol. **48**:219-242

Van Masnfeld, A. D., Baas, P. D., and H. S. Jansz, 1984. Gene A protein of bacteriophage øX174 is a highly specific single-stranded DNA nuclease and binds via a tyrosyl residue to DNA after cleavage. Adv. Exp. Med Biol. **197:** 221-230.

Vriend, G., Verduin, B. J., and M. A. Hemminga, 1986. Role of the N-terminal part of the coat protein in the assembly of cowpea chlorotic mottle virus. A 500 MHz proton nuclear magnetic resonance study and structural calculations. J. Mol. Biol. **191:** 453-60.

Wery, J. P., Reddy, V. S., Hosur, M. V., and J. E. Johnson, 1994. The refined three-dimensional structure of an insect virus at 2.8 A resolution. J. Mol. Biol. **235:** 565-86.

Wikoff, W. R., Tsai, C. J., Wang, G., Baker, T. S., and J. E. Johnson, 1997. The structure of cucumber mosaic virus: cryoelectron microscopy, X-ray crystallography, and sequence analysis. Virology **232:** 91-97.

Willits, D., Zhao, X., Olson, N., Baker, T. S., Zlotnick, A., Johnson, J. E., Douglas, T., and M. J. Young, 2003. Effects of the cowpea chlorotic mottle bromovirus β-hexamer structure on virion assembly. Virol. **306**: 280-288

Winston, F., Botstein, D., and J. H. Miller, 1979. Characterization of amber and ochre suppressors in Salmonella typhimurium. J Bacteriol. 137:433-439

Zolotukhnin, S., Potter, M., Hauswirth, W. W., Gou, J., and N. Muzyczka, 1996. A humanized green fluorescent protein cDNA adapted for high-level expression in mammalian cells. J. Virol. **70:** 4646-4654.